# Absorption Spectroscopy of Rare Earth Fluoride and Metal Vapours using Synchrotron Radiation

by

Michael Pantelouris B.Sc., A.R.C.S.

December 1986

A thesis submitted for the degree of Doctor of Philosophy
of the University of London.

Physics Department,
Imperial College,
London SW7 2AZ.

## Abstract

The inner shell $4d$ photoabsorption spectra of the fluorides $LaF_3$, $CeF_3$, $PrF_3$ and $GdF_3$ are compared with the corresponding atomic metal vapour, as well as with existing data of the metals in the solid state. An analogous comparison for the related $5d$ spectra of the actinide fluorides $ThF_4$ and $UF_4$ is also presented.

The spectra were obtained in the 100 Å wavelength region using a grazing incidence spectrograph and synchrotron radiation as a background source.

The dominating feature in all of the lanthanide spectra is a broad and intense absorption peak known as a *giant resonance* which lies in the continuum. The notation $4d \longrightarrow \overline{4,\varepsilon f}$ is used to label the giant resonance transitions and we argue that this is primarily a feature inherent to the continuum as opposed to a two-channel process such as auto-ionisation. The close similarity observed between the various spectra for each specific lanthanide indicates that the features observed in the fluoride and solid state spectra are essentially atomic in origin.

An interpretation based on the independent particle model is presented, which focusses on the important role played by the angular momentum barrier that appears in the effective radial potential for $d$ and $f$ electrons. The double valley that is thus formed in the potential together with the associated phenomenon of *wavefunction collapse* is responsible for the observed features of the lanthanide spectra, and for the suppression of Rydberg series observed.

As was expected, the actinide fluoride and solid state spectra are also dominated by giant resonance transitions $5d \longrightarrow \overline{5,\varepsilon f}$. However only the uranium atomic spectrum could be obtained and this displayed no giant resonance but only a single sharp line associated with a discrete final state. This unexpected result demonstrates the critical dependence of of the wavefunction collapse phenomenon on the depth of the inner potential well.

A parametric formula dependent on the depth and width of a simple square well representation for the radial potential is used to calculate the profiles of the giant resonances. Excellent agreement is obtained with the observed spectra, reflecting the underlying correctness of the qualitative explanation given.

# Contents

# List of Figures

# List of Tables

**Acknowledgments**

The present work would not have been possible without the cooperation and the help of a large number of people, all of whom I thank.

In particular I would like to thank the following. Michael Martin for initiation to work *down the hole*. Michael Mansfield whom I helped to obtain the $UF_4$ data so providing me with my first experience of the apparatus and working with synchrotron radiation. Ernst Radtke for advice on the furnace and spectrograph, and useful discussions about the lanthanide elements. Aslam Baig for his encouragement and friendship throughout the work. Josef Hormes for all his help and support both during and after the experimental work was completed, and in whose group it has been most enjoyable to belong. Also all my freinds in the Synchrotronstrahlungsgruppe.

I also wish to thank the directors of the Physikalisches Institut Profs. K.H. Althoff, G. Knop and G. Nöldeke for the priveledge of working at the Institut and for allowing me access to all its facilities. My thanks also to Dr. D. Husmann director of the 2.5 GeV Synchrotron for his freindly interest and support.

I am indebted to Herr H. Peschel for his expert and amazingly fast construction of an endless number of pieces of apparatus.

My warmest thanks go to Herrn P. Haas, J. Karthaus and K. Küffner who were responsible for the running of the 500 Mev Synchrotron and without whom none of this work would have been possible. Their willingness to advise and help, their encouragement and the freindly atmosphere under which this was provided made it a great pleasure and a priveledge to work with them.

My thanks also to Prof. Reg Garton for the many enjoyable discussions on both physics and diverse other subjects. His experience and vast knowledge was of great value to me.

Lastly I wish to extend my sincere thanks to my supervisor Prof. Jean–Patrick Connerade for his guidance and the inspiration behind the experiments. His encouragement throughout and his endless patience is greatly appreciated. We carried out the experiments on $LaF_3$ and $ThF_4$ together and the data ~~obtained~~ we obtained he also reduced and digitised. It was both instructive and a great pleasure to work together.

A three year studentship grant from the S.E.R.C. is also acknowledged.

# Chapter I

# Rare Earths: Ab initio theory of atomic structure

## 1.1 Summary

The strategic importance of the *rare earth* elements as a testing ground of *ab initio* theory of atomic structure is introduced by a qualitative look at the periodic table of elements.

The independent particle model is discussed as are alternatives in the shape of many-body perturbation theory and the random phase approximation with exchange which to a varying degree take account of electron correlation effects. Recently the $g$-Hartree method is beginning to hold promise of becoming a powerful tool in the treatment of atomic structure.

## 1.2 Introduction

Spectroscopy is an important method of extracting information on electronic structure, and is an area where experimental and theoretical work have always gone hand-in-hand. Advances in one have motivated advances in the other, and both are inseperably linked. Although the focus of the present work lay entirely on the experimental side, we cannot ignore the significance of the work on the theoretical *backdrop*. We therefore feel it as pertinent to begin with a general overview of the theoretical background, so as to set the *scenery* and give an indication of the spirit in which this experimental work was undertaken. We do not attempt to give an in-depth review

of the theory but instead limit ourselves to a more-or-less brief description of the salient concepts or components involved. Thus in this chapter we concentrate on introducing the various *ab initio* theories, whilst the also very significant practical incentives are presented in the next chapter.

We first present a short account of the Independent Particle Model which was developed in the 1920's. Bohr (1913) provided an explanation of the periodic table (figure 1.1) to which the concept of electron-spin (Uhlenbeck and Goudsmit 1925) and the exclusion principle (Pauli 1925) were then added. This finally led to the proposal by Hartree (1928) of the self-consistent field method on which the Hartree-Fock method (Fock 1930) was based. The periodic table not only provides evidence in support of the independent particle model, but also serves to indicate its limitations. Therefore alternative theories that implicitly involve many-body correlations are then also introduced and discussed.

In the meantime we must not forget that it was experimental work (Lukirskiĭ et al 1964, Zimkina et al 1967) that first brought to light the importance of the rare earth elements as a testing ground of fundamental theories, and that it is exactly this class of elements that we studied in the present work. But as already mentioned this will be further exemplified in chapter two.

## 1.3 The Independent particle model

The essential feature of the independent particle model are the following assumptions

- each electron moves in a time-independent potential which is due to the nucleus and the other $(N-1)$ electrons in the system
- the nucleus is point-like
- the nucleus has an infinite mass and hence absorbs momentum but not energy

Although not necessary, it is convenient to choose the static mean field so that it is spherically symmetric, in which case angular momentum is conserved. The main advantage of such a treatment is that a three dimensional

problem is essentially reduced to a single dimension involving $r$ the radial coordinate.

Nevertheless solving the radial equation is a complex problem, and an exact solution is only possible for the hydrogen atom. Otherwise numerical solutions involving an iterative procedure must be computed as indicated in this chapter.

## 1.4 The Self-consistent Field Approach

The wavefunction for a system is a solution of its Schrödinger equation and is the function that contains all the information about the systems dynamical properties (Schrödinger 1926). If the wavefunction is known, all observable properties of the system can be deduced by performing the appropriate mathematical operation.

Now the radial function $R(r)$ depends on the form of the potential $V(r)$ for each electron, which in turn is inseperably connected to the radial charge distribution $R(r)$ of all other electrons. This reflectivity can be tackled by the self-consistent field approach which was first proposed by Hartree (1928).

The Hartree method represents the atomic wavefunction as a simple product of one-electron orbitals. Initial trial wavefunctions for each electron are selected and used to calculate the corresponding potential $V(r)$, which is then used in the Schrödinger equation to evaluate a new set of wavefunctions. This procedure is reiterated until two consecutively calculated sets of wavefunctions agree to within a specified accuracy, and self-consistency is thus achieved. Fock (1930) then extended this by showing that this is essentially a variational minimum, and by including an exchange component in the potential. By expressing the wavefunction in the form of a Slater determinent (Slater 1930) the Pauli principle is automatically satisfied, and the indistinguishability of electrons is accounted for. The Hartree–Fock method however neglects electron correlation effects. Screened hydrogenic functions are usually used as initial estimates and numerical calculations can now be made using readily available computer programs.

A general computer package which goes beyond the Hartree–Fock approximation is a configuration interaction *MCHF* program (Froese-Fischer 1972). This evaluates the radial functions and configuration weightings by

numerically solving a set of integro-differential equations. It is possible to revert to the Hartree-Fock approximations by using a single configuration in the calculation, and it can be limited to a frozen-core scheme if so desired. A Hartree–Fock–Slater potential is the form of the central potential used, which include electrostatic as well as direct and exchange potential terms (Herman and Skillman 1963). This method has proved to be quite successful in computing the general size and energies of atoms. It has hence accounted for a significant part of the periodic table, but because of its limitations it cannot account for those elements where anomalies occur or for elements of high atomic number.

Even if exact calculations are done within the scheme, the calculated energy differs from the true energy. This discrepancy lies partly in the neglect of relativistic effects (Cowan and Griffin 1976). Dirac (1928) included the relativistic requirement of invarience under a Lorentz transformation and the current relativistic Dirac–Fock routines available (Desclaux 1975) are necessary for a more accurate description of high-$Z$ atoms. However there still remains a discrepancy which reflects the approximations inherent in the Hartree–Fock scheme, and many-body correlations must be considered.

## 1.5 The Periodic Table

Bohr's concept of electrons being contained in closed shells readily explains how elements with similar properties occur periodically in the list (figure 1.1).

The early part of the table upto Argon ($Z=18$), is produced by the successive filling of shells as restricted by the Pauli principle, and in ascending values of $n$ and $\ell$. From $Z=19$, there is a close competition in the ground state between the $d^n s^2$, $d^{n+1}s$ and $d^{n+2}$ configurations. These even-parity configurations interact strongly and the assignment of a definite term loses in significance. Evidence of this $s \times d$ mixing is observable even earlier in the excited states as far back as nitrogen.

Thus the first transition series is accounted for by the filling with $3d$ electrons, within this competition with the $4s$, and then followed by the filling of the filling of the $4p$ shell. The second long period ending with xenon, is similarly created by the filling of the $5s$, $4d$ and $5p$ shells.

Greater complications set in after this point. As previously the $6s$ shell

is filled, the shell closing in barium. After this the $6s$ and $5d$ electrons enter into a competition as before, but now the $4f$ states join in and predominate. The filling of the $4f$ states creates the lanthanide or rare earth elements ($Z = 58$–$71$), the subject of the present work. This is pursued further in the next chapter where a qualitative explanation for this is presented.

The filling of the $5d$ shell that was interupted by the rare earths is then resumed in hafnium to platinum, but in the process the $6s$ electrons have been displaced and have to come in again in gold and mercury, after which the $6p$ shell becomes filled. The actinide elements are then finally created in the filling of the $7s$, $6d$, and $5f$ shells, in a similar way as the lanthanides.

This competition between configurations means that the interactions within a configuration become as important as the choise of the central field itself, and hence the independent particle model suffers from a severe handicap when it comes to describing these complex regions of the periodic table. These difficulties were first experienced by Fermi (1928) and much theoretical effort ( Manson and Cooper 1968, Rau and Fano 1968, Combet-Farnoux 1969, Griffin et al 1969 ) has been applied in the past twenty years in making the independent particle model more applicable. In fact Griffin et al (1969) by choosing a suitable central field are able to describe the order of the long periods if not their total energies .

Thus we see that the *aufbau-prinzip* which is based on angular momentum works fine and only breaks down when the radial component becomes important. Text-books when discussing the periodic table gloss over the problem by talking about screening effects (eg. Herzberg 1944). This is obviously not correct because screening cannot explain why the drop down into the inner shells should take place or why this should occur suddenly.

The real answer lies in the radial form of the potential function, and the appearence in the radial potential of $\ell \geq 2$ electrons plays a key role in accounting for the complexities of the transition, rare earth and actinide elements. Thus the irregularities in the periodic table can be understood qualitatively and this will be discussed further in chapter two, as already mentioned.

We have till now assumed that photons are absorbed by a single electron and that the effects of the other electrons can be approximated by a central-field. Relaxing this approximation means that we must explicitly include the effects of other electrons and we must go to a many-body formalism. For instance, the final states available can include states of double

or multiple excitations, that are excluded in the one-electron treatment. The problem then becomes one of how to choose the two- or more electron excitations that are important in a given calculation. Various approaches to this problem that provide a prescription for such a choise are available. We now move on to briefly describe exactly such alternative theories which have been applied to calculating photoionisation cross-sections in atoms most successfully. These attempts to extend atomic calculations beyond the independent particle model, do nevertheless retain the self-consistent field approach, and indeed the one-electron model serves as a starting point for procedures such as many-body perturbation theory or the random phase approximation. In principle these require a *complete* set of eigenfunctions of a single particle Hamiltonian as a starting point.

## 1.6 Many-body Perturbation Theory

This scheme was originally developed by Brueckner (1955) and by Goldstone (1957), and its application to electron correlations in atoms has been pioneered by Kelly (1964). It is essentially an *unashamed* perturbative method and hence one cannot say anything about convergence, the computation simply being stopped when agreement is reached. It can be used on open shells as well as in the continuum. However there is no exclusive result since the end wavefunction depends on the starting wavefunction.

In a perturbation approach, the Hamiltonian of the system is split into two parts, a model unperturbed Hamiltonian $H_0$ and a perturbation $H'$. For atoms a natural choise for $H_0$ is a central-field such as the Hartree–Fock model, the eigenfunctions of which form a basis set for the description of the zeroth-order states of the many-electron system. These can then be used in a Rayleigh–Schrödinger perturbation expansion. This can however become difficult to employ beyond for instance third order, and a graphical representation is generally used to treat the theory. The matrix elements that appear in the equations can be represented by simple diagrams that are related to the Feynman diagrams introduced in field theory (Feynman 1949). This technique was first introduced by Goldstone (1957) in his treatment of the Brueckner perturbation theory, and so these diagrams are referred to as Goldstone diagrams.

The following principles are used to draw this kind of diagram:

- coulomb interactions are denoted by horizontal wavy lines
- electron states involved in the interaction are denoted by solid lines that connect with the interaction line at a vertex
- a line with an upward arrow denotes an occupied electron state
- a line with a downward arrow denotes an unoccupied electron state or hole
- the initial states point towards the interaction vertex, the final states away from the vertex
- a dashed line denotes the incoming photon
- the time axis is towards the right
- the number of wavy lines indicates the order, whereby the $n^{th}$ order diagram has n such wavy lines

Using this convention one can draw as simple examples the following diagrams representing various types of interactions:

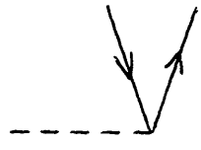

Single excitation

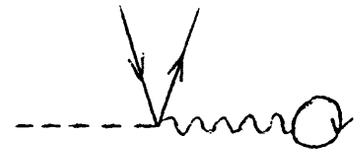

Direct interaction

Exchange interaction

Double excitation

Unfortunately the number of diagrams which must be included in higher orders is of the order of $(n-1)!$ and therefore rapidly becomes unmanagebly large. Thus the perturbation expansion can only be expanded to a certain order. Also as in all perturbation expansions the convergence of the procedure depends on the choise of the unperturbed Hamiltonian $H_0$, and there is no best choise for the basis set used since each choise essentially defines a different perturbation procedure with different terms.

Although all diagrams up to a certain order are included and that an estimate of the next order can be made, the fact that the starting wavefunctions remain frozen and are not affected by the interaction severely limits the theory. The modification of the self-consistent field which acts on the outgoing electron is thus the main effect that is accounted for in *MBPT*. However the corrections involved near to inner-shell ionisation are rather large and cannot be realistically taken into account by perturbation theory. Nevertheless the method has been applied with success to lighter open shell systems.

A comprehensive account of the theory is given by Kelly (1969, 1976) and by Lindgren and Morrison (1982).

## 1.7 Random-phase Approximation with Exchange

The name random-phase appromation was introduced originally by Bohm and Pines (1953) in discussing the properties of an electron plasma, and it essentially deals with the *average* response of a system to an applied perturbation. The application of this procedure to to atomic systems was developed by Amusia et al (1971, 1976, 1980) and Wendin (1973, 1976). A relativistic extension of the theory is also available (Band and Fomichev 1980). As applied to atomic systems it has nothing to do with with the plasma model since atomic basis wavefunctions are used and not plane-wave functions. In fact it was then named random-phase approximation *with exchange* in order to emphasise that it applies to atoms and that exchange, the intrinsic tendency of electrons to correlate their motions, is explicitely included.

*RPAE* essentially represents a certain level of approximation to the time-dependent Schrödinger equation, in that we displace the system to

a non-equilibrium position and allow the system to develop in time. The standard method is to start with time-dependent Hartree–Fock eigenfunctions and to deform them through for example, the creation of electron-hole pairs in the corresponding orbitals. Hence matrix elements describing these interactions are introduced and an infinite perturbation expansion in these matrix elements must be made in order to explicitely describe the correction to the Hartree–Fock energy. The same graphical representation described in the previous section is commonly used and leads to the *RPAE* diagrams consisting of strings of ***bubbles***. For example the expansion series representing various interactions are shown below.

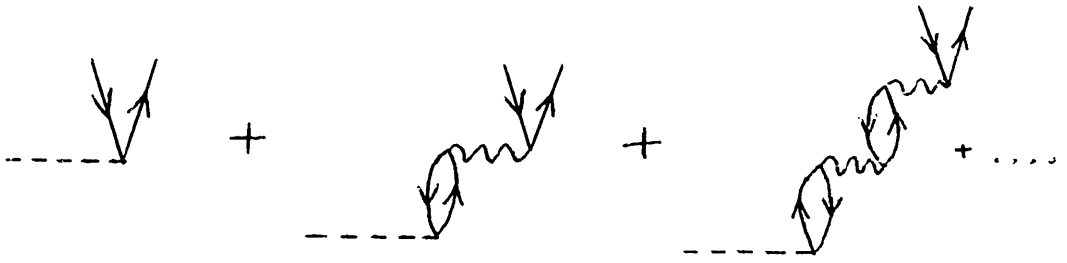

Ground state fluctuations —— correlations involving pair fluctuations in the unexcited sea of electrons

Electron–hole interaction

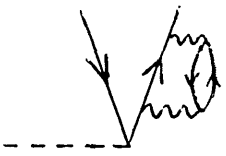

Self interaction

Relaxation of a frozen core

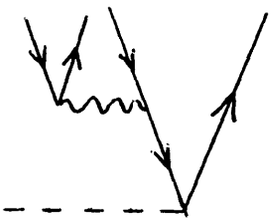

Shake–up due to positive charge of the hole

Such multiple excitations are not included in standard *RPAE*

In this method an algebraic sum to all orders of only certain diagrams is made, and unlike in many-body perturbation theory convergence is thus guaranteed within each calculation, though some truncation of terms may be necessary in practical calculations. The basic philosophy of the *RPAE* approach can therefore be thought of as concentrating on the operators which connect the initial and final states, rather than on the wavefunctions themselves. *RPAE* is however limited in that some diagrams are left out which if included could significantly alter the position and shape of the calculated ionisation cross-sections.

The importance of *RPAE* is related to the velocity of the excited electron. When an out-going electron leaves an inner shell slowly, the outer shells have time to rearrange. Thus diagrams corresponding to corrections in electron and hole self-energies as well as to electron-hole interactions have to be summed up the corresponding series to infinite order. It is however practically impossible to perform such calculations with high accuracy or if at all. The method does however try to simultaneously improve both the initial and final states in a consistent manner. Thus the random phase approximation can be used for closed shells, with open shell calculations not yet established and remaining unconvincing despite approximations that attempt to account for the above. Examples of its success are calculations of the partial photoionisation cross-sections of xenon, which are more difficult to calculate than total cross-sections, and calculations performed on closed shell atoms in general. A discussion of the theory as applied to photoabsorption is given by Johnson and Lin (1979).

## 1.8 The $g$-Hartree Method

In contrast to the previous theories, the $g$-Hartree method includes the interaction within the self-consistent field approach explicitly and so the treatment is exact within the model. It includes all second order diagrams but not higher (Dietz et al 1982).

The method essentially calculates the optimum central static mean field. This is thus time independent, and fluctuations are not included. However it is fundamental in that it is based on the quantum field-theory Lagrangian, and is thus a direct test of Quantum Field Theory (Dietz and Weymans 1984). It is fully relativistic and includes creation and annihilation of particles in its formulation. It has so far however not been applied to the continuum, but it promises to develop into a most successful theory. It does however hold a restriction, namely that the order in which annihilations and creations are considered is of importance. One would not expect this since in theory these terms should finally cancel out, but a standard ordering is necessary which differs from the direct order.

One can expand a little on the meaning of $g$, which is in fact a parameter that tunes the central field in order to get the best answer. A summation of the form

$$g\Omega_{direct} + (1-g)\Omega_{exchange} \qquad 0 \leq g \leq 1$$

is made and in principle $g$ should disappear if a summation to infinite order is carried out. Now we see that

| | | |
|---|---|---|
| $g = 1$ | corresponds to | Hartree equations : direct terms only |
| $g = 0$ | corresponds to | "Fock" : pure exchange only |

and with $g = 1/2$ one would expect that the Hartree–Fock equations would result but this is not the case. Since $g$-Hartree is more fundamentaly derived, this seems to indicate that the Hartree–Fock method is not quite correct. This is probably due to the fact that in the Hartree–Fock scheme just the Slater determinents are used whereas any linear combination of these would do, although this is conveniently forgotten.

Calculations can be made in two ways. One can choose a value of $g$ and apply Hartree–Fock, reiterating for various $g$. One can then trace $g$ against, for example, the total energy, which yields a curve with a turning point. Alternatively we can choose $g$ so that the calculated value of the total energy fits with the observed value. This value of $g$ can then be used

to calculate further quantities. This by definition gives the best possible central field and means that other quantities such as spin-orbit splitting will also agree with experiment, as long as we have not left anything out in our theory, and this is the be-all and end-all of the method. Such calculations have till now only been done for $Ba^+$ (Connerade et al 1984), and the motivation and interest in this will be discussed in later chapters.

## 1.9 Conclusion

As we have seen there exist theoretical techniques of varying complexity that can be used to calculate atomic photoionisation cross-sections. Single electron processes are generally represented well in terms of the effects of particle-hole electron correlations, but actual two-electron excitation processes are as yet not well established. When the excited electron becomes resonantly localised in the region of the core-hole, the latter collective effects become of great importance and involvement of these correlations is still under development. This is particularly necessary when dealing with transitions of the kind $n\ell \longrightarrow n(\ell+1)$ and especially when the $n(\ell+1)$ shell starts to fill. Thus interesting sequences of the periodic table are the lanthanide and actinide elements. We studied these and specifically looked at the energy region where $4d$ and $5d$ electrons are excited. This area is a proving ground for the various methods and critically test the prescriptions used in specifying the choise of electron correlations that are important. This is why we began by looking at the theoretical background and we hope that the present experiments will serve to extend the empirical database with which theoretical calculations can be compared.

The Periodic Table of Elements

Figure 1.1

| | | | | | | | | | | | | | | | | | |
|---|---|---|---|---|---|---|---|---|---|---|---|---|---|---|---|---|---|
| 1 H $1s^1$ | | | | | | | | | | | | | | | | | 2 He $1s^2$ |
| 3 Li $2s^1$ | 4 Be $2s^2$ | | | | | | | | | | | 5 B $2s^2 2p^1$ | 6 C $2s^2 2p^2$ | 7 N $2s^2 2p^3$ | 8 O $2s^2 2p^4$ | 9 F $2s^2 2p^5$ | 10 Ne $2s^2 2p^6$ |
| 11 Na $3s^1$ | 12 Mg $3s^2$ | | | | | | | | | | | 13 Al $3s^2 3p^1$ | 14 Si $3s^2 3p^2$ | 15 P $3s^2 3p^3$ | 16 S $3s^2 3p^4$ | 17 Cl $3s^2 3p^5$ | 18 Ar $3s^2 3p^6$ |
| 19 K $4s^1$ | 20 Ca $4s^2$ | 21 Sc $3d^1 4s^2$ | 22 Ti $3d^2 4s^2$ | 23 V $3d^3 4s^2$ | 24 Cr $3d^5 4s^1$ | 25 Mn $3d^5 4s^2$ | 26 Fe $3d^6 4s^2$ | 27 Co $3d^7 4s^2$ | 28 Ni $3d^8 4s^2$ | 29 Cu $3d^{10} 4s^1$ | 30 Zn $3d^{10} 4s^2$ | 31 Ga $4s^2 4p^1$ | 32 Ge $4s^2 4p^2$ | 33 As $4s^2 4p^3$ | 34 Se $4s^2 4p^4$ | 35 Br $4s^2 4p^5$ | 36 Kr $4s^2 4p^6$ |
| 37 Rb $5s^1$ | 38 Sr $5s^2$ | 39 Y $4d^1 5s^2$ | 40 Zr $4d^2 5s^2$ | 41 Nb $4d^4 5s^1$ | 42 Mo $4d^5 5s^1$ | 43 Tc $4d^5 5s^2$ | 44 Ru $4d^7 5s^2$ | 45 Rh $4d^8 5s^1$ | 46 Pd $4d^{10}$ | 47 Ag $4d^{10} 5s^1$ | 48 Cd $4d^{10} 5s^2$ | 49 In $5s^2 5p^1$ | 50 Sn $5s^2 5p^2$ | 51 Sb $5s^2 5p^3$ | 52 Te $5s^2 5p^4$ | 53 I $5s^2 5p^5$ | 54 Xe $5s^2 5p^6$ |
| 55 Cs $6s^1$ | 56 Ba $6s^2$ | 57 La $5d^1 6s^2$ | 72 Hf $5d^2 6s^2$ | 73 Ta $5d^3 6s^2$ | 74 W $5d^4 6s^2$ | 75 Re $5d^5 6s^2$ | 76 Os $5d^6 6s^2$ | 77 Ir $5d^7 6s^2$ | 78 Pt $5d^9 6s^1$ | 79 Au $5d^{10} 6s^1$ | 80 Hg $5d^{10} 6s^2$ | 81 Tl $6s^2 6p^1$ | 82 Pb $6s^2 6p^2$ | 83 Bi $6s^2 6p^3$ | 84 Po $6s^2 6p^4$ | 85 At $6s^2 6p^5$ | 86 Rn $6s^2 6p^6$ |
| 87 Fr $7s^1$ | 88 Ra $7s^2$ | 89 Ac $6d^1 7s^2$ | | | | | | | | | | | | | | | |

| | | | | | | | | | | | | | |
|---|---|---|---|---|---|---|---|---|---|---|---|---|---|
| 58 Ce $4f^1 5d^1 6s^2$ | 59 Pr $4f^3 6s^2$ | 60 Nd $4f^4 6s^2$ | 61 Pm $4f^5 6s^2$ | 62 Sm $4f^6 6s^2$ | 63 Eu $4f^7 6s^2$ | 64 Gd $4f^7 5d^1 6s^2$ | 65 Tb $4f^9 6s^2$ | 66 Dy $4f^{10} 6s^2$ | 67 Ho $4f^{11} 6s^2$ | 68 Er $4f^{12} 6s^2$ | 69 Tm $4f^{13} 6s^2$ | 70 Yb $4f^{14} 6s^2$ | 71 Lu $4f^{14} 5d^1 6s^2$ |
| 90 Th $6d^2 7s^2$ | 91 Pa $5f^2 6d^1 7s^2$ | 92 U $5f^3 6d^1 7s^2$ | 93 Np $5f^4 6d^1 7s^2$ | 94 Pu $5f^6 7s^2$ | 95 Am $5f^7 7s^2$ | 96 Cm $5f^7 6d^1 7s^2$ | 97 Bk $5f^9 7s^2$ | 98 Cf $5f^{10} 7s^2$ | 99 Es $5f^{11} 7s^2$ | 100 Fm $5f^{12} 7s^2$ | 101 Md $5f^{13} 7s^2$ | 102 No $5f^{14} 7s^2$ | 103 Lw $5f^{14} 6d^1 7s^2$ |

# Chapter II

# Rare Earths: A qualitative picture

## 2.1 Summary

A general picture of the formation of double valleys in the effective radial potential is given using qualitative arguments, and wavefunction *collapse* as well as *giant resonances* are introduced. The aim of our work is discussed and subsequent chapters will present experimental data observed when wavefunction collapse manifests itself.

## 2.2 Introduction

The spectroscopy of atoms and molecules has attracted much attention as an important method of yielding information on the electronic structure of the material in question. This information is also of considerable importance for a variety of problems relating to plasma physics, astrophysics and solid state physics.

Vacuum ultra-violet radiation can either excite valence electrons to high-energy continuum states, or deeply bound core electrons to bound states below and above the ionisation threshold. As already indicated in the previous chapter, spectra are strongly influenced by the interaction between different excitation channels. Hence although phenomena in the VUV region can in general be understood within the general framework of the independent particle model, it is inadequate in describing such features as

autoionisation or the *simultaneous* excitation of more than one electron.

At high photon energies ( $>1\,\mathrm{keV}$ , $\lambda < 10\,\text{Å}$ ) deep inner-shell electrons are excited and the attracting nuclear field is the dominating force experienced by the electrons. Thus many-body effects such as the repulsive electron-electron interactions can be incorporated into the nuclear field with the use of screening factors that do not alter its coulombic character. The observed absorption spectra can in general be successfully described using the independent particle model. Similarly at low energies a valence electron is excited and the resulting spectra are also generally well understood (Pratt et al 1973).

At intermediate energies inner valence electrons or electrons from the outermost inner shells are excited and the situation becomes more complex. Electron correlations are so significant that they can lead to a complete breakdown of the independent particle approximation.

Let us first take a brief look at why this occurs. The collapse of $\ell > 2$ wavefunctions is one of the principal causes of so-called non-Rydberg phenomena observed in atoms (Griffin et al 1969). The term non-Rydberg spectroscopy was first coined by Connerade (1978) and used to describe the study of atomic systems where the traditional concepts of Rydberg series breakdown. Then the monotonic variation in the characteristics of a series of neutral atoms during the filling of a shell, or within an isoelectronic series, are not observed.

The importance of the $\ell(\ell+1)/2m_e r^2$ term in the Schrödinger equation was first stressed by Fermi (1928) who showed that the radius of the $4f$ orbit decreases abruptly as the atomic number is increased from 55 to 60. Solutions of the Schrödinger equation using a statistical Thomas–Fermi potential indicated that the radial wavefunction reverts, from being in an outer orbit, into an inner localised orbit that penetrates the core. The problem was studied in more detail by Goeppert-Mayer (1941) on the basis of the same statistical potential. She looked at changes in the nature of the $4f$ and $5f$ eigenfunctions at the beginning of the lanthanide and actinide groups of the periodic table. She showed that the reason for the phenomenon lay in the particular shape of the effective potential in which the $f$ electrons move. This displays two wells that are separated by a potential barrier. An increase in nuclear charge causes a deepening of the inner well which eventually leads to a sharp decrease in the mean orbit of the electron. This is responsible for the existence of the rare earth elements.

Due to the limitations of the statistical potential used, Goeppert-Mayer was only able to apply this to $f$ electrons. Much more recently it has been shown that collapse also occurs in the same way for $d$ electrons (Griffin et al 1969). Thus the mechanism for *all* the long Periods in Mendeleev's table is substantially the same, and $d$- and $f$- contraction have the same physical origin.

The collapse leads to important changes, of up to orders of magnitudes, in various quantities which depend on the wave function of an excited electron *viz* the mean distance from nucleus, the binding energy, the spin-orbit interaction, as well as the oscillator strengths. Evidence of these changes can be directly observed as anomalous features in photoabsorption spectra.

Similarly when a free electron moves in the field of an atom that possesses an effective potential with a double well, then when the electron energy is near to the threshold energy, a sudden penetration of the free electrons radial wavefunction into the atom occurrs. The effect of this is that resonances appear in photoionisation spectra and in the scattering cross-section when electrons are scattered off atoms.

Such features have been observed in the absorption spectra of molecules and solids and the aim of this study is to present and exemplify this very point. The lack of a systematic classification of data on collapse in atoms and molecules will, it is hoped, be partially rectified.

## 2.3 Theoretical Incentives

These have to a large extent been dealt with in chapter one. However the theories discussed depend on detailed numerical computations, and although of importance do not give us a physical picture of what is happening. As an aid to their interpretation and understanding we therefore outline a simple model which more readily allows us to visualise the actual physics involved.

### 2.3.1 The Effective Radial Potential

We will consider the conditions for the formation of a double valley potential on the basis of a one-electron model within the central field approximation. Assuming the wavefunction of an atom to be the antisymmetrical product of

one electron wavefunctions (with coupled spins), this allows us to separate the angular, spin and radial components of the one-electron wavefunctions.

The Schrödinger equation for an electron in an arbitrary centrally symmetric field $V(r)$ has the form

$$\nabla^2\psi + \frac{2m_e}{\hbar^2}[E - V(r)]\psi = 0$$

Angular momentum is conserved during motion in a central field and the eigenfunctions can be seperated into the product of a radial and an angular function

$$\psi = R(r)\, Y_{\ell m_\ell}(\theta, \varphi)$$

The spherical harmonic functions $Y_{\ell m_\ell}(\theta, \varphi)$ are known as the associated Legendre polynomials, and the assignment of quantum numbers $\ell$ and $m_\ell$ characterise each stationary state.

The angular functions are easily solved and since they are independent of the potential $V(r)$, they remain identical for all atoms (Schiff 1968). Thus only the radial part depends on the properties of the particular atom. This is still one of the most difficult problems to solve as it is essentially a many-body problem which cannot be solved exactly. Hence the various theories depend on approximations of varying simplicity for the computation of numerical solutions.

The radial Schrödinger equation may be written as

$$\frac{1}{r}\frac{d}{dr}\left(r^2\frac{dR_{n\ell m}}{dr}\right) - \frac{\ell(\ell+1)}{r^2}R_{n\ell m} + \frac{2m_e}{\hbar^2}[E - V(r)]R_{n\ell m} = 0$$

and it is required that the radial function $R_{n\ell m}$ be finite everywhere and equal to zero at $r = 0$, hence the equation has finite and continuous solutions only for certain values of $E$.

The radial wavefunctions are determined by the effective potential in which each electron moves, which in atomic units can be defined as

$$V_{eff}(r) = V(r) + \frac{\ell(\ell+1)}{2r^2}$$

where $V(r)$ is the potential of the electrostatic field resulting from the nucleus and other electrons, whereas the second term corresponds to the classical centrifugal energy.

It is the attractive electrostatic field that presents the problems and which is the subject of approximation, however it can be represented by

$$V(r) = -\frac{Z(r)}{r}$$

where $Z(r)$ is the effective nuclear charge and depends on the distance of the electron from the nucleus.

In the hydrogen-like approximation $Z(r)$ can be treated as a constant

$$Z^{hyd} = Z - \sigma(n, \ell)$$

where $\sigma(n, \ell)$ is the screening constant and $Z$ the nuclear charge

However this only gives rise to a single well in $V_{eff}(r)$. The effective nuclear charge must depend on $r$ in order that competition with the centrifugal term results in a more elaborate double well potential.

As has already been mentioned this condition is met within a Thomas–Fermi potential. The nuclear charge can be approximated by (Fano and Cooper 1968)

$$Z^{TF}(r) = 0.42\frac{Z^{\frac{2}{3}}}{r}$$

The formation of a double valley potential then depends on the magnitude of the centrifugal term, and for $\ell > 2$ electrons a positive potential barrier appears in the Thomas–Fermi effective potential. This restriction to only $f$ electrons can be extended to $d$ electrons when the asymptotic form of this potential is corrected by a $-2/r$ term (Cowan 1967).

A better approximation is the Hartree–Fock potential. For a single electron in an $n\ell$ excited shell, the charge derived from the Hartree–Fock equations (Hartree 1957) for the average energy is given by

$$Z^{HF}_{n,\ell}(r) = Z - \sum_{\substack{n'\ell' \\ n'\ell' \neq n\ell}} N_{n'\ell'}\, Y_o(n'\ell', n'\ell') + Z^{exc}_{n,\ell}(r)$$

where $Y_o(n'\ell', n'\ell')$ is the screening effect of the $n'\ell'$ electron on the $n\ell$ electron, $N_{n'\ell'}$ is the number of electrons in the $n'\ell'$ shell, and

$$Y_o(n\ell, n\ell) = \int_0^r P^2(r)dr + r\int_r^\infty \frac{P^2(r)}{r}dr$$

where $P(r)$ is the radial one-electron wavefunction.

The term $Z^{exc}$ comes from the exchange part of the Hartree–Fock equations, and usually plays an insignificant part in deriving the effective potential. However for excited core configurations this is not always true and the Hartree–Fock equations must be solved for each term, and term dependent exchange parts must be incorporated, which can play an important role in the formatation of a potential barrier (Froese-Fischer 1977).

Such complicated forms for the electrostatic potential are necessary for the sophisticated numerical calculations. However for a qualitative understanding they are not necessary and as we will see, can even be replaced by a simple square well.

### 2.3.2 The Double Valley Potential

As already mentioned the interplay between the attractive coulomb potential and the repulsive centrifugal term can lead to the formation of a double valley potential as depicted in figure 2.1. Despite the complicated and intricate mathematics involved in calculating the electrostatic potential, the formation of a double valley potential can be intuitively presented as follows.

For small values of $r$, the effective charge approaches a constant value and $V_{eff}$ is dominated by the repulsive centrifugal term which prevents $\ell \neq 0$ electrons from entering the nuclear volume. As we move outwards, the coulomb attraction of the nucleus becomes comparable to the centrifugal term. A potential well is then formed because $Z(r)$ falls off with increasing $r$ as the nucleus is screened off by the inner electrons. At some point the centrifugal term may predominate again and a small positive potential barrier can be formed at $\sim$1–3 a.u.. The strength of the centrifugal term however drops rapidly with further increases in $r$. For large $r$ the effective potential is determined by the coulomb potential, then $Z(r) \approx 1$ and a hydrogen-like external potential well occurs which is wide but shallow because of the slow decay of the coulomb potential.

The actual size of the potential barrier formed is a determining factor for which of the two wells an electron will prefer. If the barrier was infinite, two independent energy level systems would exist which would distribute themselves between the two wells. However since the inner well is narrow, it can only contain a certain number of levels and this is highly dependent on the atomic number $Z$. Connerade (1982) has proposed using a Morse

potential (Morse 1929) as an analytic function to represent the inner well. The number of eigenstates the inner well can support then becomes dependent on a parameter $\xi$ that is related to the depth and width of the well. When the inner well is not deep enough to contain any levels, the principal maxima of the wavefunction are situated in the outer well, far from the core. As $Z$ increases, the well becomes deeper and broader, and can accommodate an energy level which moves down in energy as the well becomes deeper. As it acquires an energy level that lies below the first level in the outer well, a sudden displacement of the wavefunction to the inner well can takes place, and for $\ell \geq 3$ the transfer of the eigenfunctions occurs abruptly and we therefore refer to wavefunction *collapse*. One node of the collapsed radial wavefunction shifts into the inner well, the other wavefunctions become similar to the $n$–1 uncollapsed wavefunctions, and the quantum defect changes by one (Cheng and Froese-Fischer 1983). Linked to this is the scattering phase shift $\delta$ which must also change abruptly when the quantum defect changes. Levinsons theorem (Taylor 1972) specifies that $\delta$ be equal to $\pi$-times the number of bound states. Thus the appearance of a new discrete level in the inner well should cause a sudden increase of $\pi$ in the phase-shift (Connerade 1983).

### 2.3.3 Giant Resonances

The situation can be readily understood if we introduce an analogy to one-dimensional potential well theory of elementary quantum mechanics, as illustrated in figure 2.2. On the basis of this model, it has been shown how as the well deepens it suddenly becomes able to support a discrete eigenstate of its own (Connerade 1978). For elements which are almost, but not quite, capable of supporting a bound state in the inner well a small perturbation can precipitate wavefunction collapse. These $E > 0$ levels are not bound and are considered as *virtual* states. As figure 2.2 indicates, the levels would be bound states if the barrier was infinitely thick.

However when an electron of appropriate kinetic energy is excited it *knows* that there is a virtual level there, and a resonantly localised continuum state with large amplitude in the inner well can exist. This leads to the so-called *giant resonances* immediately above the corresponding $d$ or $f$ ionisation thresholds. The $\varepsilon f$ continuum wavefunction of the outer well emulates a $4f$ in the inner well, and we can therefore consider the double

valley problem as an amalgamation of short- and long-range potentials each with their associated wavefunctions. Such states have been labelled $\overline{4,\varepsilon}\, f$ states because of their hybrid nature (Mansfield and Connerade 1976).

As we will see in chapter four, the phenomena of delayed onset, giant resonance and potential barrier tunneling are directly linked to the form of the effective radial potential, and although each of these phenomena is distinct, they are nevertheless closely related. This whole subject is thoroughly presented in the review articles of Connerade (1978b) and more recently Karaziya (1982).

## 2.4 The Question of Molecular and Solid State Effects

The resonances in the $4d \longrightarrow f$ absorption spectra of the lanthanide elements were first observed by Zimkina et al (1967), who worked with thin metallic films. Although these were spectra of the elements in the solid phase, it was correctly deduced that the prominent absorption peak present in all spectra up to ytterbium were atomic in origin (see figure 2.3). This approach was proved correct when atomic vapour spectra were eventually obtained and shown to be identical (Mansfield and Connerade 1976, Wolff et al 1976). That this giant resonance feature persists in the corresponding spectra of solids and molecules is due to its being associated to the short-range inner potential well and hence is not greatly influenced by the external environment.

## 2.5 Aim of Experiments

Our aim was to continue this line of research and to try and extend our study to the $5d \longrightarrow f$ transitions in the actinide sequence of elements. The $5d$ absorption spectra of solid uranium and thorium had revealed a feature very similar to the giant resonance in the lanthanides (Cukier et al 1974, 1978). Since the $5f$ wavefunction extends further into the outer well than the $4f$ it was debatable to what extent the solid state environment influenced the spectra, and we wished to clarify this.

Parallel to this we wished to investigate lanthanide and actinide fluoride

vapours and so to monitor the influence of the fluorine *cage* on the spectra, and so hopefully find an example of where the inner well is critically binding.

## 2.6 Further Practical Incentives

As we have seen, double wells enable the existence of adaptable wavefunctions and the significance of this is reaching into other areas of research. Resonant photon-stimulated desorption of ions has become a standard tool in solid state spectroscopy as a local probe for the determination of surface valency (Koel et al 1982). It has also been suggested that the hybrid nature of $d$- and $f$- electrons is very closely connected to the problems of catalysis and superconductivity.

Smith and Kmetko (1983) have constructed a quasi-periodic table in which the five long periods are arranged in order of decreasing localisation. This effectively equates the $d$ and $f$ metals since the boundary between super-conductivity and magnetism follows the locus of the atomic giant resonances (see chapter five).

Further the capability of lanthanides as hydrogen storage materials are currently research areas of great interest. The capacity of for example lanthanum to act as a storage material for hydrogen is closely related to wavefunction collapse. In fact a car has been run on such a system in Japan.

Thus we see that studying *pure* atomic profiles of $d \longrightarrow f$ transitions is of direct interest to other branches of physics, and the direct practical applications added further incentive for the present work.

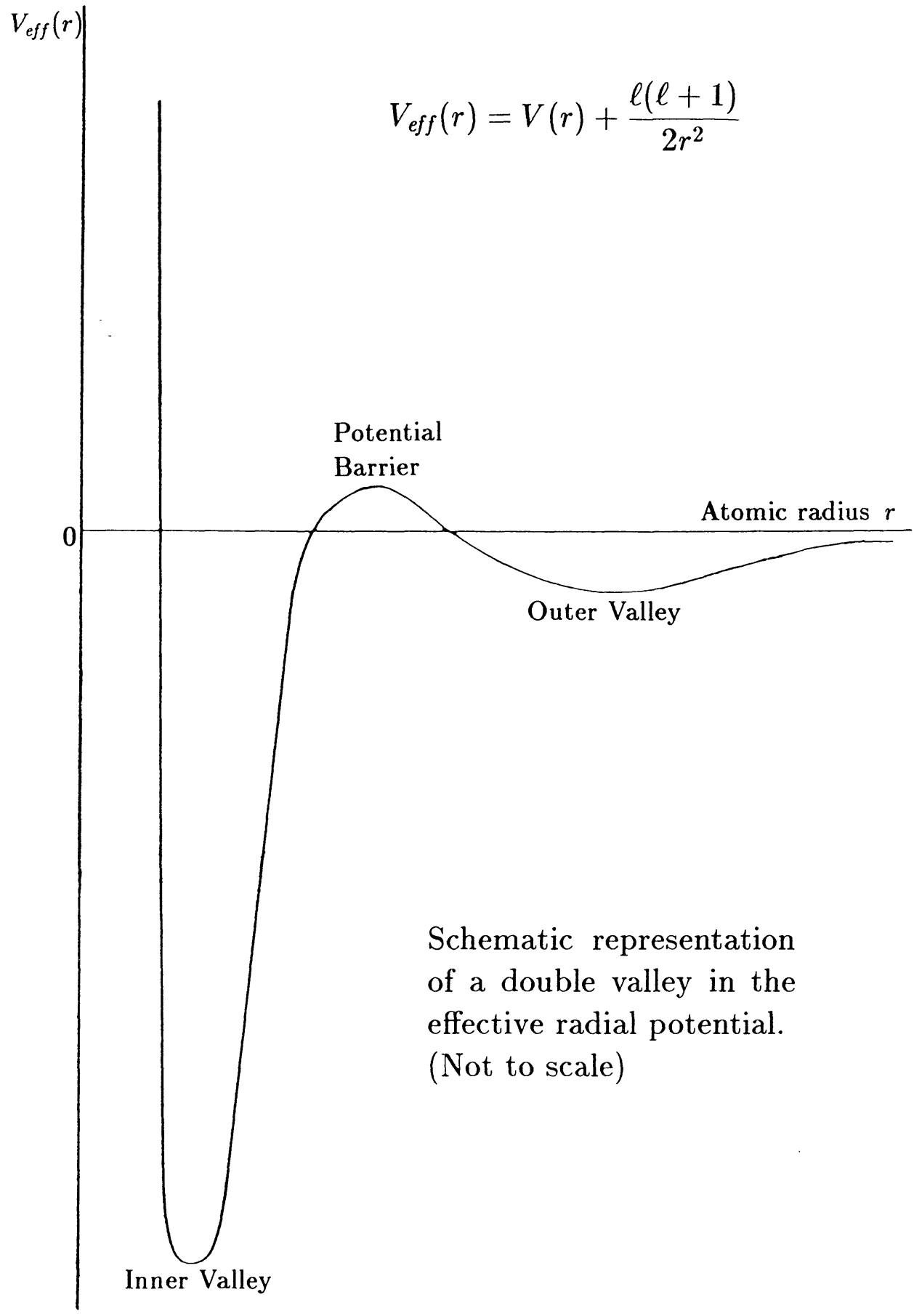


Schematic representation of a double valley in the effective radial potential. (Not to scale)

Figure 2.1

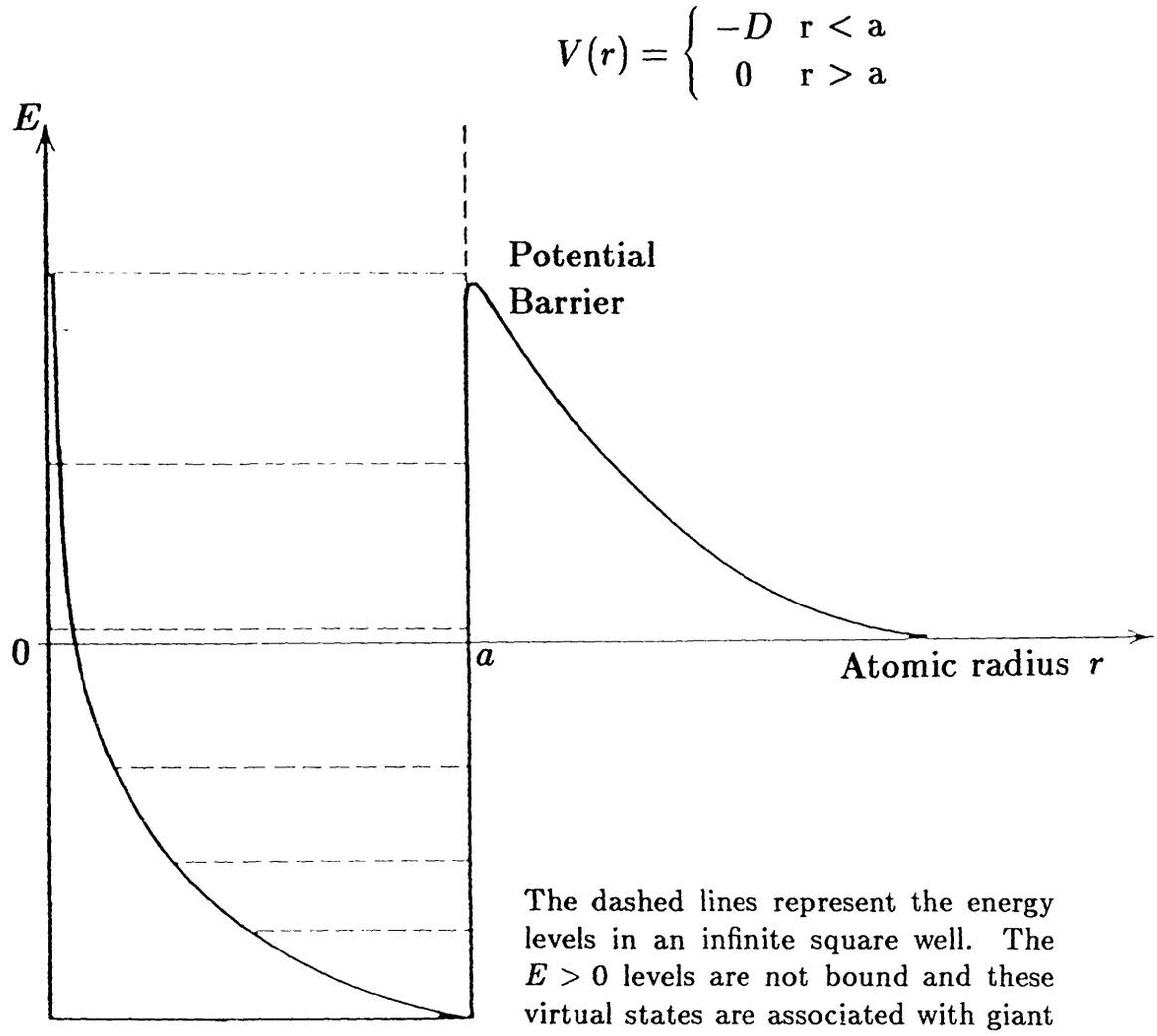


Showing the effective radial potential with a square well of range $a$.

Figure 2.2

Although the data are for metallic samples, it was correctly deduced that the peaks are atomic in origin. The almost identical spectra of the corresponding vapours confirmed this view.

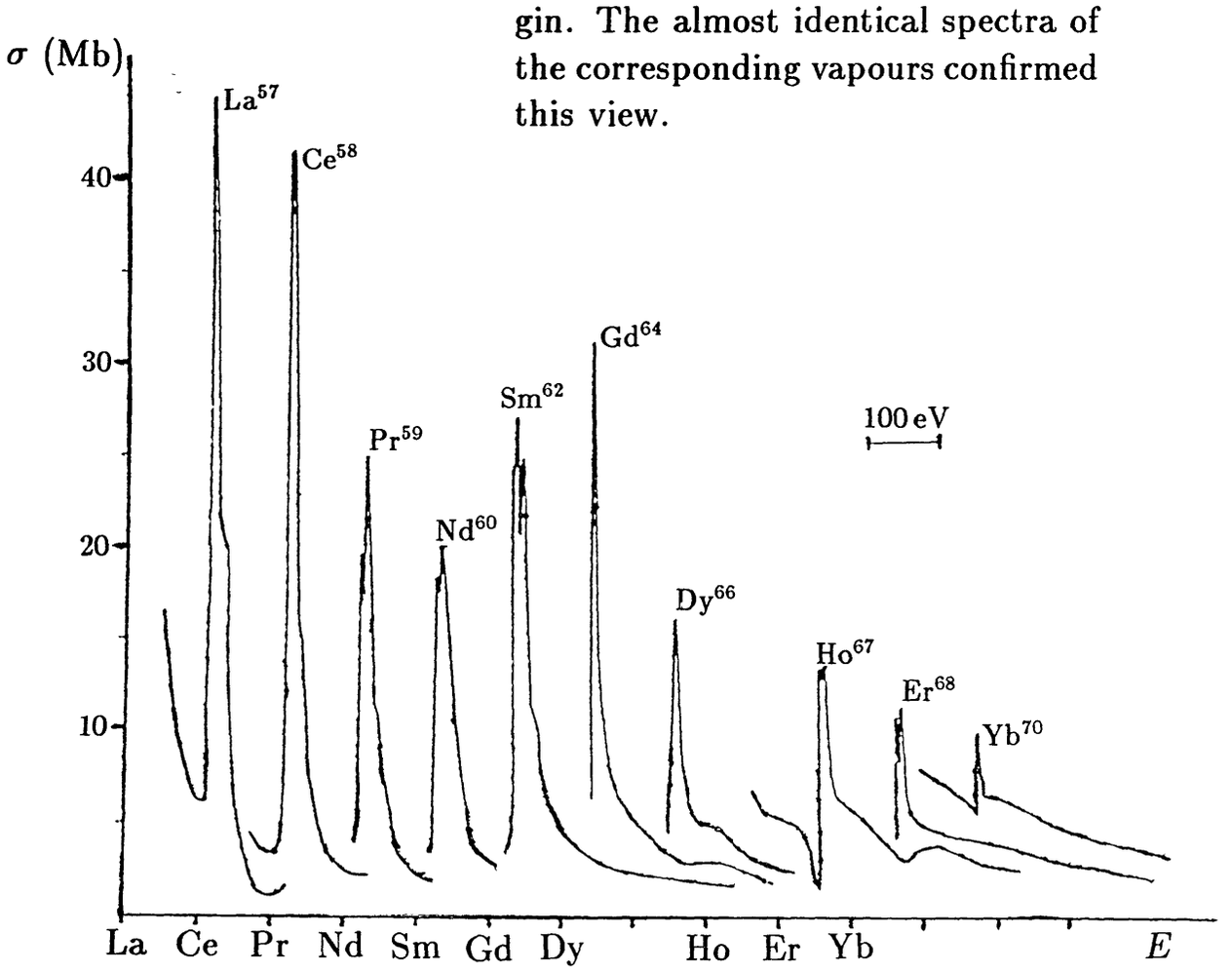


Absorption spectra of the rare-earth elements.
(after Zimkina and Gribovskiĭ 1971)

Figure 2.3

# Chapter III

# Experimental Details

## 3.1 Summary

The present work was performed using the facilities available at the 500 MeV electron synchrotron in the Physikalisches Institut of Bonn University, West Germany. The instruments employed and the experimental techniques necessary for photoaborption studies are discussed in this chapter.

## 3.2 Introduction

Investigations of absorption spectra in the vacuum ultraviolet require a source that provides a continuous spectrum over the relevant spectral region. The first such practical source was the continuous spectrum emitted by the hydrogen molecule, a high current discharge being used to produce a continuum that extends from the visible down to 1600 Å. With the construction of a so-called disruptive discharge flash tube by Lyman (1924), an uninterrupted continuum down to 900 Å was available. This used a microfarad capacitor and an external gap for high breakdown voltages to give an impulsive discharge through a helium filled capillary. The main discharge takes place in eroded wall material and hence any low pressure gas can be used, though helium has the advantage of transparency down to lower wavelength. Although various improved designs were developed (Rathenau 1934, Collins and Price 1934), the short lifetime of the capillary remained the major disadvantage of the Lyman source.

This difficulty was overcome by Garton (1959) who designed a large-bore

coaxial flash tube giving a very intense continuum down to 300 Å which is essentially free of overlying absorption or emission lines. The high current densities required are achieved by minimising the inductance of the discharge tube and circuit. Below 300 Å a line spectrum is obtained which can be utilised as a calibration source in the grazing incidence region (Radtke 1980).

A source of emission continuum valuable for work in the range 100–600 Å, originally described by Ballafet et al (1961) and subsequently improved by Garton et al (1969), is known as the BRV flash source. The radiation is emitted by a high density–high temperature plasma in the vicinity of a small diameter anode. The anode material must be of high atomic number and uranium which also has good refractory properties is most often used.

Continua emitted by rare gases have also been widely used in absorption spectroscopy and can be excited by either a condensed or microwave discharge. The Hopfield emission continuum (Hopfield 1930) extends from 600–1000 Å and is due to a transition from a stable upper state to the unstable ground state of the helium molecule. Similar discharges in the rare gases neon through to xenon yeild continua that jointly allow the range 600–2000 Å to be covered, although rather high pressures of pure gases are required.

A comprehensive review of the traditional light sources mentioned above is offered by Garton (1966) as well as in the work of Samson (1967).

The disadvantages however of these continua sources include limited spectral range, poor reproducibility, as well as the prescence of overlying absorption and emission lines. A source of a completely different kind eliminating these problems is found in the radiation obtainable from electron synchrotrons and storage rings.

This is an almost perfect background continuum source for photoabsorption experiments and has become increasingly used for such work. The accelerating electrons in the synchrotron emit radiation with a clean continuous spectrum resembling that of a high-temperature black-body. The radiation encompasses the x-ray to infra-red spectral regions, and is polarised, highly directional and time-modulated.

## 3.3 Synchrotron Radiation

The major source of energy loss in a synchrotron is the radiation emitted as the radiation emitted as the electrons undergo centripetal acceleration. Although a quantum mechanical treatment is necessary for atomic orbitals, classical theory is sufficient to describe electrons confined to a circular orbit in a synchrotron. A very thorough treatment is given by Schwinger (1949). Comprehensive reviews on the applications of synchrotrons are given by Godwin (1969), Codling (1973), Kunz (1979) and by Winick and Doniach (1980).

Electrons have a small rest mass of about 0.5 MeV and for kinetic energies above 100 MeV the electrons travel at velocities close to the speed of light. At such high energies, the toroidal radiation pattern is distorted because of relativistic effects. Thus almost all the power is concentrated into a very small cone in the direction of motion (see figure 3.1). The mean half-angle of divergence which is energy dependent and typically of the order of milliradians is given by

$$\vartheta_{\text{mean}} \simeq \frac{1}{\gamma} = \frac{E_o}{E} = \frac{0.511}{E(\text{MeV})}$$

with

$$\gamma = (1-\beta^2)^{-1/2} = \frac{E}{m_o c^2} \quad ; \quad \beta = \frac{v}{c}$$

where $m_o$ is the electron rest mass and $E$ the actual electron energy. However the actual divergence is wavelength dependent, being less at shorter wavelength.

The instantaneous power radiated by a single relativistic electron is

$$I \simeq \frac{2e^2 c}{3R^2}\left(\frac{E}{m_o c^2}\right)^4$$

where $R$ is the orbital radius of the electron in metres, and the energy radiated per revolution is given by

$$\Delta E\ (\text{keV}\, rev^{-1}) = \frac{2\pi IR}{c} \simeq \frac{88.5\,[E(\text{GeV})]^4}{R(\text{m})}$$

Thus it can be seen that the radiation losses increase as the fourth power of the electron energy. This is therefore the limiting factor in high energy

electron synchrotrons, but is not such a great problem for protons because of the large difference in rest mass.

This radiated energy can only be observed in a tangential direction to the orbit when we observe the radiating electrons travelling towards us. The ensuing Doppler effect causes the radiation to lie predominately in the x-ray and vacuum ultraviolet regions. The variation of the total instantaneous power with wavelength was given by Tomboulin and Hartman (1956)

$$I(\lambda) = \left(\frac{3^{5/2}}{16\pi^2}\right)\left(\frac{e^2 c}{R^3}\right)\left(\frac{E}{m_o c^2}\right)^7 G(y)$$

with

$$G(y) = y^3 \int_y^\infty K_{5/3}(\eta) d\eta$$

and

$$y = \frac{4\pi R}{3\lambda}\left(\frac{m_o c^2}{E}\right)^3 = \frac{\lambda_c}{\lambda}$$

where $K_{5/3}$ is a modified Bessel function of the second kind. The quantity $\lambda_c$ is the critical wavelength and can be simplified to

$$\lambda_c\ (\text{Å}) = \frac{5.59\, R(\text{m})}{[E\,(\text{GeV})]^3}$$

The critical wavelength is related to the wavelength at the maximum intensity by

$$\lambda_{\max} = 0.42\, \lambda_c$$

Thus the intensity maximum shifts to shorter wavelength as the energy increases, and for a constant $R$ an increase in energy causes an increase in the power radiated at shorter wavelength.This can be seen in figure 3.2 which shows the intensity distribution curves at various energies for the Bonn 500 MeV synchrotron.

Lastly the radiation is linearly polarised in the plane of the electron orbit, although the radiation seen by the experimental equipment in practice is usually elliptically polarised. This is due to a small component polarised perpendicular to the orbital plane which arises from radiation coming from above and below the orbit plane due to the finite electron beam size. Nevertheless the overall degree of polarisation when the components are integrated over all angles and wavelengths is about 75%, independent of both the radius and the electron energy.

## 3.4 Bonn Synchrotron Facility

When this work was done, there were two electron synchrotrons available, with maximum energies of 500 MeV and 2.5 GeV. The former has in the meantime been removed in order to make way for *ELSA*, a 3.5 GeV electron stretcher and accelerator (Husmann 1983). Althoff et al (1968) provide a comprehensive description of the 2.5 Gev maschine which remains available and will also be used as the electron source for *ELSA*.

The present work was carried out on equipment installed on the 500 MeV machine, a plan of which is shown in figure 3.3. Completed in 1958 it was the first European synchrotron to use a strong focussing system. Electrons produced by a Van der Graff accelerator were injected into the synchrotron at an energy of 3 MeV. A total of nine magnets with a mean field gradient of 1000 G $cm^{-1}$ held the electrons in an orbit of 1.7 metres radius, and the repetition cycle was 50 Hertz.

There were three main beam lines, one of which was further sub-divided into 3 lines with the aid of gold-coated cylindrical mirrors. The present work was done using the 2 m grazing incidence spectrograph situated on the direct beam. For all experiments the synchrotron was run at an energy of 450 MeV, this being the most appropriate for our investigations in the 40–200 Å wavelength range.

The absorption cell containing the sample, together with the line source used for calibrating the spectra, were situated in the space of 9 metres available between the synchrotron and the spectrograph. The absorption cell was windowless and so the synchrotron light was first deflected on reaching the spectrograph grating. The light could be observed directly, using a flat mirror, and was of an intense bluish-white hue. The small cross-piece containing the mirror and the viewing window was mounted just before the spectrograph so that a constant visual check of the light *spot* on the entrance slit was possible and this was important for alignment purposes.

Very experienced operators looked after the maschine during the day. However most of work was carried out during the night since the synchrotron was then much more stable and so functioned better for our purposes. This meant that not only did we have to run the experiment but also at the same time to operate the synchrotron and deal with all the problems that inevitably occured.

## 3.5 The Absorption Cell

The sample being investigated was vapourised inside a windowless absorption cell, which essentially consisted of a high-temperature furnace and a vapour containment system.

The furnace which was inductively heated was an improved version on the design of Tomkins and Ercoli (1967). The furnace has been described by Radtke (1975) and includes a theoretical treatment of the problem of inductively heated hollow cylinders. A schematic diagram of the furnace is shown in figure 3.4. In short the induction furnace consisted of a 60 cm long alumina tube that acted as a vacuum chamber and which held a water-cooled copper cylinder. The cylinder was slotted along its whole length and was henced unaffected by the high-frequency magnetic field. It conducted away the radiated heat and so ensured that the temperature of the vacuum chamber only rose to about 100 °C, even when the inner furnace tube was at a temperature of 2600 °C. Nevertheless in order to limit the amount of radiated heat escaping, a radiation shield (a slotted tantalum tube) was situated immediately inside the copper cylinder and so reflected heat back into the furnace. It was inside this shield that the actual furnace tube was placed. The 42 cm long furnace tube was supported by thin beryllia rings and was thus both electrically and thermally isolated from the radiation shield. The shield was similarly isolated from the copper cylinder. The maximum working temperature of beryllia is 2773 °C and this was hence the limiting temperature attainable with the furnace.

The whole assembly was placed within a coiled copper tube which was connected to the power supply, an RF generator working at 450 kHz and capable of upto 10 kW output. The eddy currents induced in the furnace tube heated it directly. The furnace was very efficient and the rise from ambient temperature to the working temperature of two thousand degrees took as little as 20 seconds. Similarly the temperature would drop as abruptly as soon as the power generator was switched off. This enabled the sample to be conserved between exposures for the time required to change the photographic plate and evacuate the spectrograph.

The tantalum furnace tubes used had a wall thickness of 1 mm and an outer diameter of 15 mm. To minimise the mass-loss rate of the furnace three baffles at 15 mm intervals were placed at each end and these supported a tightly fitting impedence tube down the centre of our furnace. The impe-

dence tube had a diameter of 4 mm and ten 1 mm vapour inlets at its centre that lay above the boat holding the sample. Tracy (1975) showed that such a configuration has a loss rate of about $0.5\,g\,hr^{-1}$. Material diffusing out of the furnace condensed on the wall of the vacuum system and so neither the synchrotron or the spectrograph entrance slit were contaminated.

The induction furnace could only be used at temperatures above 1000 °C and for the samples for which lower temperatures were necessary a resistance heated furnace was used instead. In this case a stainless steel furnace tube containing an impedence tube was externally heated using a clam-shell arrangement as described by Connerade and Mansfield (1973). It was however a very inefficient system as compared to the induction furnace because it suffered from an extremely large thermal lag. Thus stable temperatures could only be achieved by heating the furnace gradually over a period of one hour, with an accompanying loss of material.

## 3.6 The Calibration Line Source

As mentioned earlier, a Garton flash tube as modified by Wheaton (1964) can be used as a line source in the 40–200 Å range. In this region a dense reference emission spectrum with about one line per angstrom is obtained when the flash tube is run at $\sim 10\,kV$ with a vacuum of $10^{-5}$ Torr. The predominant lines emitted are Al IV–VII, C V, F V–VII, O V and O VI. Their wavelengths are listed by Kelly and Palumbo (1973) and Edlén (1975).

The flash tube was permanently situated in the beam-line at a distance of 45 cm from the spectrograph entrance slit. After a plate had been exposed using synchrotron light, a calibration spectrum could be superimposed if so wished. Usually about 15 flashes were necessary to give strong emission lines without obliterating the underlying absorption spectrum. For each sample investigated several plates were so calibrated.

About 80 emission lines were sufficient to determine the non-linear wavelength scale using a least-squares Chebychev polynomial fit program and gave a standard deviation of 0.006 Å. This was far more accurate than using rare gas absorption edges as reference lines (Ar 50 Å, Kr 133 Å) and interpolating over a large wavelength range. A densitometer trace of a typical calibration spectrum is shown in figure 3.5, and the emission lines are identified in table 3a.

## 3.7 The Spectrograph

The spectra were recorded on Ilford Q2 photographic plates using a 2 m grazing incidence spectrograph, manufactured by Hilgar and Watts to a design by Gabriel et al (1965). Light enters through an $8 \pm 2\mu m$ wide fixed-jaw slit and strikes the grating at an 88° angle of incidence. The platinised replica grating has a radius of curvature of 2 m and is mounted on a *Rowland circle*. The grating used was ruled with 1200 lines/mm and was blazed at an angle of 1 ° 47′ (Bauch and Lomb: catalogue number 35-52-40-700). This grating was found to be remarkably free of higher orders (Connerade and Mansfield 1973). The resolution of the spectrograph at short wavelengths is limited by the slit width and not by the grating. Hence the resolution is a constant and can be determined empirically by taking advantage of the dense emission lines of the calibration source. The grating can resolve lines with a $\delta\lambda \simeq 0.043$ Å.

Only one exposure could be made on each plate and hence the spectrograph had to be repeatedly let up to air and reloaded after each exposure. Evacuation to a pressure of $5 \times 10^{-5}$ took about 20 minutes and between 10–15 exposures at different temperature were taken for each sample.

## 3.8 Experimental Procedure

The absorption spectra were measured using the arrangement described above. Typically a small tantalum boat containing about one gram of 99.99% pure sample was loaded into the induction furnace. The vacuum system was then sealed and pumped down to a pressure of $1 \times 10^{-5}$ Torr. The clam-shell furnace system was used only for caesium and $UF_4$ and in these cases considerably more material was required.

Each sample was de-gassed over a period of one hour by raising the temperature to a few hundred degrees Celsius. With the furnace then cold (no absorption), a background plate was made of the synchrotron light. Exposures were then made for vapour pressures varying between 0.05 and 2 Torr. The exposure time varied between 3 to 10 minutes, depending on the synchrotron light intensity. Several of the spectra were additionally calibrated.

Densitometer traces of the plates were then obtained with a Joyce

Loebel microphotometer. The position of the absorption and emission lines were measured from the plates with a Zeiss Abbé microcomparator. The traces were digitised and plotted on a linear scale using a Hewlett Packard 7221 plotter and the VAX 11/780 computer facility at the Physikalisches Institut. As a further check of our calibration the position of the absorption and emission lines were also measured from the traces using the digitising capability of the plotter. No objective criteria for error limits are feasible without digital data, and since the photographic plate is an analog device the errors must be based on the experimentalists judgement. We estimate the systematic errors to be not larger than 0.02 Å and is indicated in all wavelength lists. We must also emphasise that on all figures that show our spectra absorption is arbitrarily normalised. Thus comparisons of the cross-section magnitudes between different elements are not meaningful.

## 3.9 The Elements and Compounds Studied

The metals and fluoride compounds which we studied in the vapour phase are listed in table 3b. Some physical properties of the lanthanide and actinide fluorides are collected in table 3c (colour, melting points and crystal structure). Table 3d then contains vapour pressure data for the fluorides and figure 3.6 data for the metals. The data especially for the fluorides is very sparse and often contradictory, and the data is at best accurate to only 10%. The data was nevertheless of value to us since it gave us an idea of what temperatures we would need in order to obtain our spectra.

## 3.10 Specific Details

The aggressive nature of the gadolinium and uranium liquids meant that they could not simply be contained in tantalum boats as for the other elements. This metallurgical problem was overcome for gadolinium by using a tungsten boat. Uranium on the other hand also attacked the tungsten, and we eventually found that a tantalum carbide boat was resistent to attack. As an added precaution the loaded boats were placed within a tungsten tube. This tube, which was split along its length, fitted snugly inside our tantalum furnace tube. The 1 mm gap was sealed with a strip of carbon foil. Figure 3.7 shows a schematic picture of the furnace set-up.

| Line | Å | | Line | Å | | Line | Å | |
|---|---|---|---|---|---|---|---|---|
| 1 | 158.926 | O V | 47 | 122.122 | F VI | 93 | 92.636 | Al VI |
| 2 | 158.601 | F IV | 48 | 120.116 | F VI | 94 | 91.332 | Al VI |
| 3 | 157.515 | F V | 49 | 118.984 | Al V | 95 | 90.858 | Al VI |
| 4 | 156.247 | F VI | 50 | 118.500 | Al V | 96 | 90.701 | Al V |
| 5 | 155.673 | F IV | 51 | 117.400 | O VI | 97 | 90.200 | Al VI |
| 6 | 154.506 | F VI | 52 | 116.419 | O VI | 98 | 88.636 | Al V |
| 7 | 153.952 | O V | 53 | 115.824 | O VI | 99 | 88.273 | Al VI |
| 8 | 152.511 | F V | 54 | 114.737 | Al IV | 100 | 88.033 | Al VII |
| 9 | 151.547 | O V | 55 | 114.313 | Al IV | 101 | 87.655 | Al VI |
| 10 | 150.124 | O VI | 56 | 113.756 | Al VI | 102 | 87.334 | Al VI |
| 11 | 149.078 | O V | 57 | 113.437 | Al VI | 103 | 87.060 | Al VII |
| 12 | 148.653 | F VI | 58 | 112.955 | F VII | 104 | 86.887 | Al VII |
| 13 | 148.002 | F V | 59 | 111.781 | Al IV | 105 | 86.097 | Al VI |
| 14 | 147.261 | O V | 60 | 111.589 | Al IV | 106 | 85.817 | Al VI |
| 15 | 146.676 | F VI | 61 | 111.196 | Al IV | 107 | 85.622 | Al V |
| 16 | 145.691 | F VI | 62 | 110.220 | O VI | 108 | 84.098 | Al VII |
| 17 | 144.837 | O V | 63 | 109.843 | Al VI | 109 | 83.831 | Al VII |
| 18 | 143.897 | F V | 64 | 109.514 | Al VI | 110 | 83.635 | Al VIII |
| 19 | 142.120 | O V | 65 | 108.975 | F VI | 111 | 83.335 | Al |
| 20 | 141.154 | F VI | 66 | 108.616 | Al V | 112 | 83.102 | Al |
| 21 | 139.900 | F VI | 67 | 108.385 | Al V | 113 | 82.543 | Al VIII |
| 22 | 139.029 | O V | 68 | 108.004 | Al V | 114 | 81.806 | Al VII |
| 23 | 138.109 | O V | 69 | 107.620 | Al VI | 115 | 81.234 | Al VII |
| 24 | 136.955 | F V | 70 | 106.790 | O VI | 116 | 80.770 | Al VI |
| 25 | 136.249 | Al V | 71 | 106.471 | Al | 117 | 79.952 | Al VII |
| 26 | 135.523 | O V | 72 | 104.811 | O VI | 118 | 79.557 | Al |
| 27 | 134.882 | F VII | 73 | 104.344 | Al VI | 119 | 79.197 | Al VII |
| 28 | 134.539 | F V | 74 | 104.047 | Al VI | 120 | 79.012 | Al VII |
| 29 | 133.521 | O V | 75 | 103.260 | O VI | 121 | 78.327 | Al VII |
| 30 | 132.819 | F V | 76 | 102.300 | O VI | 122 | 77.896 | Al VII |
| 31 | 132.312 | O VI | 77 | 101.570 | O VI | 123 | 76.953 | Al VI |
| 32 | 131.750 | O V | 78 | 101.027 | Al VI | 124 | 76.572 | Al VII |
| 33 | 131.441 | Al V | 79 | 100.616 | Al VI | 125 | 76.383 | Al VII |
| 34 | 131.003 | Al V | 80 | 99.680 | O V | 126 | 75.850 | Al VII |
| 35 | 130.413 | Al V | 81 | 99.290 | Al V | 127 | 75.302 | Al VII |
| 36 | 129.872 | O VI | 82 | 96.442 | Al VI | 128 | 74.892 | Al VI |
| 37 | 128.297 | O V | 83 | 95.965 | Al VII | 129 | 74.592 | Al VI |
| 38 | 127.796 | F VII | 84 | 95.775 | F VII | 130 | 74.444 | Al VI |
| 39 | 126.923 | F VI | 85 | 95.436 | Al VI | 131 | 74.321 | Al |
| 40 | 126.065 | Al V | 86 | 95.020 | O VI | 132 | 72.674 | Al |
| 41 | 125.525 | Al V | 87 | 94.394 | Al V | 133 | 72.270 | Al VII |
| 42 | 124.543 | Al IV | 88 | 94.117 | Al V | 134 | 71.987 | Al |
| 43 | 124.440 | F VI | 89 | 93.955 | Al V | 135 | 71.590 | Al |
| 44 | 124.038 | Al IV | 90 | 93.542 | Al VII | 136 | 71.139 | Al |
| 45 | 123.744 | F V | 91 | 93.295 | Al VII | | | |
| 46 | 123.175 | F VI | 92 | 92.875 | Al VI | | | |

Table 3a: Wavelength list for the calibration spectrum in figure 3.5

| *Samples studied* | *Atomic number Z of the metal atom* | *Ground state configuration of the metal atom* |
|---|---|---|
| Cs | 55 | $4d^{10}5s^25p^66s$ |
| $BaF_2$ | 56 | $6s^2$ |
| $LaF_3$ | 57 | $5d6s^2$ |
| Ce<br>$CeF_3$ | 58 | $4f5d6s^2$ |
| Pr<br>$PrF_3$ | 59 | $4f^36s^2$ |
| Gd<br>$GdF_3$ | 64 | $4f^75d6s^2$ |
| $ThF_4$ | 90 | $5d^{10}6s^26p^65f^06d^27s^2$ |
| U<br>$UF_4$ | 92 | $5f^36d7s^2$ |

Table 3b: The elements and fluorides studied

| | *Crystal Structure* | *Colour* | *Melting Point* °C |
|---|---|---|---|
| $BaF_2$ | cubic | white | 1280 |
| $LaF_3$ | hexagonal | white | $1495 \pm 3$ [a] |
| $CeF_3$ | hexagonal | white | $1429 \pm 3$ [a] |
| $PrF_3$ | hexagonal | green | $1399 \pm 3$ [b] |
| $GdF_3$ | rhombic | white | $1230 \pm 3$ [c] |
| $ThF_4$ | monoclinic | white | 1110 |
| $UF_4$ | monoclinic | green | 1036 |

*a* Dworkin and Bredig 1971
*b* Spedding and Henderson 1971
*c* Spedding et al 1974

Table 3c: Physical properties of the lanthanide and actinide fluorides

| | *p in Torr, T in Kelvin* | °C *for 1 Torr* | °C *for the metal* |
|---|---|---|---|
| $BaF_2$ [a] | $\lg p = -\frac{20330}{T} - 5.03 \lg T + 12.489$ | 1436 | 937 |
| $LaF_3$ [b] | $\lg p = -\frac{21730}{T} + 12.489$ | 1467 | 2127 |
| $CeF_3$ [c] | $\lg p = -\frac{20460}{T} + 12.086$ | 1420 | 2217 |
| $PrF_3$ [d] | $\lg p = -\frac{21090}{T} + 12.252$ | 1448 | 1947 |
| $GdF_3$ [e] | $\lg p = -\frac{22056}{T} + 12.400$ | 1505 | 2027 |
| $ThF_4$ [f] | $\lg p = -\frac{15270}{T} + 10.821$ | 1138 | 3027 |
| $UF_4$ [g] | $\lg p = -\frac{16840}{T} - 7.549 \lg T + 37.086$ | 949 | 2627 |

A factor of $\lg 760 = 2.88$ has been added to the constant term in order to convert to Torr.

*a* Kubaschewski et al 1967
*b* Mar and Searcy 1967
*c* Lim and Searcy 1966
*d* Skinner and Searcy 1968
*e* McCreary and Thorn 1973
*f* Darnell and Keneshea 1958
*g* Brown 1968

Table 3d: Vapour pressure data for the fluorides

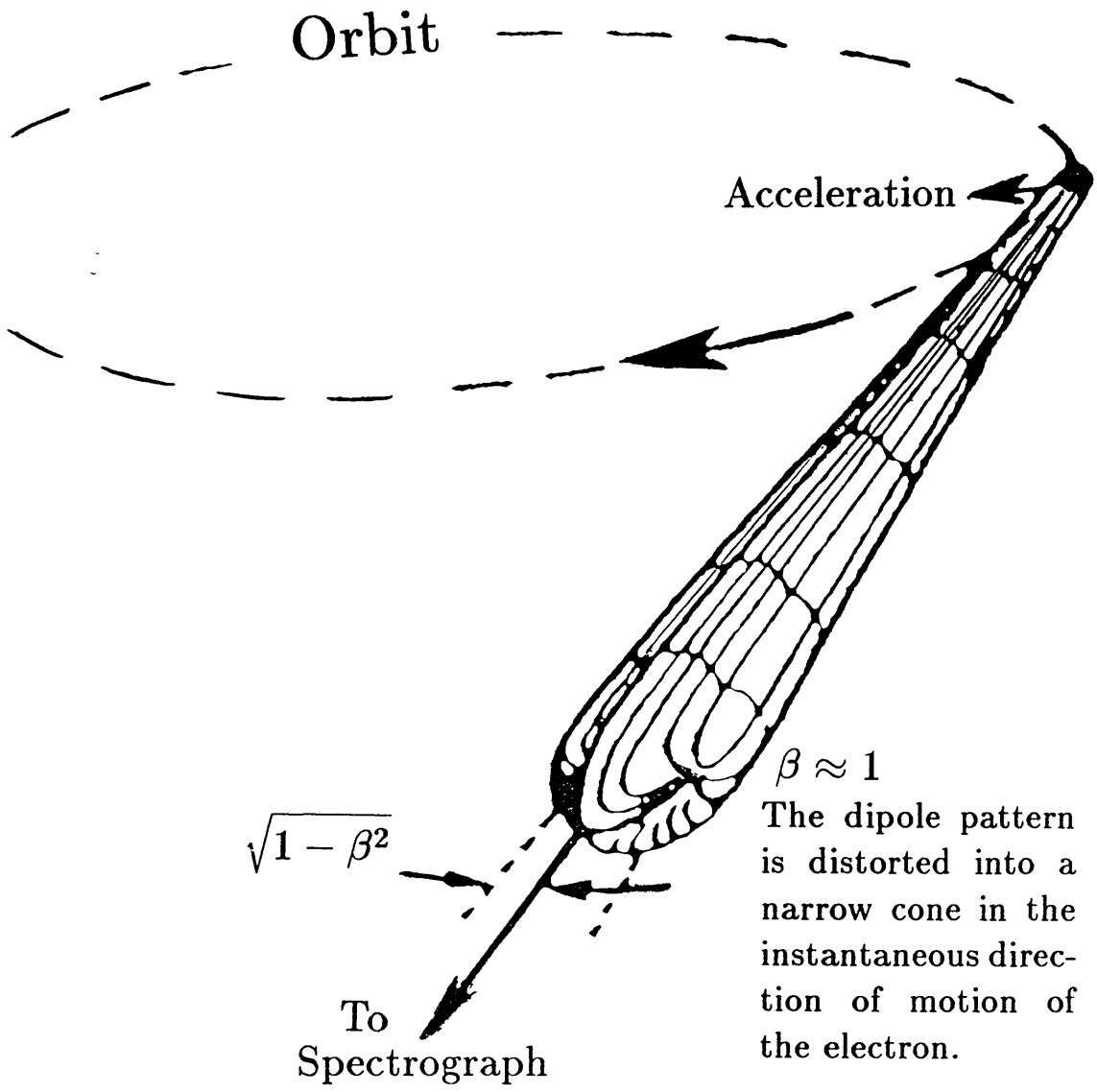


Emitted radiation pattern from a relativistic electron in a circular orbit.
(after Tomboulin and Hartman 1956)

Figure 3.1

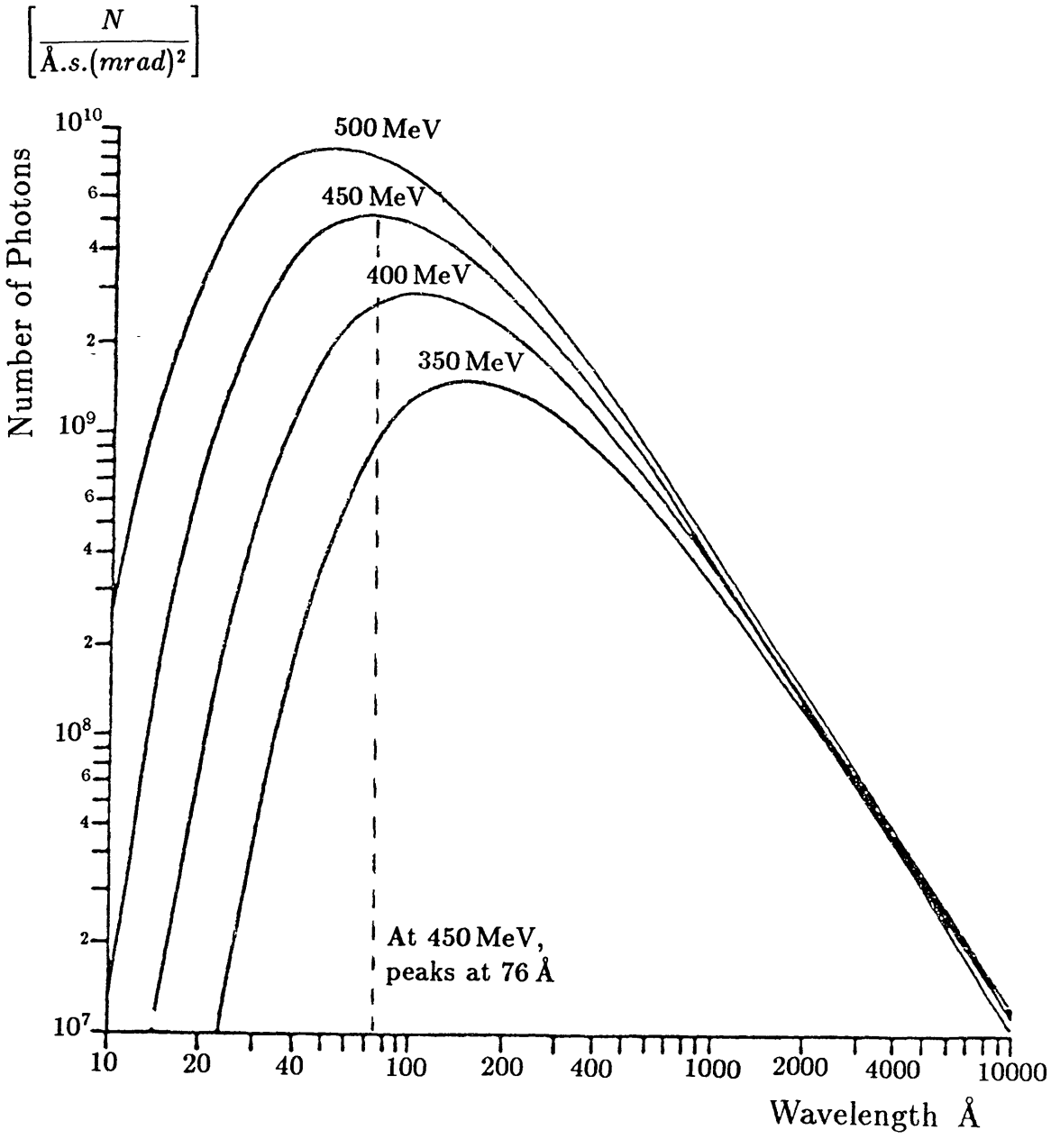


Intensity distribution curve for the Bonn 500 MeV electron synchrotron.
(after Thimm 1965)

Figure 3.2

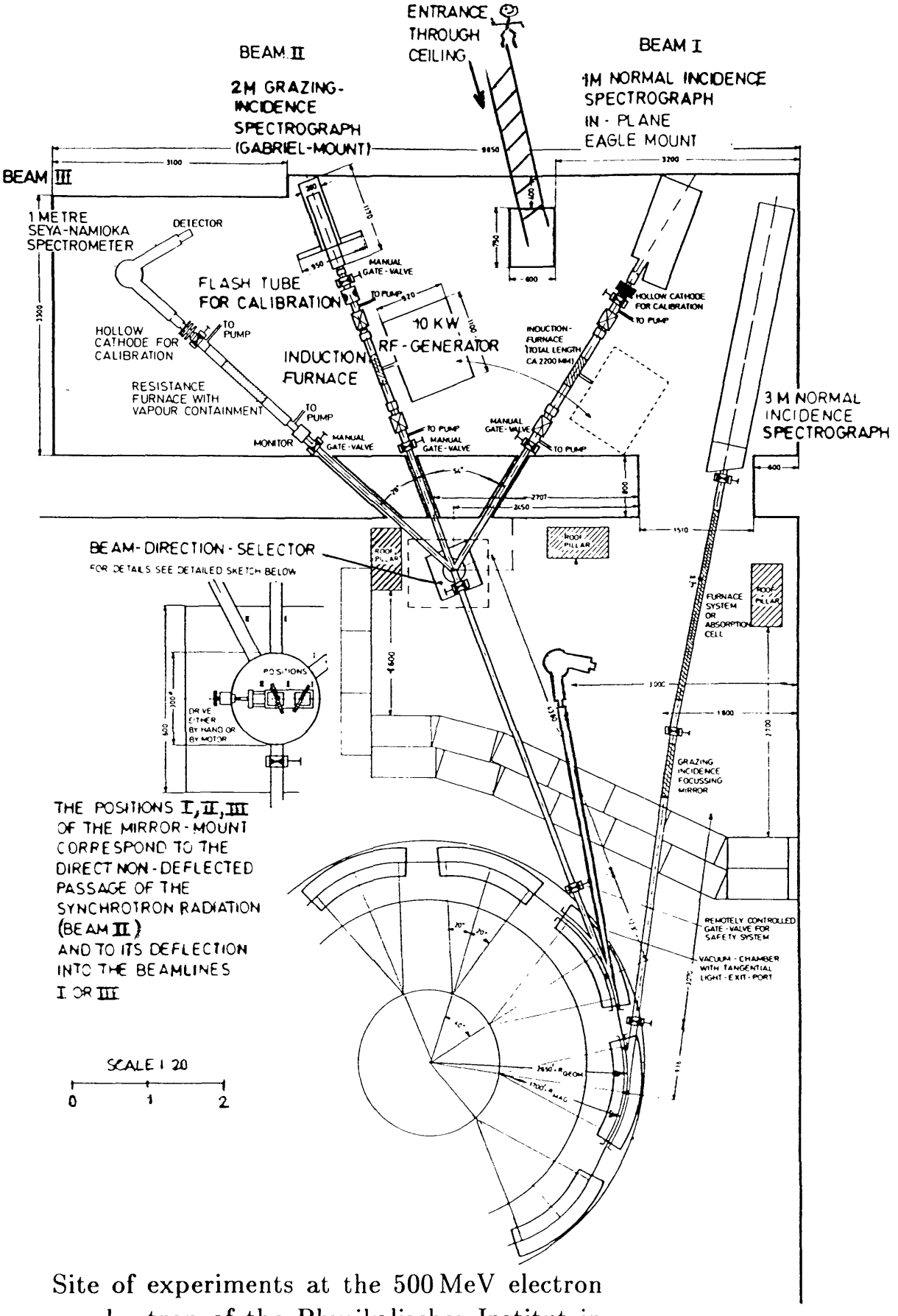


Site of experiments at the 500 MeV electron synchrotron of the Physikalisches Institut in Bonn. (after Connerade et al 1974)

Figure 3.3

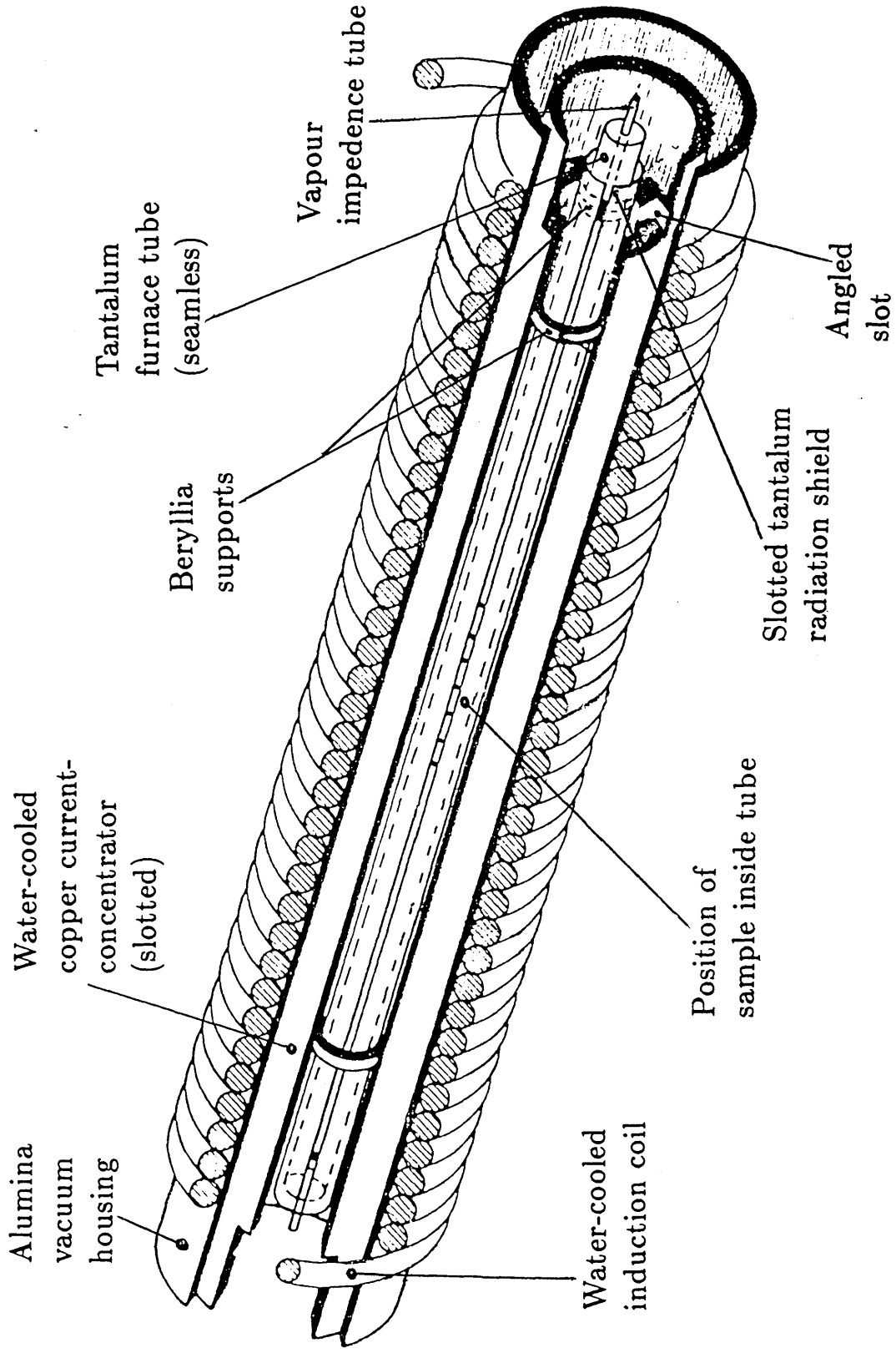


Diagram of the induction furnace.
(after Radtke 1980)

Figure 3.4

The emission lines are identified and a full wavelength list is given in Table 3a

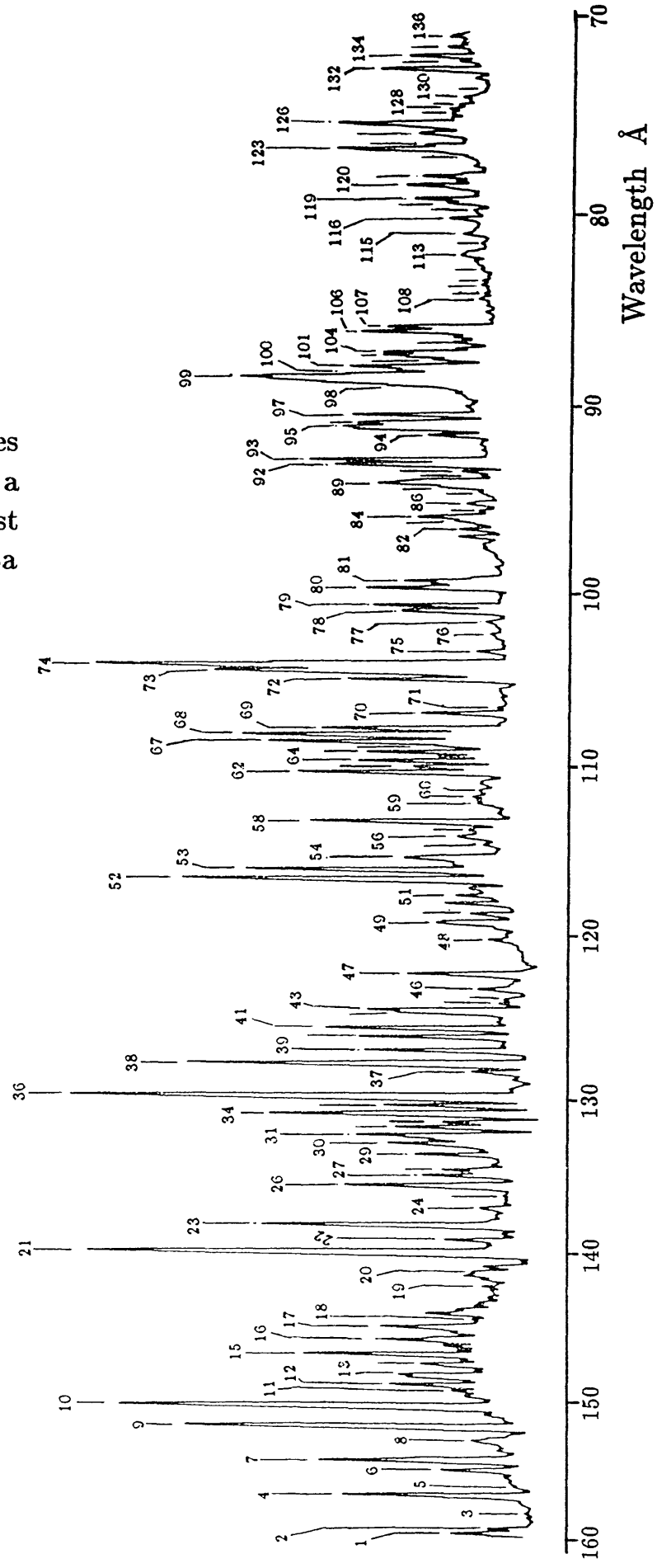


A typical calibration emission spectrum.

Figure 3.5

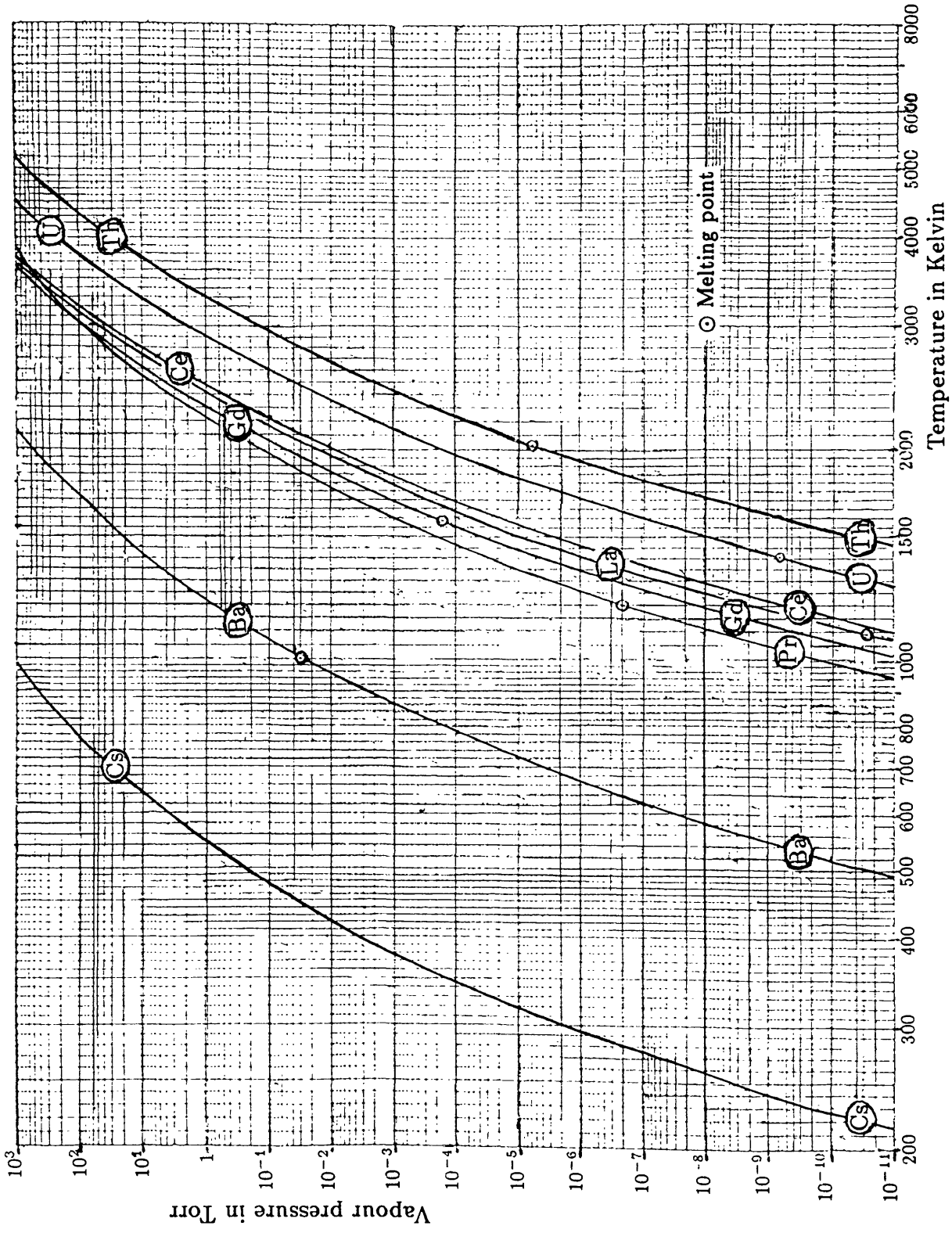


Vapour pressure curves for the elements studied.

Figure 3.6

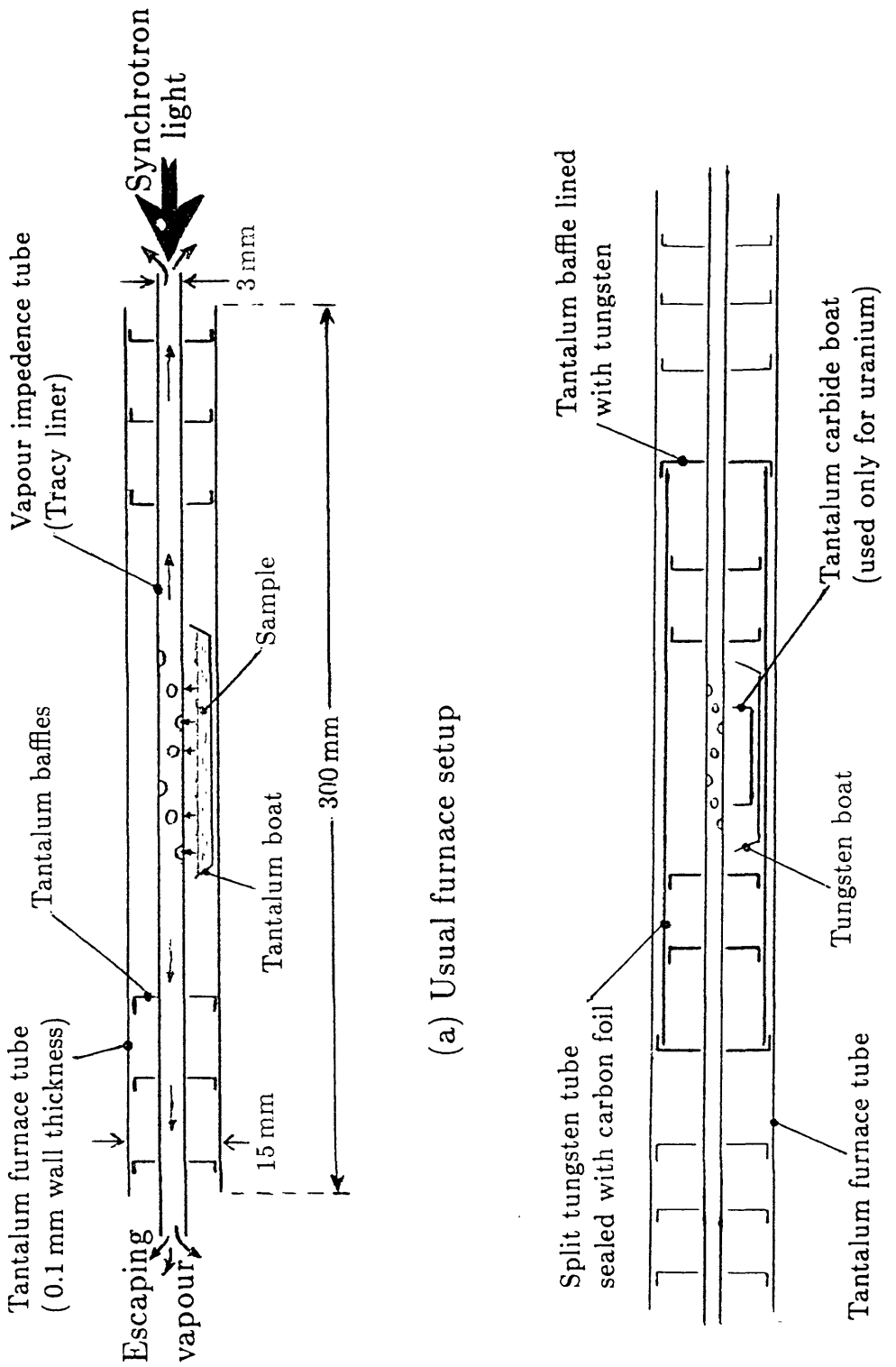


Schematic diagram of the furnace insert.
(not to scale)

Figure 3.7

# Chapter IV

# Caesium, $BaF_2$ and $LaF_3$

## 4.1 Summary

The $4d$ absorption spectrum of caesium is presented as an example of delayed onset. In contrast the spectra of $BaF_2$ and $LaF_3$ then serve to illustrate a giant resonance transition. Comparison of the the spectra we observed with the metal vapour and solid state spectra justifies our argument that they are atomic in origin.

## 4.2 Introduction

As explained in chapter three, there are severe experimental constraints coming from furnace design and metallurgy considerations. We must therefore combine an understanding of double wells and theory done to date, with what is practicable in making vapour columns. The whole subject therefore advances by a mixture of theory and experiment as outlined in chapter two.

As pointed out in the first two chapters, theoretical considerations suggest the following

- that the $Z$- dependence of the problem is of great importance
- that we should look at the lanthanide and actinide elements
- that we should look especially for *pure* examples where the $f$ subshell group theory does not lead to too much structure and hence allowing us to pick up purely radial effects.

- that we should try to find sensitive examples where the inner well is critically binding

and the above points were essentially what we aimed to explore.

Most of the lanthanides are accessible and some had already been done in Bonn by Radtke (1979b,1980) who made a systematic comparison between the lanthanide atomic and solid spectra. However the actinides are much more difficult, requiring high temperatures as well as being very aggresive in the liquid phase.

After looking at all this we decided to study volatile compounds, initially because what little information we had suggested that $UF_4$ and $ThF_4$ could be more easily studied than the metals. These fluorides are not aggresive, have much lower melting points, and have high enough vapour pressures at the temperatures we can attain with our furnace (see table 3d). Again the theory was useful because it told us that the giant resonances are formed in the inner well and so should be fairly insensitive to the external environment. Thus the spectra should resemble the atomic vapours.

The next step in this line of thought was to realise that the fluorine *cage* effect (Rosen 1979) could actually *tune* the double well problem. Instrumental in this thinking was the work of Dehmer (1974) on small molecules.

This broad plan developed gradually as the experiments progressed, building up to the important experiment on uranium vapour which actually demonstrates the molecular tuning of radial functions refered to above.

In this and subsequent chapters we build up progressively from the lanthanides and associated fluoride compounds, through to the purest giant resonance that we found in gadolinium. We have interpreted this giant resonance with the aid of a simple model based on scattering theory. We then move on to the actinides.

This chapter deals with the early lanthanides for which $f$ shell complications are not great. We discuss our results in relation to earlier work and show how the fluorine atoms affect lanthanum, the first evidence of molecular effects on wavefunctions.

## 4.3 The Delayed Onset of Photoionisation

As already alluded to in chapter two, delayed onset is distinct to but closely connected to giant resonances. The crucial difference is that it arises mainly

from what is happening in the outer well of our double well potential, unlike giant resonances which are essentially an inner well phenomenom. This cannot be stressed enough since in the literature both are persistently treated as being the same effect. This is particularly so for the case of xenon, and a typical example of such confusion is to be found in the first paragraph of the paper by Cheng and Johnson (1983).

Delayed onset of continuous absorption was first observed in the $4d$ spectrum of xenon (Lukirskiĭ and Zimkina 1963, Ederer and Toumboulin 1964) and came as a surprise. Till that time it had been thought that continuous absorption would rise sharply just above threshold and would then decrease uniformly with increasing energy (saw-tooth shape). Instead it was seen that there is little absorption immeadiatly above threshold but that absorption rises to a maximum some 30 eV higher and then falls off (see figure 4.1). The explanation for this behaviour once again lies in the effect of the $\ell(\ell+1)/2m_e r$ term in the effective potential.

This term gives the atom a hard repulsive centre for electrons of $\ell \geq 2$, and hence tend to keep electrons away from the nucleus. The reason for delayed onset is qualitatively illustrated in figure 4.2 which is adapted from Manson and Cooper (1968). It shows an initial $3d$ wavefunction, as well as an outgoing $\varepsilon f$ continuum function. At threshold the $\varepsilon f$ wavefunction hardly penetrates the core region and the spatial overlap of the initial and final wavefunctions is small. As the kinetic energy of the outgoing electron increases so does its ability to penetrate the barrier and the overlap with the $3d$ core wavefunction increases appreciably. This continues till the $\varepsilon f$ wavefunction has an energy comparable with the barrier height when it penetrates deeply, and the overlap reaches a maximum. With increasing energy the negative part of the continuum function overlaps the initial wavefunction, and phase cancellation leads to the overlap integral falling off. Since the photoionisation cross-section is proportional to the square of the overlap we can thus envisage why the delayed onset effect occurs. This concept is transferable to the $4d$ wavefunctions.

However the bulk of the continuum wavefunction remains in the outer well as comparison with figure 2.1 reveals. The inner well is centred at $r \sim 1$ a.u. (1 a.u = 0.529 Å) and the outer well is centred at $r \sim \ell(\ell+1)$ a.u..

## 4.4 The $4d$ spectrum of Caesium

Delayed onset has been observed in many elements. We studied caesium as an example lying with an atomic number of $Z = 55$ close to the beginning of the lanthanide series. The spectrum of caesium is of particular interest because it lies at the delineation of uncollapsed and collapsed $f$ wavefunctions and it has therefore also attracted much theoretical attention (Dehmer et al 1971, Wendin 1972, Lin 1974, Amusia et al 1976, Wendin and Starace 1978).

Figures 4.3 and 4.4 show our data for the caesium $4d$ spectrum at different vapour pressures. The spectra of figure 4.3 were taken at a vapour pressure of 1 Torr and 2 Torr, and that of figure 4.4 at a temperature of 320 °C corresponding to a pressure of 4 Torr. About 10 g of pure caesium metal in glass ampoules was loaded in the furnace, and the ampoule broken in a counter-flow of argon immediately before the apparatus was evacuated.

The caesium spectrum in this region of $4d$ excitation has been studied in previous work by Petersen et al (1975), and was confirmed by Connerade and Mansfield (1976) who concentrated however on the $3d$ spectrum.

However the work of Petersen et al (1975) is incomplete since problems with *stray light and higher order background* only allowed them to present a tentative curve in the region of maximum absorption. Further the spectrum is assembled from spectra obtained under differing conditions and adjustments were necessary in creating the one spectrum. Our spectra do not suffer from these drawbacks and we recorded features previously not observed.

At the short wavelength below 80 Å we have structure due to excitation of a $4p$ electron to $s$- and $d$- symmetric states

$$4p^6 4d^{10} 5s^2 5p^6 6s\ (^2\mathrm{S}) \longrightarrow 4p^5 4d^{10} 5s^2 5p^6 6s \quad \begin{matrix} ns & n \geq 6 \\ n'd & n' \geq 5 \end{matrix}$$

Simultaneous excitation of an $6s$ electron also leads to double excitations, for example

$$4p^6 4d^{10} 5s^2 5p^6 6s \longrightarrow 4p^5 4d^{10} 5s^2 5p^6 5d^2$$

Of course the excitation of two electrons by one photon is not possible within an independent particle model where interactions between electrons are not included, and in a sense double excitations can be thought of as

resulting from the excitation of a single electron in an atom which is in a competing ground state configuration.

Similar excitations, now involving a $5p$ electron in addition to the $4d$ electron, cause the structures superimposed on the broad continuum maximum *viz*

$$4p^6 4d^{10} 5s^2 5p^6 6s \longrightarrow 4p^6 4d^9 5s^2 5p^5 \begin{matrix} 6s6p^2 \\ 6s5d^2 \\ 6s^2 5d \end{matrix}$$

The weak structure between 80–120 Å that is especially evident on the high vapour density spectrum (figure 4.4) were reported by Petersen et al (1975). However they failed to pick up the two window type excitations marked $I$ and $H$, which are especially evident in the two lower density traces of figure 4.3. These window resonances are also probably due to double excitations. Also not reported in the previous work of Petersen et al (1975) are the features labelled $G$. These minima are probably caused by interference between transitions to the underlying continua

$$4d \longrightarrow \varepsilon f \quad \text{and} \quad 4d \longrightarrow \varepsilon p$$

The discrete structure above 150 Å is displayed at a greater magnification in figure 4.5, and a wavelength list of the most prominent lines is also included. This discrete structure is due to transitions of the type

$$4d^{10} 5s^2 5p^6 6s \longrightarrow 4d^9 5s^2 5p^6 6s\ np \quad n>5$$

These transitions corresponding to the discrete structure were assigned by Petersen et al (1975). The separation of the two groups of lines $BC$ and $EF$ is attributed to the splitting by the spin-orbit interaction of the $4d$ subshell into $4d_{3/2}$ and $4d_{5/2}$, and the multiplet structure to electrostatic interaction of $6s$ and $6p$ electrons.

However of far more interest to us is the pronounced delayed onset of continuous absorption that encompasses a width of $\sim$ 30 eV, peaking about 20 eV above the $4d$ thresholds. We have already given a qualitative picture of how it arises and have seen that it is essentially an outer well effect, in that it involves $\varepsilon f$ continuum states. Nevertheless as we will see, delayed onset can still be termed a *quasi*-resonant effect that leads to a large concentration of oscillator strength above the ionisation threshold.

## 4.5 The Collapse of $4f$ states in Caesium

Provided the barrier of the double valley potential is high enough, then the $4f$ eigenfunctions are approximately eigenstates of either the inner or the outer valley. Only in the case of an infinate barrier can the eigenstates be exact.

For neutral caesium in the ground state the $4f$ wavefunction is concentrated in the outer well. However calculations of the $4d^9 4f$ configuration within a Hartree–Fock model (Connerade 1978, Cheng and Froese-Fischer 1983) indicate that the $4f$ wavefunction in $4d$ excited $Cs^+$ is localised (ie. collapsed) in the inner well. Chiang et al (1980) by studying the Auger shift spectra of solid CsCl appear to confirm this. Radler and Sonntag (1976) measured the absorption spectra of CsCl both in the solid and the vapour phase. Comparison of these absorption profiles and that of atomic caesium does not show any dramatic difference as would perhaps be expected. Thus nothing is revealed about the nature of the final $f$ wavefunctions involved from such a qualitative inspection. Hence caution is perhaps called for and the transition to a collapsed $4f$ wavefunction is possibly not so abrupt or complete in going from Cs to $Cs^+$ as calculations lead us to believe. This is perhaps also a comment on the actual ionicity of the chemical bond. The above also applies for the configuration $3d^9 4f$ , as a comparison of the atomic vapour data (Connerade and Mansfield 1976) and the data for the $Cs^+$ ion (Maĭste et al 1980) shows.

It is then also interesting and perhaps an oversimplification to maintain that delayed onset is purely an outer well phenomenom since one would then expect it to be greatly influenced by the external environment. This emphasises how closely related delayed onset and giant resonances are. Hence the confusion in the literature is perhaps to be excused since our understanding of the subject is still limited and far from profound.

## 4.6 The Giant Resonance in Barium

Following caesium in the periodic table, with atomic number $Z = 56$, is barium which has a filled $6s$ subshell in the ground state.

Barium has been at the focus of much experimental (Connerade and Mansfield 1974, Rabe et al 1974, Ederer et al 1975, Lucatorto et al 1981)

and theoretical effort (Wendin 1973b and 1976, Fliflet et al 1974, Hansen et al 1975, Zangwill and Sovel 1980, Connerade and Mansfield 1982, Connerade et al 1984) and still remains a challenging problem.

We have already seen in chapter two how the properties of the rare earth elements depend on the sudden decrease in energy and size of the $4f$ wavefunction, and how this collapse occurs because of the specific features of the effective potential for the $f$ electrons. The $4f$ is not collapsed in the ground state and hence barium possesses no $4f$ electrons. However wavefunction collapse can occur even in such elements because the inner well may become capable of supporting a collapsed $4f$ orbital once a core electron is excited. However as we will see, the collapse can be configuration dependent (Hansen et al 1975).

If we look at the spectrum of barium fluoride in figure 4.6, we immediately see a significant difference to the caesium spectrum. The broad absorption maximum peaks about 14 eV above threshold and has a width of only $\sim 15$ eV. This rapid rise of the absorption cross-section above threshold is in contrast to the delayed onset observed in caesium, and such a profile is typical of the so-called *giant resonances*.

The inner well of the effective potential for elements of $Z \geq 56$ is now deep and wide enough for the $4f$ wavefunction to collapse. This means that the overlap of the $4d$ and $4f$ wavefunction should increase dramatically, whereas the overlap with higher n$f$ orbitals remain small since these remain located in the outer well. One would therefore expect to see an intense absorption line below threshold, corresponding to the $4d \longrightarrow 4f$ transition, as for the $3d$ case. This is not what we observe and two apparently conflicting explanations have been suggested. The most widely quoted interpretation is that of Dehmer et al (1971), who base their interpretation on an average of configuration approach. They state that the exchange interaction is so large that it splits the $4d^9 4f^{N+1}$ configuration pushing some multiplets well above threshold. Autoionisation then broadens these levels, with most of the oscillator strength becoming concentrated in these higher levels. The result of the process

$$4d^{10}4f^N \longrightarrow 4d^9 4f^{N+1} \overset{\text{autoionisation}}{\longrightarrow} 4d^9 4f^N \varepsilon f$$

is the giant absorption resonance seen above threshold. On the other hand, Hansen et al (1975) point out that this implies a very unusual behaviour of the n$f$ series since it is normally impossible for a bound state to autoionise

into its own continuum. The latter authors argue that the $4f\ ^1$P state in actual fact lies below threshold and that the absorption peak observed represents a transition to an $\varepsilon f$ continuum state. The reason why two formally equivalent computational schemes lead to different interpretations is that electron correlations are so strong that the concept of electronic configurations breaks down. The problem then becomes one of definitions, either one classifies a wavefunction by the main component of the basis set expansion or one counts the nodes of the resultant wavefunction.

Now in the configuration average basis calculation for Barium the $4f_{av}$ eigenstate is collapsed and localised in the inner well, with the $5f_{av}$ being the lowest energy eigenstate of the outer well. In this configuration average approach, the radial functions are taken to be the same for all the terms in the configuration. The variational calculation is performed giving the average energy of the configuration, and then the energies of the various $LS$ terms are computed in terms of slater integrals, as deviations from the average energy. Thus diagonalisation of the isolated $4d^9 4f$ configuration suggests that the $^1$P state is pushed above the $4d^9$ threshold (Ederer et al 1975).

The alternative analysis of Hansen et al (1975) uses $LS$-dependent basis functions and the variational calculation is carried out seperately on each possible term, hence the various terms are included from right at the start. This method indicates that the $4d^9 4f\ ^1$P is infact an eigenstate of the outer well and lies below threshold. The $^3$P and $^1$D states are however collapsed and hence the collapse is configuration dependent. Since the $4f\ ^1$P state is effectively in the outer well the overlap with the $4d$ initial state is small and so this transition carries little oscillator strength and is not responsible for the giant resonance. Instead continuum $\varepsilon f$ states are becoming resonantly localised and takeover the oscillator strength originally associated with the $4d^9 4f_{av}$ configuration. This happens because at an energy a little above threshold the $4d^9 \varepsilon f\ ^1$P wavefunctions becomes resonant in the inner valley and closely resembles the eigenfunction the well would have supported if it were slightly deeper. It was for this reason that Mansfield and Coner-ade (1976) suggested that a hybrid wavefunction $\overline{4,\varepsilon f}$ that resembles a $4f$ wavefunction in the core region and an $\varepsilon f$ wavefunction outside describes the situation better. This notation has generally been accepted and giant resonances are labelled as $4d \longrightarrow \overline{4,\varepsilon f}$ transitions.

Nevertheless Wendin and Starace (1978) demonstrated the essential

equivalence of the two interpretations and showed that the $nf$ $^1$P wavefunction infact resembles the $(n+1)f_{av}$ wavefunction and that this is due to the exceptionaly large correlations that occur. There are now two points to consider

- There now arises a possible inconsistency with our previous assertion that giant resonances are primarily an inner well phenomenom, unlike delayed onset. That the process is closely related too the delayed onset picture cannot be denied but a difference exists. Although continuum wavefunctions are still involved, they become resonantly enhanced in the inner well region and in appearance very much like a discrete state localised in the inner well of the potential. The dynamics of this process is not known, but it occurs when the inner well is deep enough to support collapsed $4f$ wavefunctions of only certain terms. This is supported by the the difference in absorption profile in going from one element to another. In chapter 6 we will show that a giant resonance is associated with a typical absorption profile and that it differs fundamentally from an autoionising line profile.

- Calculations support this interpretation for the giant resonances in barium and lanthanum, which have no $4f$ in the ground state, but is this transferable to the other lanthanides where the $4f$ is localised in the ground state. It is possible that even here only certain multiplets are localised in the inner well and that some lie in the outer well. The resultant correlations would lead to the $4f$ oscillator strength transferring to the continuum states. However calculations do not exist because of the rapidly increasing number of $LS$-multiplets as the number of $f$ electrons increase. Whatever the exact mixing mechanism we empirically know that giant resonances are present for most of the lanthanides and as long as the profile is characteristic we will still label them as $4d \longrightarrow \overline{4,\varepsilon}f$ transitions.

## 4.7 The $4d$ spectrum of $BaF_2$

In figure 4.6 we present the $4d$ absorption spectrum of $BaF_2$ vapour and compare it with previous data of barium vapour (Connerade and Mansfield 1974). The wavelengths of the marked features are given in the table within

the figure. These features appear consistently on all our plates and have been marked on our figure even though some are very weak structures, and could almost be thought of as *figments of the imagination*. We see that both are very similar in particular the shoulder at 105 Å is evident in both spectra. This shoulder is probably due to the double excitation of a $4d$ and a $5p$ electron (Wendin 1973a). However the discrete structure at longer wavelength differs, barium having much more complex structure. The calculations of Connerade and Mansfield (1975) show that the plethora of structure is due to $s \times d$ mixing between $6s$ and $5d$ states. The absorption spectra of barium metal and solid $BaF_2$ measured by Rabe (1974) also show similar discrete structure as in our $BaF_2$ vapour data. However there appears to be structure present within the giant resonance in the solid state $BaF_2$ data.

Barium is divalent and therefore the two valence $6s$ electrons are effectively removed in both the metal and $BaF_2$. In the metal they enter the conduction band and in $BaF_2$ they are transferred to the fluoride ion. Hence they are not available for interaction with $5d$ states, and this could explain the decrease in structure in comparison to barium vapour.

## 4.8 The Ba, $Ba^+$ and $Ba^{2+}$ spectra

The possible consequences of collapse of the $4f$ wavefunction were illustrated in the absorption spectra of Ba, $Ba^+$ and $Ba^{2+}$ by Lucatorto et al (1981). As figure 4.7 shows, the barium and $Ba^+$ spectra are similar with a giant resonance as the main feature. Of particular interest however is the $Ba^{2+}$ spectrum which exhibits several discrete lines instead, and Lucatorto et al (1981) attributed the sudden change to the collapse of the $4f$ wavefunction. The interpretation was however not clear since even after the $4f$ collapses one would expect only one line, with the transitions to higher $nf$ states still being suppressed by the potential barrier. Without presenting a detailed identification, Connerade and Mansfield (1982) showed that the discrete structure in the $Ba^{2+}$ spectrum is due to $4d \longrightarrow nf$ transitions. Their calculations revealed that in moving down the barium ionic sequence the $4f\,{}^1P$ eigenfunction, that in neutral barium remains in the outer well, is collapsed in $Ba^{2+}$. A parallel tendency of the other $nf$ wavefunctions ($n \geq 5$) to gain comparable amplitude on both sides of the potential barrier,

and so become hybrid wavefunctions of both wells, explained the profusion of lines observed. Using a different theoretical approach, Nuroh et al (1982) were in agreement with this general interpretation, although there were considerable discrepancies in the identification of individual lines. Connerade (1983) then gave a fuller classification of the discrete structure than had previously been achieved. Using multi-channel quantum defect theory[a] (Seaton 1966, Lu and Fano 1970), it was made clear that the $4f\,^1\mathrm{P}$ level is indeed the lowest level in the $nf\,^1\mathrm{P}$ series as it ought to be. Independently, Cheng and Froese–Fischer (1983) gave a similar interpretation for the observed spectra. Now as we progress from Ba to $Ba^{2+}$ the effective nuclear charge increases, and the inner well of the effective potential seen by the $f$ electrons deepens. However the calculations of Cheng and Froese–Fischer (1983) show that a parallel weakening of the potential barrier also takes place. Thus the inner well becomes deep enough to support the $4f\,^1\mathrm{P}$ wavefunction, but the removal of the barrier allows the other $nf$ states to interact with the collapsed $4f$ states and so gain amplitude in the inner well. Thus discrete transitions to the higher $nf$ states are possible, leading to the observed lines. It is also evident from figure 4.7 that the $4d$ thresholds move to higher energy. This in some way hinders the continuum $\varepsilon f$ wavefunction from becoming resonantly localised in the inner well, and so the giant resonance disappears, allowing the discrete transitions to dominate the spectrum. In $Ba^+$ it appears that an intermediate situation has been reached, with the discrete lines beginning to come through superimposed within the giant resonance feature.

Barium ionic series thus provides us with an example of *tuning* of the potential by the nuclear charge and we see that when wavefunctions are in a knife-edge situation a small change to the inner well can precipitate a dramatic change in the observed spectra.

---

[a] *MQDT* is a method whereby with the use of 3 fundamental dynamical parameters that are slowly varying functions of energy, together with the position of the series limits, one can form the basis for a complete description of a Rydberg spectrum (see Seaton 1978 and references therein). In particular most of the information describing a two-limit Rydberg system can then be represented within a two-dimensional Lu–Fano graph.

## 4.9 The *abnormal* $4f$ binding energy

As is the case with barium, lanthanum has also been the focus of much theoretical attention (Dehmer et al 1971, Dehmer and Starace 1972, Amusia and Sheftel 1976a). Lanthanum lies on the boundary on which the $4f$ state appears in the ground state configuration. The question of the $4f$ character of lanthanum was controversial though it is now generally accepted that if there is one then it is very small and the $4f$ first appears in the ground state for cerium. Lanthanum hence has the ground state configuration $4d^{10}5s^25d6s^2$ (see also table 3b).

Thus when a $4f$ electron is added in cerium there are eleven electrons in shells with higher principle quantum number (or only ten when the $5d$ disappears) and this prevails throughout the lanthanide sequence. This means that the $4f$ electrons have a lower energy than the $5s$, $5p$ and $6s$ electrons. Tabulated values of electron binding energies in atoms (Lotz 1970) show that the $6s$ electrons have comparable binding energies as the $4f$ electrons. This however does not mean that the $6s$ electrons ought to transfer to the $4f$ subshell. Although as $4f$ electrons they would have a lower energy it would somehow result in a net raising of the energy of the atom as a whole. Also the $6s$ electrons act as the valence electrons (Ley and Cardona 1979) which the $4f$ electrons localised in the inner well would not be able to play this role in the same way. On the other hand the $5s$ and $5p$ electrons retain binding energies many times greater than the $4f$'s, and this abnormal situation remains till well after the $4f$ subshell has been filled (with respect to the $5s$ till $Z=84$). The whole problem as we have seen hinges on the strong dependence of the effective potential for $f$ electrons on the effective nuclear charge. Putting a $5s$ electron in a $4f$ orbital would destroy the balance enough to shift the $4f$ wavefunction into the outer well. We are however effectively arguing in circles and the explanation is still somewhat opaque.

As Griffin et al (1969) pointed out the situation of the transition metals with respect to the $d$ and $s$ electrons is somewhat different. Looking at the periodic table (figure 1.1) shows us that there are only ever two $s$ electrons with higher principal quantum number than the $d$ electrons.

## 4.10 The $4d$ spectrum of $LaF_3$

In figure 4.8 we compare our absorption spectra for $LaF_3$ with the spectra of lanthanum vapour (Radtke 1979a) and lanthanum metal (Rabe 1974). The absorption spectrum for $LaF_3$ solid is also available (Suzuki et al 1975, Olson and Lynch 1982). We find good agreement between the energies of the peaks in all the data. The giant resonance is labelled as a hybrid $\overline{4,\varepsilon f}$ state as discussed previously and the other two features are identified as the triplet states as comparison with theory (Dehmer et al 1971, Sugar 1972) suggests.

This infact was the experiment that served as a check for our reasoning that the spectra of the lanthanide and actinide fluoride compounds can act as a substitute for the atomic spectra that were inaccessable directly. The experiment also established that as is the case with the metallic spectra the fluoride spectrum is of atomic origin. However the giant resonance in $LaF_3$ is narrower than in lanthanum vapour or metal. This indicates that the fluorine atoms increase the localisation of the $\overline{4,\varepsilon f}$ state. The interpretation is that the highly electronegative fluorine atoms draw electrons from the metal atom, thus causing the well to become deeper and so enhancing the localisation (Connerade et al 1980).

In the subsequent two chapters we will see that the effect of the fluorine *cage* is less pronounced than in lanthanum. The photoemission partial yield spectrum of $LaB_6$ (Aono et al 1980) is also like the lanthanum spectrum and further demonstrates the relative insensitivity of the spectra to the external environment.

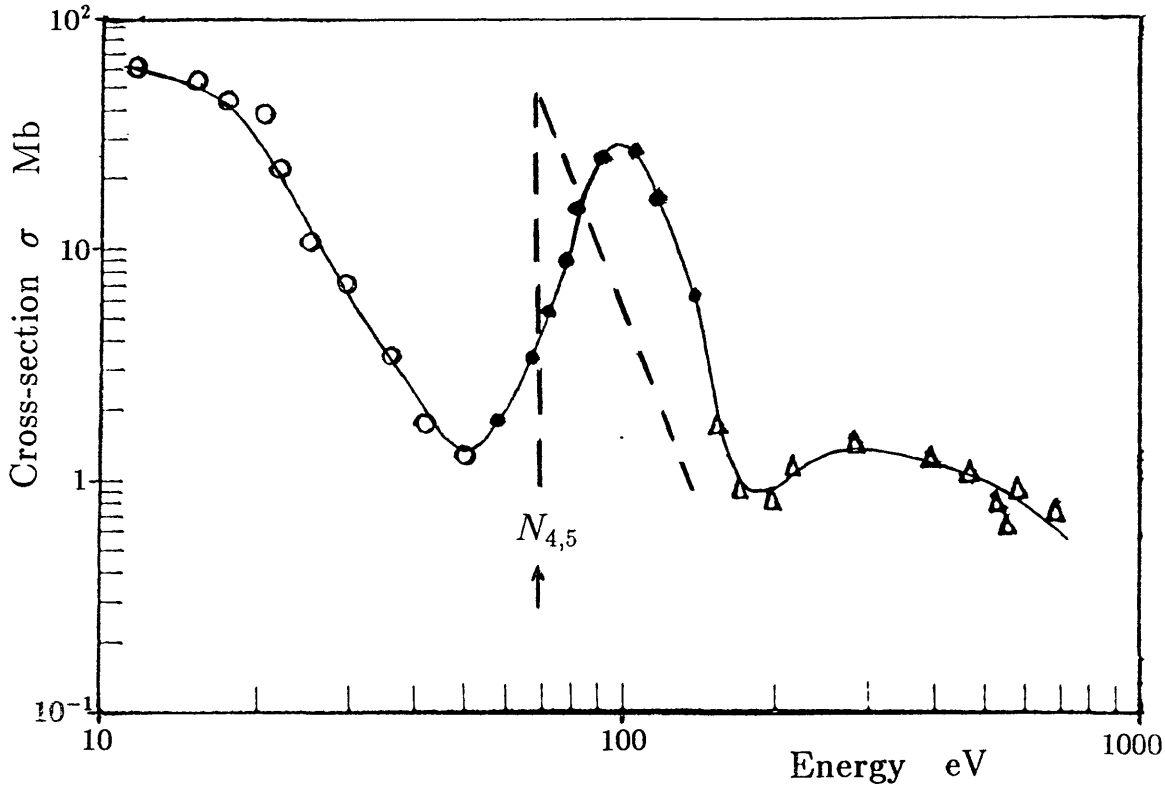


– – – Hydrogenic approximation

——— Experimental results

- ○ Samson (1966)
- ● Ederer (1964)
- ▲ Lukirskiĭ et al (1964)

The $4d$ photoionisation spectrum of xenon.
(after Fano and Cooper 1968)

Figure 4.1

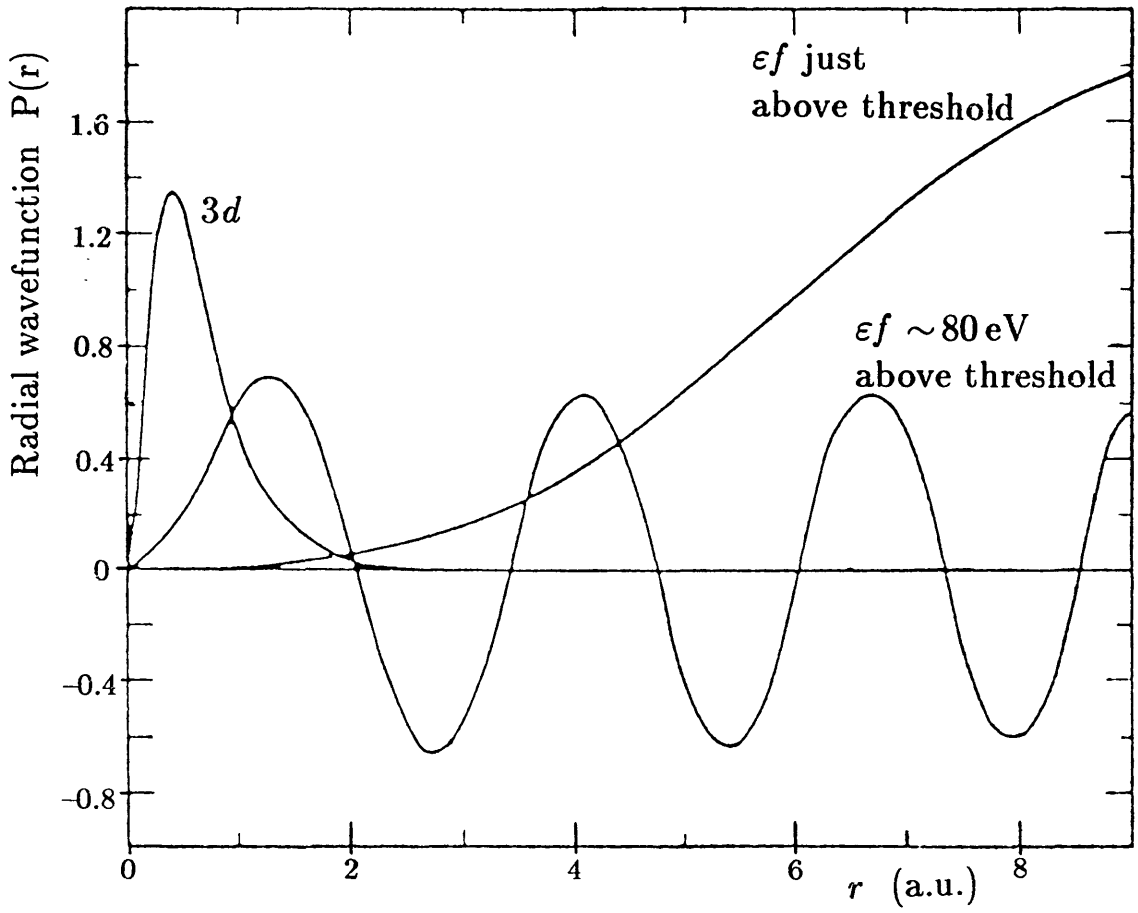


The variation in spatial overlap between the $3d$ wavefunction and the $\varepsilon f$ wavefunctions of different energies, is a result of the potential barrier in the effective radial potential.

A qualitative explanation for the delayed onset of photoionisation. (after Manson and Cooper 1968)

Figure 4.2

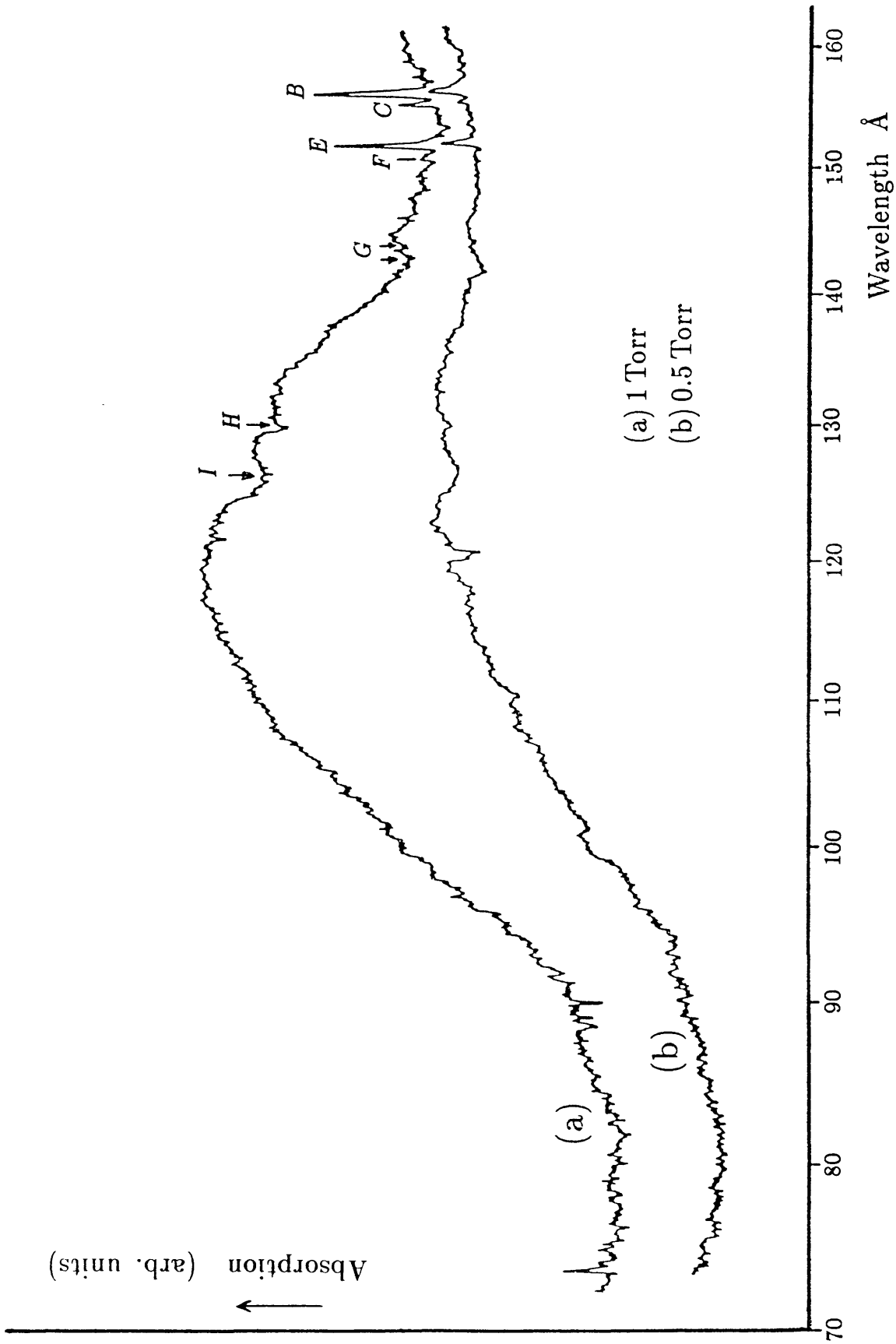


The $4d$ absorption spectrum of caesium
— at low vapour pressures

Figure 4.3

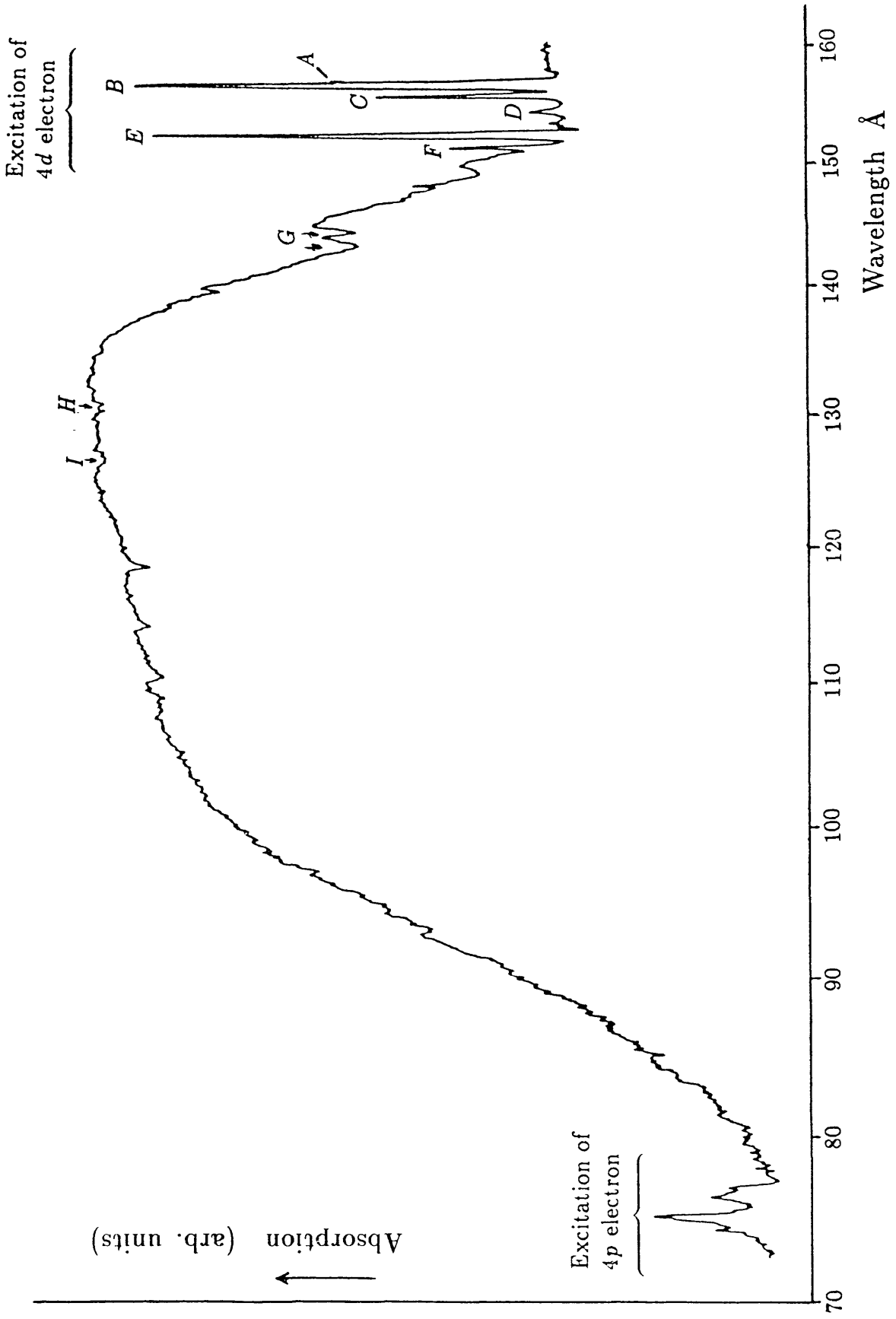


The $4d$ absorption spectrum of caesium
— at high vapour pressure (4 Torr)

Figure 4.4

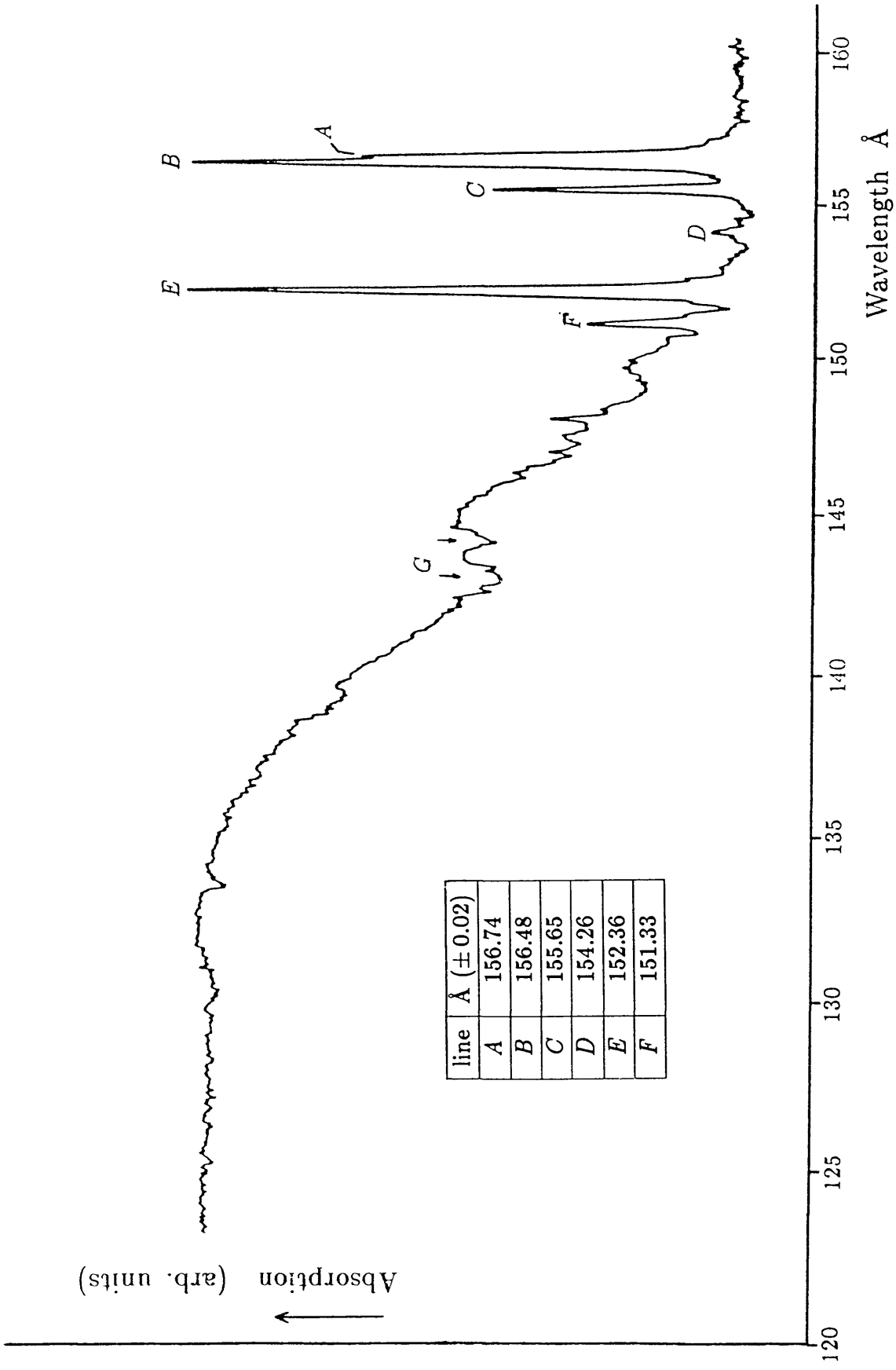


| line | Å (±0.02) |
|---|---|
| *A* | 156.74 |
| *B* | 156.48 |
| *C* | 155.65 |
| *D* | 154.26 |
| *E* | 152.36 |
| *F* | 151.33 |

Magnified trace of the caesium spectrum
— showing the discrete structure.

Figure 4.5

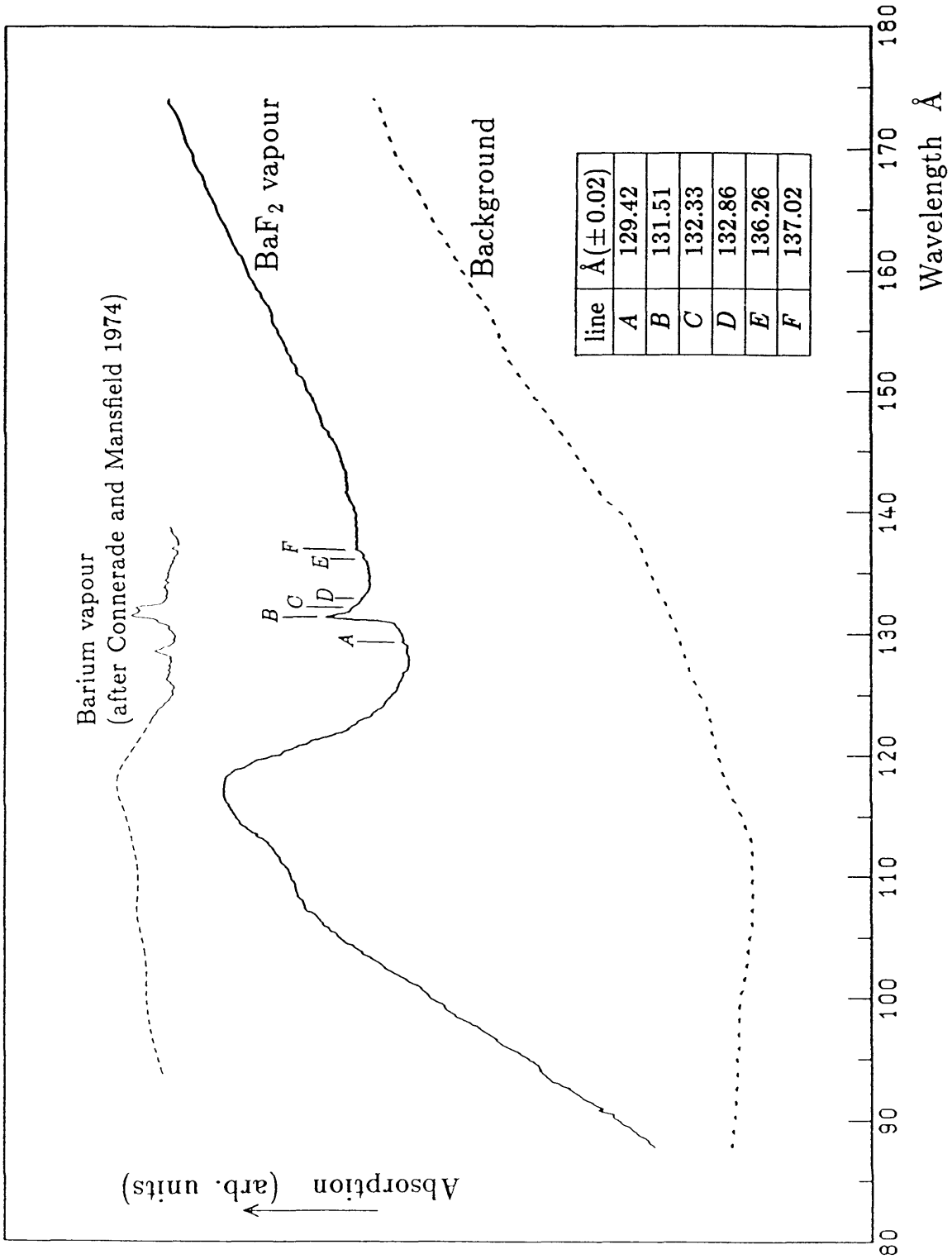


| line | Å(±0.02) |
|---|---|
| *A* | 129.42 |
| *B* | 131.51 |
| *C* | 132.33 |
| *D* | 132.86 |
| *E* | 136.26 |
| *F* | 137.02 |

The absorption spectrum of $BaF_2$ vapour.

Figure 4.6

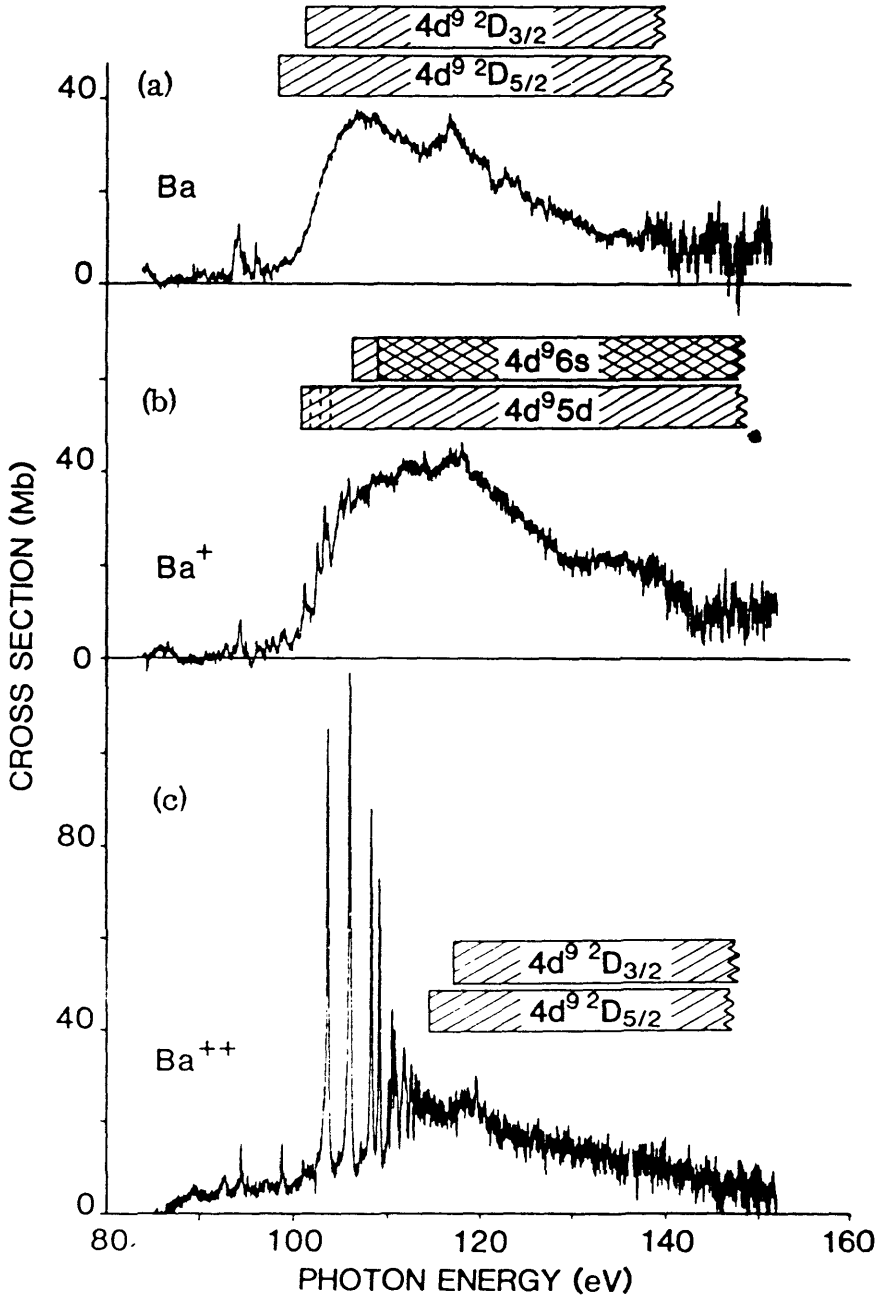


The absorption spectra of Ba, $Ba^+$ and $Ba^{2+}$ (from Lucatorto et al 1981)

Figure 4.7

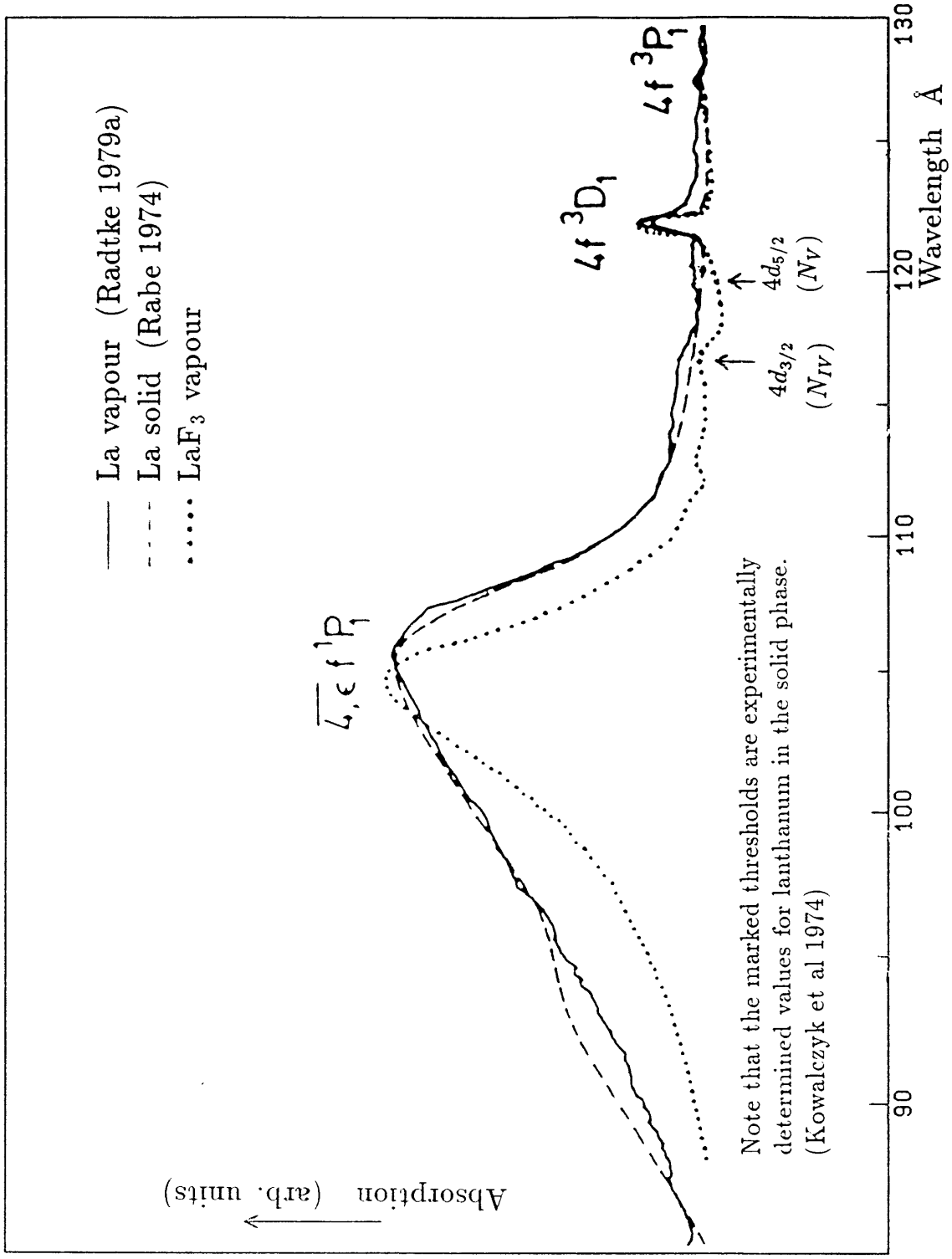


Comparison of the absorption spectra of lanthanum vapour, metallic lanthanum and $LaF_3$ vapour.

Figure 4.8

# Chapter V

# Cerium and Praseodymium

## 5.1 Summary

The $4d$ absorption spectra of cerium and praseodymium together with their trifluoride $CeF_3$ and $PrF_3$ are presented and a qualitative inter-comparison of all these spectra is made.

## 5.2 Introduction

As we discussed in the previous chapter we embarked on this study because theory tells us to look for the $Z$-dependence of radial effects. This chapter shows how this approach is frustrated by multiplet structure. This causes a non-systematic enhancement or quenching of discrete structure and overlapping of resonances, when we compare an atomic lanthanide spectrum with the corresponding trifluoride vapour. So far there is no theory available and without this we can offer no concrete interpretation of the spectra observed. We first point out that the particular interest in these elements is because of their chemical and physical properties and that these can be attributed to the behaviour of the $4f$ electrons.

### 5.2.1 The Interest in the Early Lanthanides

Cerium is the first element in the lanthanide sequence with occupied $f$ orbitals, and hence should have the spatially most extended $4f$ wavefunctions. Cerium exhibits fascinating chemical and physical attributes. Particularly

the anomalous properties when cooled below room temperature or when exposed to external pressure, make both cerium and several of its compounds of special interest.

Cerium possesses a complicated temperature–pressure phase diagram, and can exist in three different phases. These range from a low density $\gamma$–Ce to a volume collapsed high-density $\alpha$–Ce. The latter can be brought about by low temperature or a pressure of $\sim$ 7 kbar at room temperature (Koskenmake and Gschneider 1979). Both forms however retain a face-centred cube crystal structure, but the transformation is accompanied by a change from magnetic to non-magnetic behaviour. Further cerium becomes a superconductor at very low temperature and high pressure, and is thus the only element which can be magnetic, non-magnetic and superconducting according to the pressure or temperature considered (Coqblin 1977). The $4f$ electrons of cerium are usually held responsible for these anomalous properties, as well as the mixed valency displayed in various of its compounds. It is however still not established exactly how this comes about and it appears that the $4f$ state is localised in some compounds and delocalised in others (Johanson et al 1981). Various explanations have been put forward to account for the observed behaviour (Platau and Karlsson 1978, and references therein), but the understanding of this ambivalent behaviour continues to present a major challenge.

Our $4d$ spectra for cerium and cerium trifluoride, which probe the $4f$ states are of obvious interest, and especially now so, because of the related desorption of ions properties which have recently been determined and which we will discuss later in this chapter.

The spectroscopy of praseodymium dates back many years, though interest in praseodymium trifluoride has been particularly stimulated by recent observations of laser action within $PrF_3$ crystals at low temperatures (Hegarty and Yen 1980). Although Radtke (1980) reported the spectrum of praseodymium, the discrete structure was not well resolved. We therefore recorded the $4d$ spectrum of not only $PrF_3$, but also of the metal vapour, and observed much structure that had previously been missed.

## 5.3 Cerium and $CeF_3$

The absorption spectra of cerium and $CeF_3$ in the wavelength range 60–150 Å (80–190 eV) are shown in figures 5.1 and 5.2, together with the observed background. Absorption is in arbitrary units since the length of the vapour column was not defined. The wavelength positions of the observed peaks in this region are presented in tables 5a and 5b.

As in our previous spectra, the dominant feature in the cerium vapour data is the large absorption $\overline{4,\varepsilon f}$ resonance peak. However the spectrum exhibit complex structure below threshold due to the $4d^9 4f$ interaction, between the $4d$ hole and the $4f$ electron. The number of peaks exceeds that reported for metallic cerium (Haensel et al 1970) and many of the peaks appear to possess shoulders. We also observed considerable structure within the giant resonance itself which was to be seen on all plates taken with various vapour pressures (figure 5.3). There is no evidence of such structure in the published data on cerium vapour by Wolff et al (1976), a smooth curve representing the giant resonance. However the shoulder evident at 95 Å is also present in their data.

Comparison with our $CeF_3$ spectrum (figure 5.4) is very good. The width of the giant resonance is essentially the same at *FWHM* and there is no shift in energy between the two spectra. The discrete structure in the trifluoride corresponds to that of the atomic vapour but is considerably sharper. However the shoulder on the giant resonance is not so apparent in $CeF_3$ although there does appear to be structure present at this wavelength. The small blip at the maximum of the resonance in $CeF_3$ appears only at high vapour pressure for which the discrete structure was optimum.

The almost perfect agreement between the two spectra suggests that the outer $5d6s^2$ electrons hardly influence the spectra. In the trivalent fluoride they are the electrons involved in the bonding, and are thus effectively removed. The $5d$ and $6s$ radial wavefunctions cannot then overlap appreciably with the core $4d$ and $4f$ orbitals which are localised within the $5s^2 5p^6$ closed shells.

Olson and Lynch (1982) have measured the solid phase $CeF_3$ photoabsorption spectrum in the same energy range as we (figure 5.5). The discrete structure of our $CeF_3$ vapour spectrum agrees well with that of the solid $CeF_3$, but the latter has more structure that is better resolved. However there is a striking difference in the continuum resonance. We did not ob-

serve any such double maximum. The authors themselves suggest that it *seems to depend on sample quality, either strain or purity or both*, as this feature has not been observed before in any solid state measurement. A similar double maximum has however been observed in a photoemission study of cerium metal by Kowalczyk et al (1974), but in this case the spectrum is shifted by $\sim 15\,\mathrm{eV}$ and is not directly comparable to photoabsorption spectra since other selection rules apply.

## 5.4 Praseodymium and $PrF_3$

Figure 5.6 and 5.7 show our spectra with the background subtracted for praseodymium and $PrF_3$ vapours respectively, and the positions of the marked absorption peaks are collected in tables within the figures.

The metal vapour exhibits the giant resonance but with much inlaid structure clearly evident. This structure is very prominent compared to the cerium spectrum, and present over the whole range of the resonance. The discrete structure below threshold is very sharp and quite evenly spaced out and the intensity distribution is a little strange, there appearing to be a small minimum before onset of the continuum absorption.

In comparison, the giant resonance in the trifluoride is narrower and two maxima are to be seen. The discrete structure is not so profuse but appears to correspond to some of the structure in praseodymium (figure 5.8). We do not observe the broad shoulder that is seen in the solid state data of Olson and Lynch (1982) for $PrF_3$ (figure 5.9). In the latter data, the two peaks in the broad maximum are more pronounced than in our vapour data but with no shift in energy. This double maximum is also to be seen in the metal data of Gudat and Kunz (1972) but is not so pronounced in the earlier work of Haensel et al (1970).

One further interesting point is that the spectra of praseodymium and its oxide in the solid phase are identical. However for CeO, the large absorption peak is shifted to higher energies as compared to the metal and the discrete structure is different (Haensel et al 1970).

Dehmer et al (1971) and Sugar (1972) have calculated the transitions and relative oscillator strengths within an $LS$–coupling scheme for the triply ionised cerium and praseodymium. The discrete structure has to a large extent been relatively well described as

$$Ce^{3+} \quad 4d^{10}4f \longrightarrow 4d^{9}4f^{2}$$
$$Pr^{3+} \quad 4d^{10}4f^{2} \longrightarrow 4d^{9}4f^{3}$$

transitions. The giant absorption peak is then regarded as resulting from those levels that are pushed into the continuum by the large exchange interaction, and which then autoionise. This is the most widely quoted explanation. However as already indicated in chapter four, this picture is not really the whole truth since the giant resonance is an integral part of the continuum and not a two-channel process as in autoionisation, and we will pursue this further in the next chapter. It suffices to say that the profile of a giant resonance has as yet not been sufficiently well described by *ab initio* theory, and that confusion in its interpretation still persist. There is a corresponding lack of reliable values for the $4d$ electron binding energies for the lanthanides.

## 5.5 The Pseudo-Periodic Table

Recently Koel et al (1982) have reported on the observed resonant photon-stimulated desorption of ions from oxidised cerium in the region of $4d$ excitation. It was seen that the desorption spectrum of ionic hydrogen from the oxide replicated the absorption spectrum of cerium, even down to the discrete structure. Although there is no explanation of this fact it would again appear that the $4f$ electrons once again play a crucial role, the hydrogen being ejected as a result of rearrangement within the core after a $4d$ electron has been ejected. This is of great interest because of the possibilities associated with hydrogen storage, a poignant topic of research at present. It is therefore of interest to know as much as possible about the giant resonance in cerium as well as the whole spectrum in this region of $4d$ excitation.

It is interesting to note the position at which cerium lies in the quasi-periodic table constructed by Smith and Kmetko (1983). The five long periods when arranged in order of increasing localisation leads to the diagram reproduced in figure 5.10. The boundary between conductivity and magnetism (itinerent or localised $f$ and $d$ behaviour) can be traced empirically diagonally down this table. The elements in this boundary region can display widely varying behaviour that can be influenced by the external environment. The elements close to this cross-over region exhibit such

qualities as itinerent magnetism, hydrogen storage, catalysis, intermediate valence, structural instabilities and many other seemingly unrelated phenomena. It is interesting to note that this diagonal effectively coincides with the appearance of atomic giant resonances. It is therefore not surprising to find that cerium, that exhibits such anomalous properties, should lie on this diagonal.

## 5.6 Conclusion

We have therefore essentially presented our data for cerium and praseodymium vapours, in conjunction with their trifluoride vapours, without offering concrete answers to the many questions that the observed spectra raise.

We confirm however that the observed structures arising from the excitation of a $4d$ electron in both the trifluoride and the metallic spectrum are atomic in origin. We assign the large absorption resonance we observe as a $4d \longrightarrow \overline{4,\varepsilon} f$ transition as discussed in the previous chapter, and as such cannot simply be termed as autoionising lines.

However there remains the following

- Why is the giant resonance narrower in $PrF_3$ as compared to praseodymium and not in the case of cerium and its fluoride.
- Why is there so much structure within the giant resonance of both these elements as compared to lanthanum, and why is this structure so much more prominent in praseodymium.
- We offer no explanation for the double maximum in $PrF_3$.
- Why is the discrete structure in $CeF_3$ vapour sharper than in cerium, whereas in $PrF_3$ it is not as prominent as in praseodymium. That the multiplet structure in cerium and its trifluoride remain so similar is probably because the $f$ electron configuration remains the same in both. For praseodymium this is not the case, an $f$ electron in the trifluoride having to involve itself in bonding.

Although we can give no consistent interpretation we report and discuss our spectra in order to allow others to recognise that problems exist and to increase the available experimantal data base.

We conclude that the analysis is very difficult without sophisticated *ab initio* calculations beyond existing theory, namely how to calculate wave-function collapse with many open shell structure effects and complicated group theory present. This ties in with the considerations on open shells in the first two chapters but points to the need for data in which structure is not obtrusive.

| Line | Å ± 0.02 | Line | Å ± 0.02 |
|---|---|---|---|
| 1 | 88.70 | A | 111.12 |
| 2 | 89.16 | B | 112.02 |
| 3 | 89.51 | C | 112.30 |
| 4 | 90.92 | D | 112.58 |
| 5 | 94.05 | E | 113.66 |
| 6 | 96.40 | F | 114.39 |
| 7 | 100.55 | G | 114.66 |
| 8 | 102.77 | H | 114.97 |
| 9 | 103.87 | I | 115.20 |
| 10 | 104.44 | J | 115.50 |
| 11 | 105.18 | K | 115.82 |
| 12 | 105.59 | L | 116.17 |
| 13 | 106.43 | M | 116.63 |
| 14 | 107.18 | N | 117.02 |
| | | O | 117.34 |
| | | P | 118.47 |
| | | Q | 118.72 |
| | | R | 119.49 |
| | | S | 119.77 |
| | | T | 120.06 |

Table 5a: Wavelength list for cerium (figure 5.1)

| Line | Å ± 0.02 | Line | Å ± 0.02 |
|---|---|---|---|
| 1 | 102.26 | A | 111.23 |
| 2 | 102.87 | B | 112.32 |
| 3 | 104.54 | C | 113.03 |
| 4 | 105.34 | D | 114.63 |
| 5 | 106.86 | E | 116.33 |
| 6 | 107.91 | F | 116.58 |
| 7 | 109.48 | G | 117.36 |
| | | H | 117.64 |
| | | I | 119.24 |
| | | J | 119.93 |
| | | K | 120.50 |
| | | L | 121.49 |

Table 5a: Wavelength list for $CeF_3$ (figure 5.2)

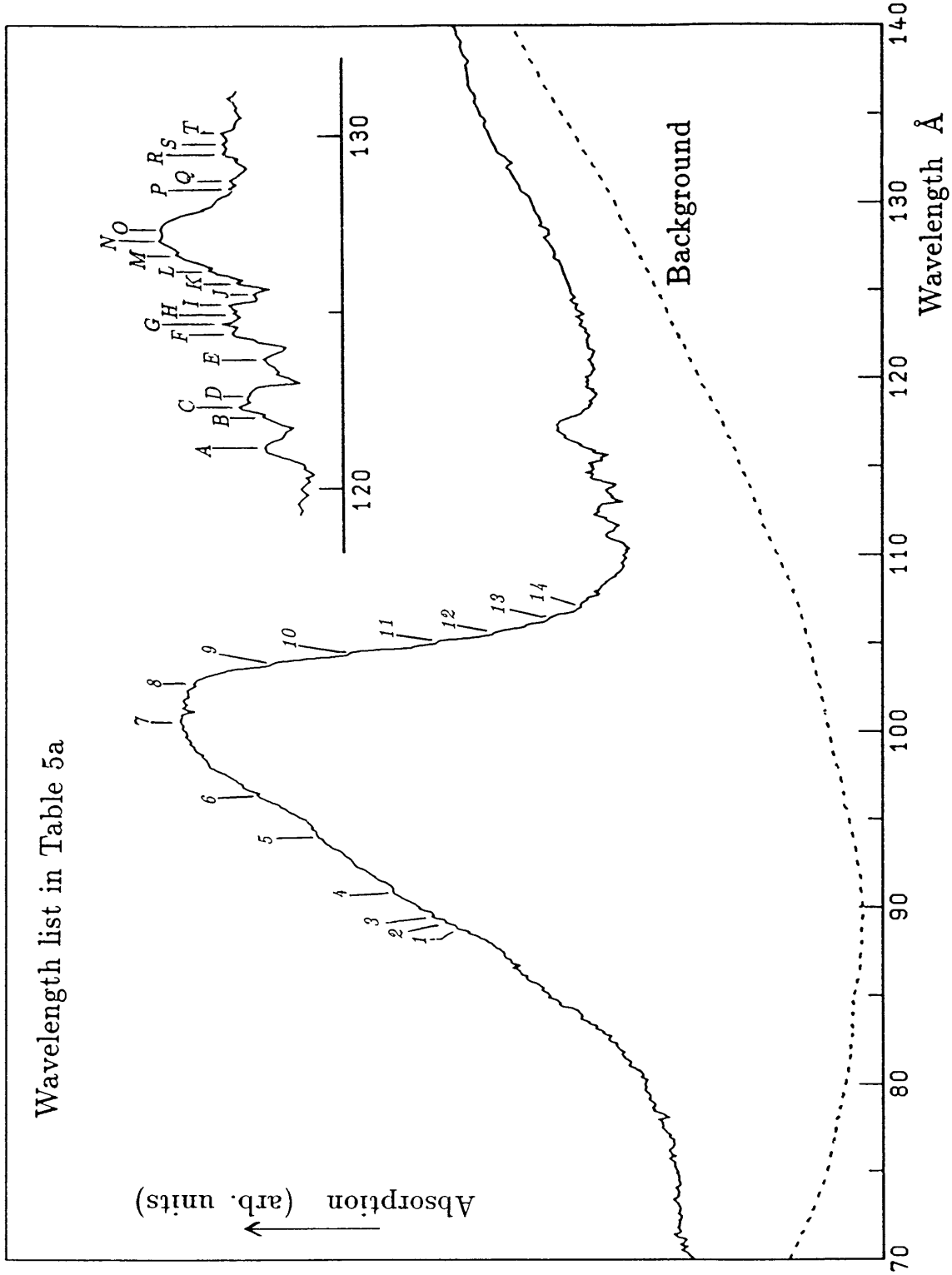


The $4d$ absorption spectrum of Cerium vapour.

Figure 5.1

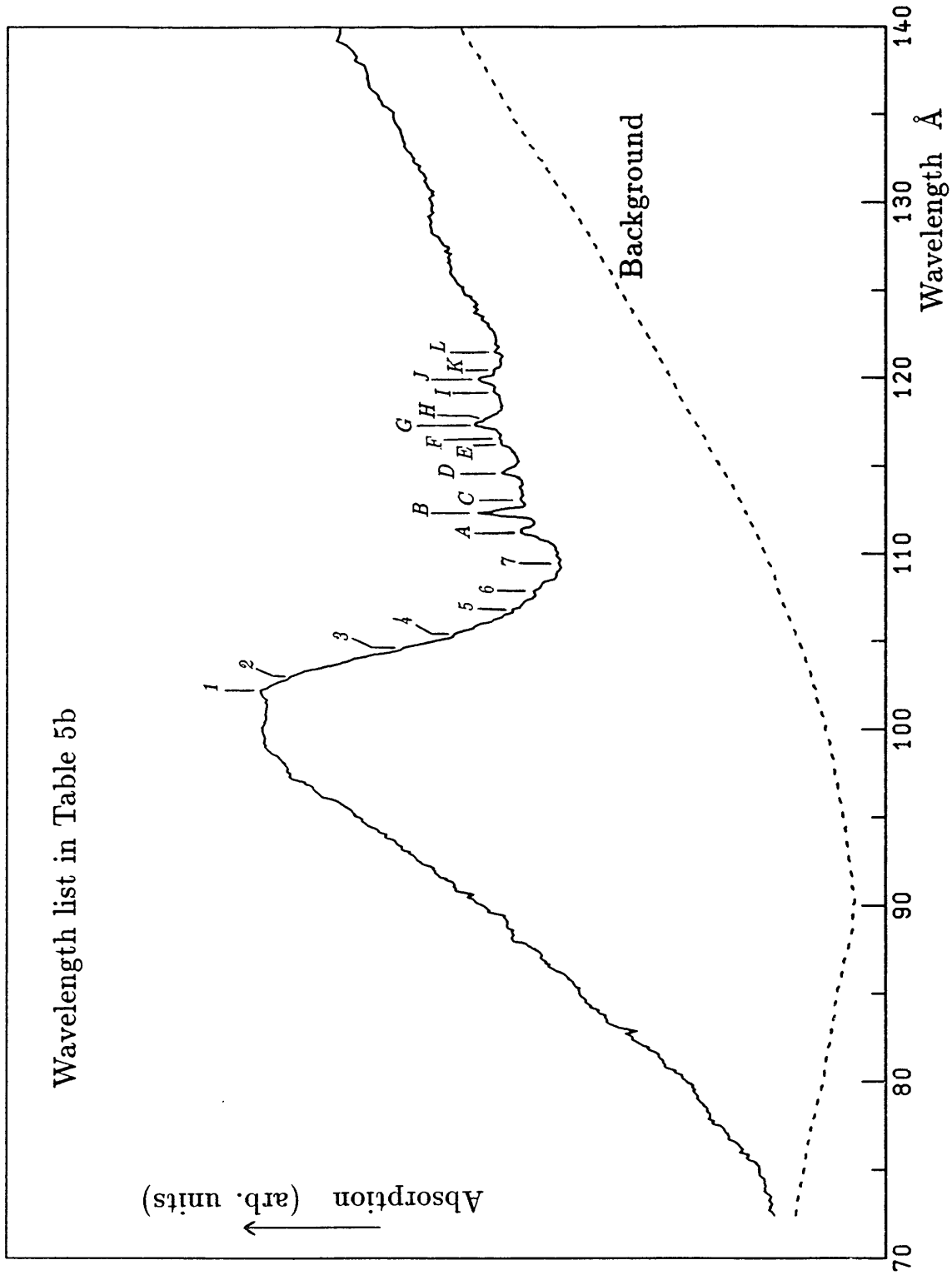


The $4d$ absorption spectrum of $CeF_3$ vapour.

**Figure 5.2**

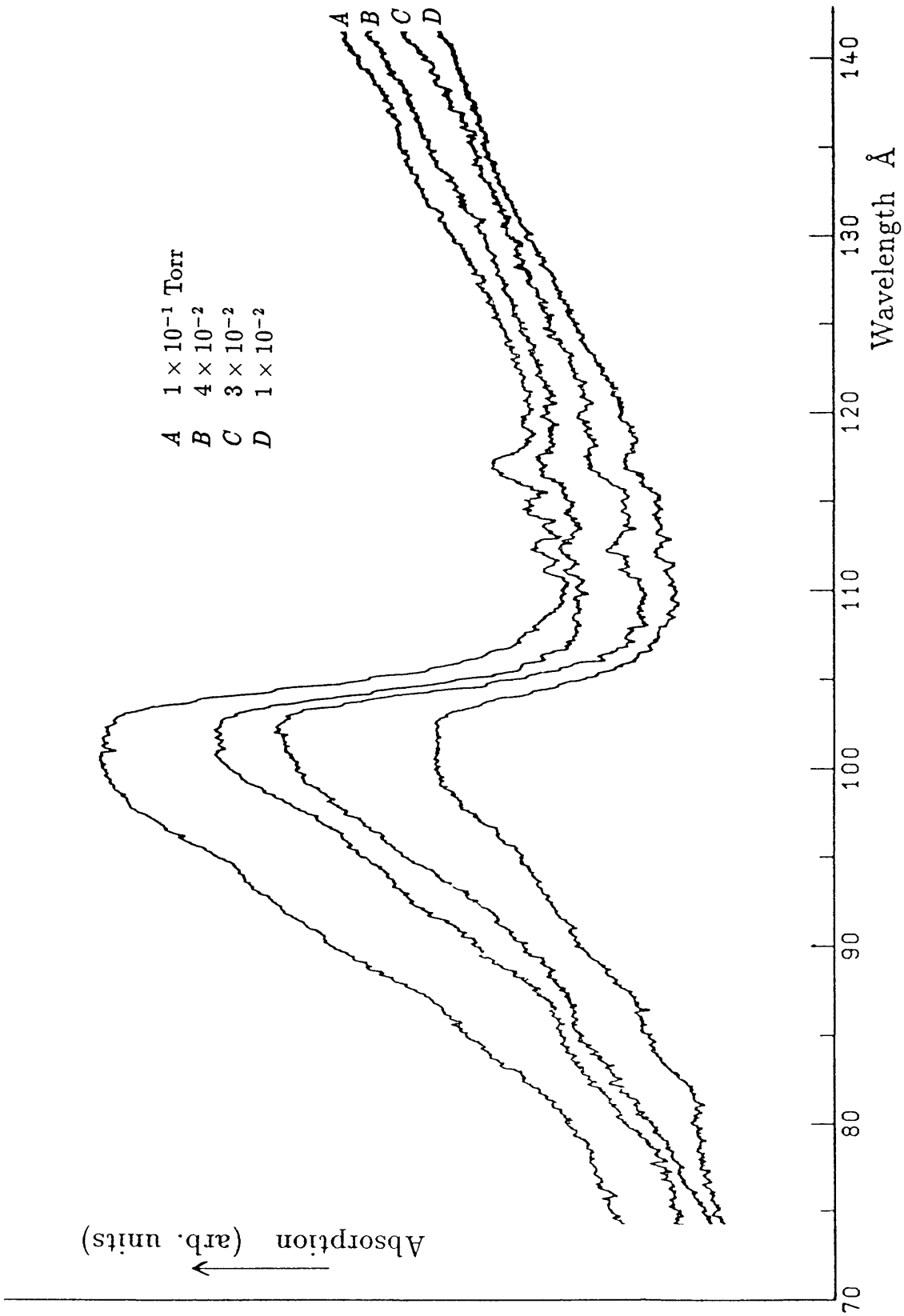


Cerium spectra at various vapour densities
— the structure within the giant
resonance appears consistently

Figure 5.3

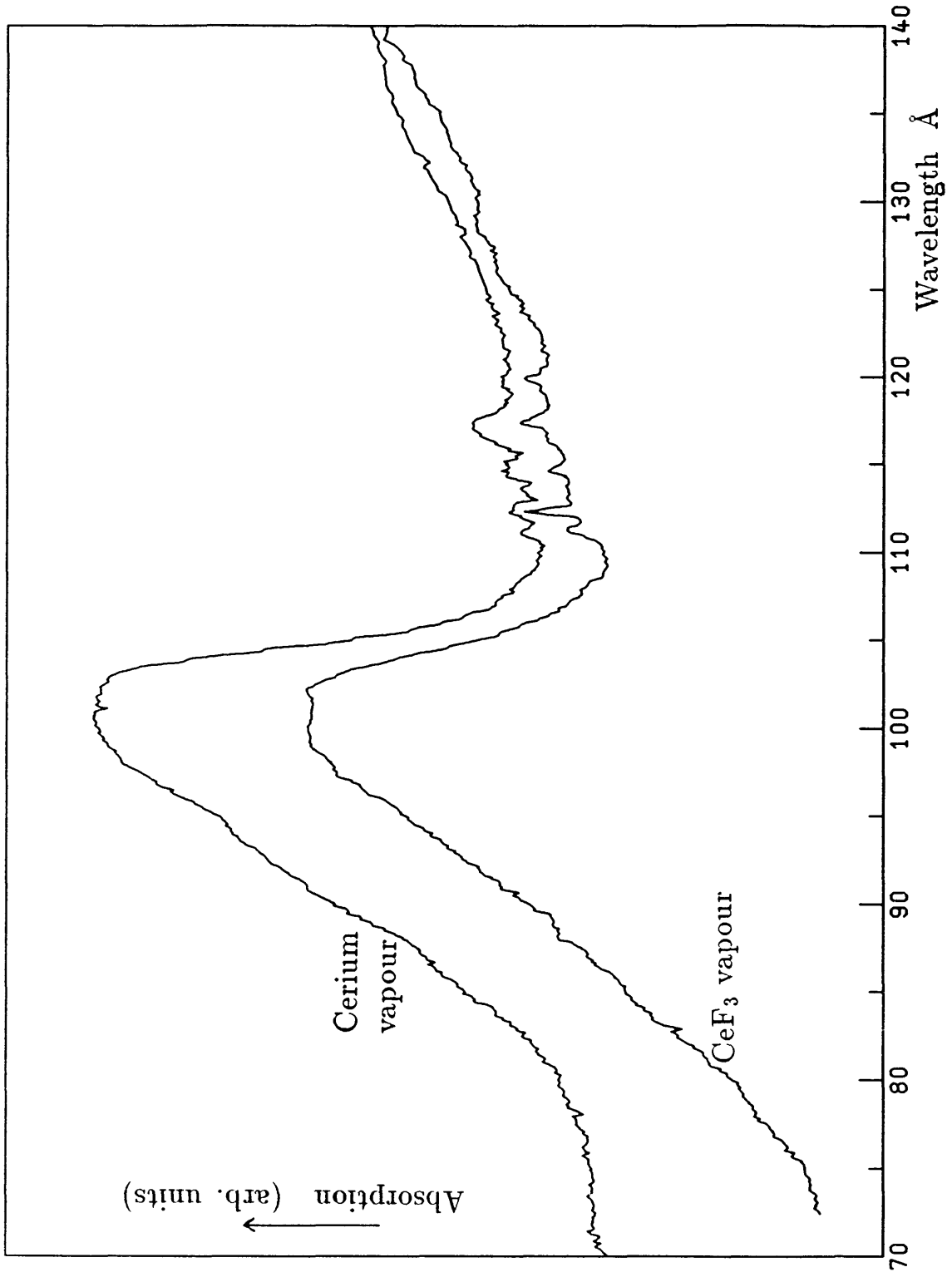


Comparison of the Cerium and $CeF_3$ spectra.

Figure 5.4

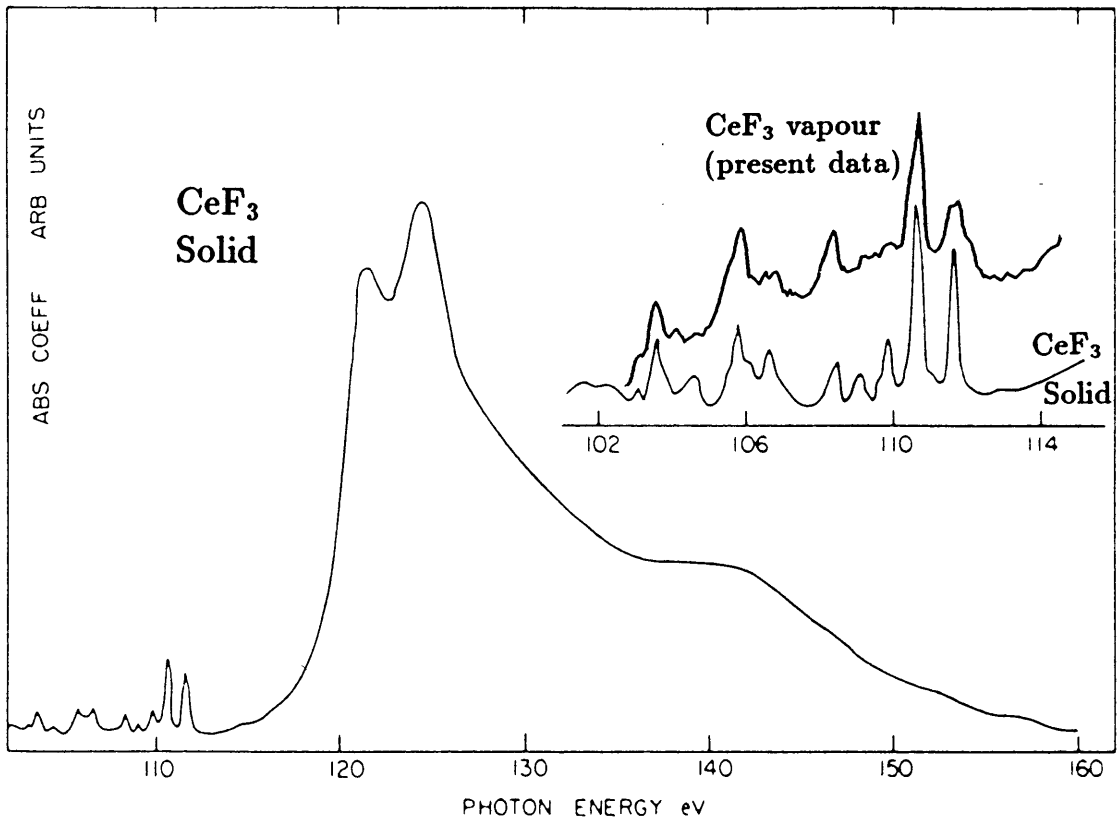


Absorption spectrum of solid $CeF_3$
(after Olson and Lynch 1982)

Figure 5.5

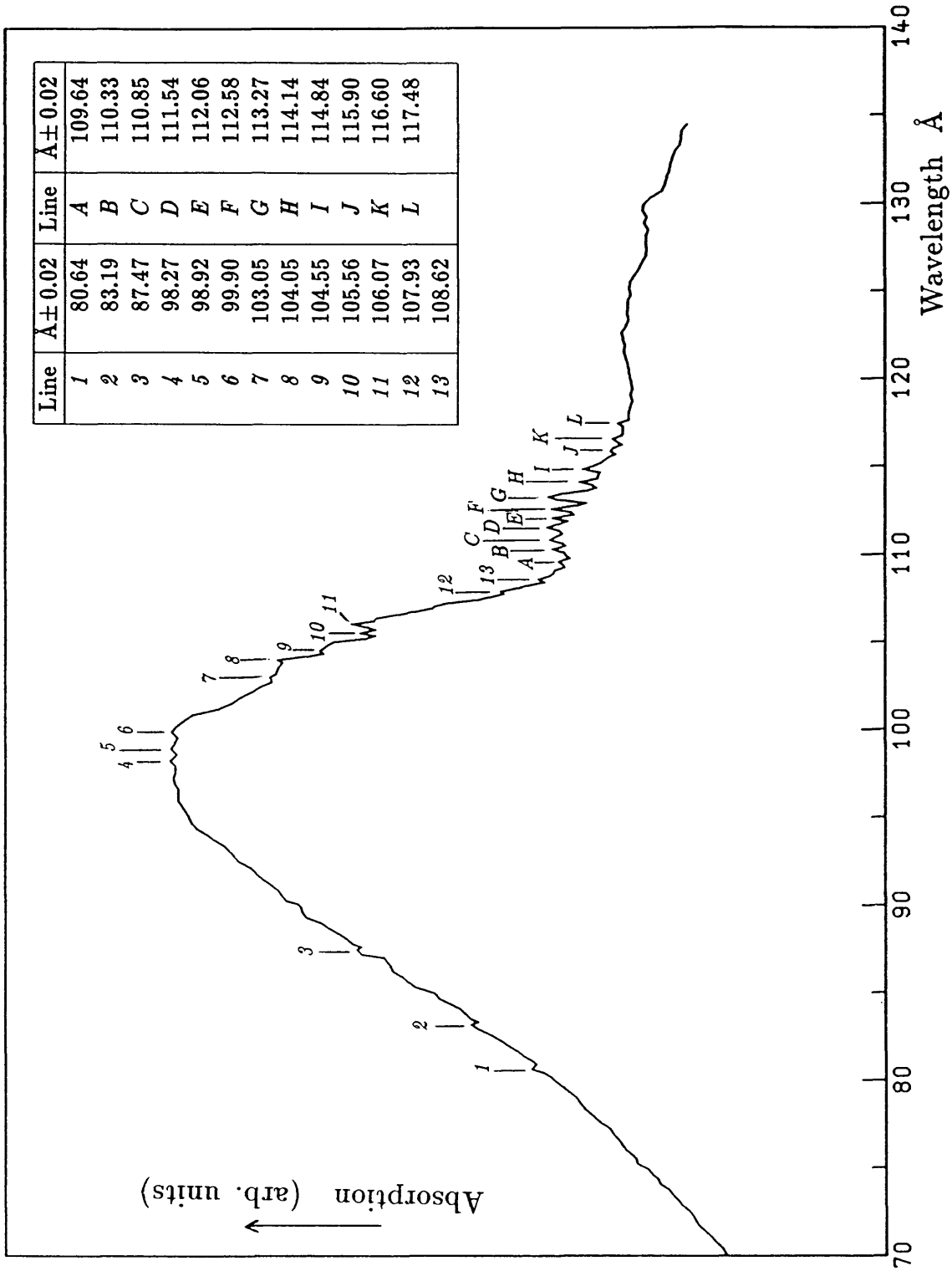


| Line | Å± 0.02 | Line | Å± 0.02 |
|---|---|---|---|
| 1 | 80.64 | A | 109.64 |
| 2 | 83.19 | B | 110.33 |
| 3 | 87.47 | C | 110.85 |
| 4 | 98.27 | D | 111.54 |
| 5 | 98.92 | E | 112.06 |
| 6 | 99.90 | F | 112.58 |
| 7 | 103.05 | G | 113.27 |
| 8 | 104.05 | H | 114.14 |
| 9 | 104.55 | I | 114.84 |
| 10 | 105.56 | J | 115.90 |
| 11 | 106.07 | K | 116.60 |
| 12 | 107.93 | L | 117.48 |
| 13 | 108.62 | | |

The $4d$ absorption spectrum of praseodymium vapour.

Figure 5.6

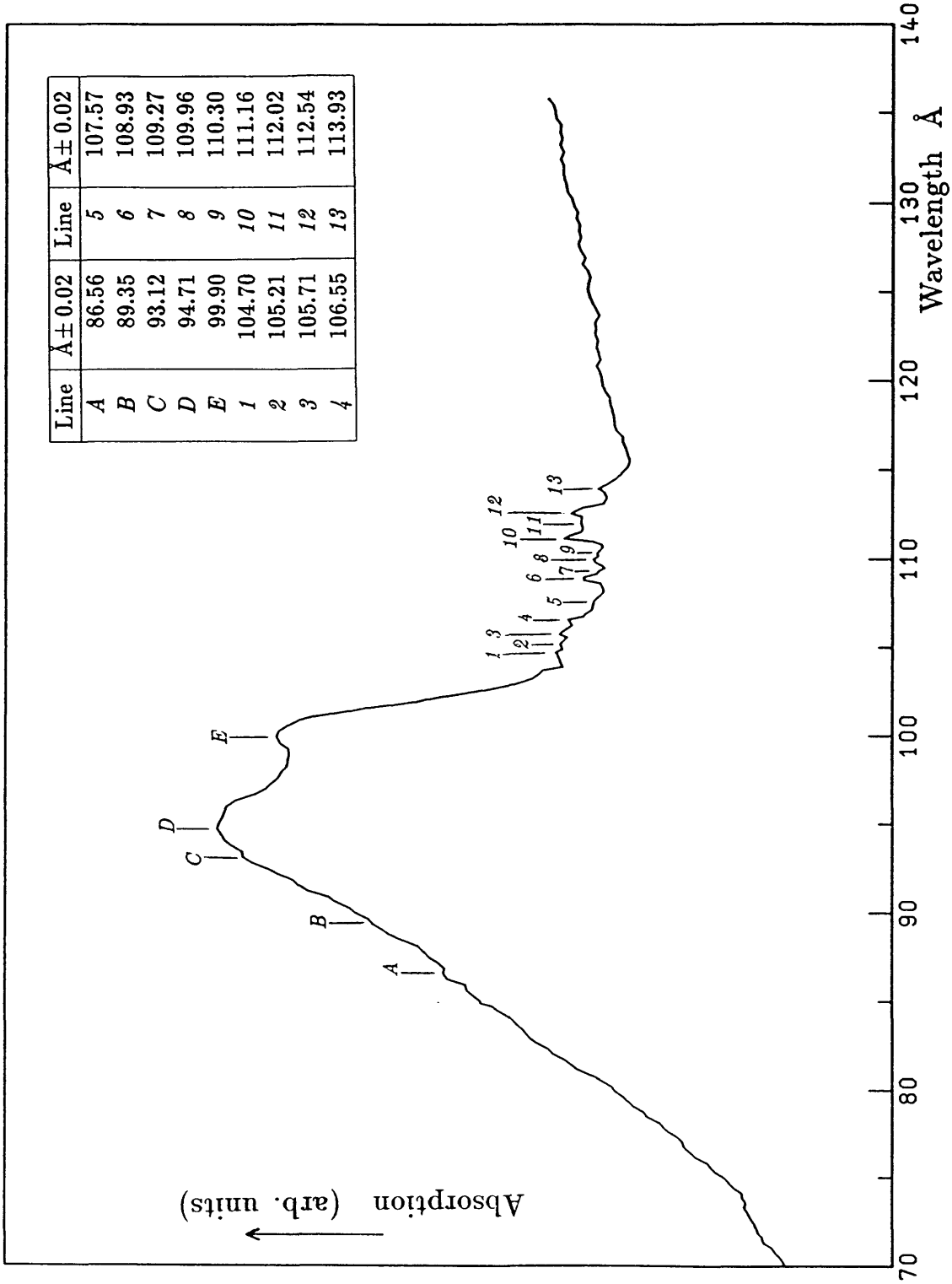


| Line | Å ± 0.02 | Line | Å ± 0.02 |
|---|---|---|---|
| *A* | 86.56 | *5* | 107.57 |
| *B* | 89.35 | *6* | 108.93 |
| *C* | 93.12 | *7* | 109.27 |
| *D* | 94.71 | *8* | 109.96 |
| *E* | 99.90 | *9* | 110.30 |
| *1* | 104.70 | *10* | 111.16 |
| *2* | 105.21 | *11* | 112.02 |
| *3* | 105.71 | *12* | 112.54 |
| *4* | 106.55 | *13* | 113.93 |

The $4d$ absorption spectrum of $PrF_3$ vapour.

Figure 5.7

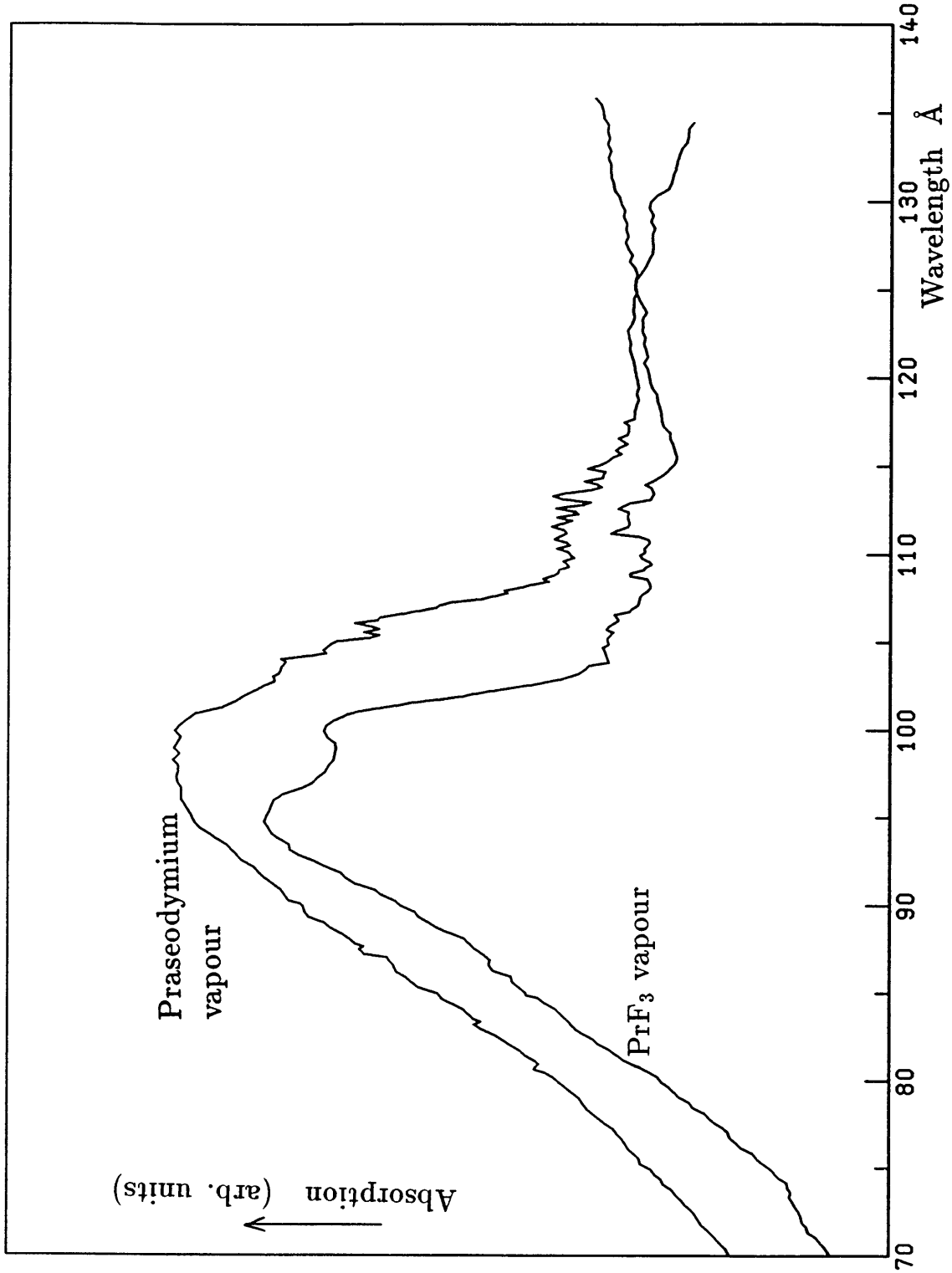


Comparison of the Praseodymium and $PrF_3$ spectra.

Figure 5.8

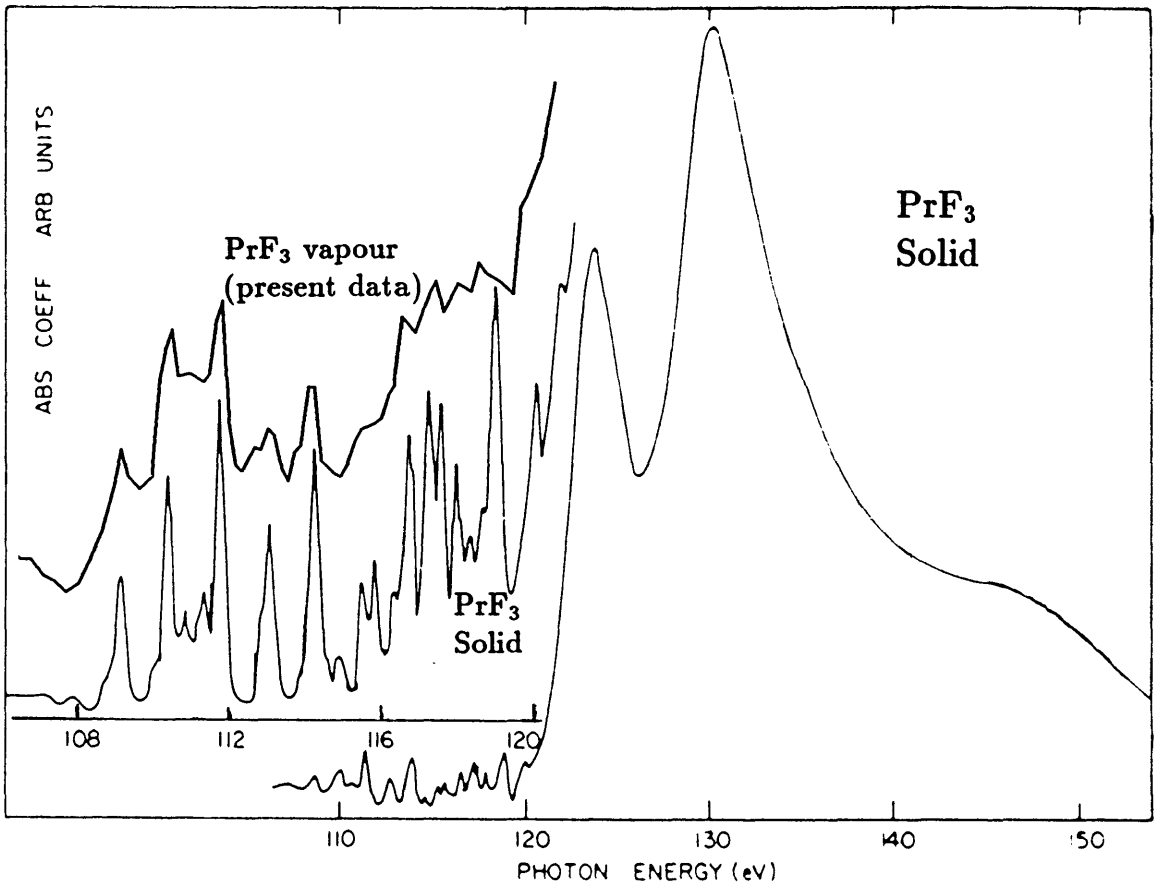


Absorption spectrum of solid $PrF_3$
(after Olson and Lynch 1982)

Figure 5.9

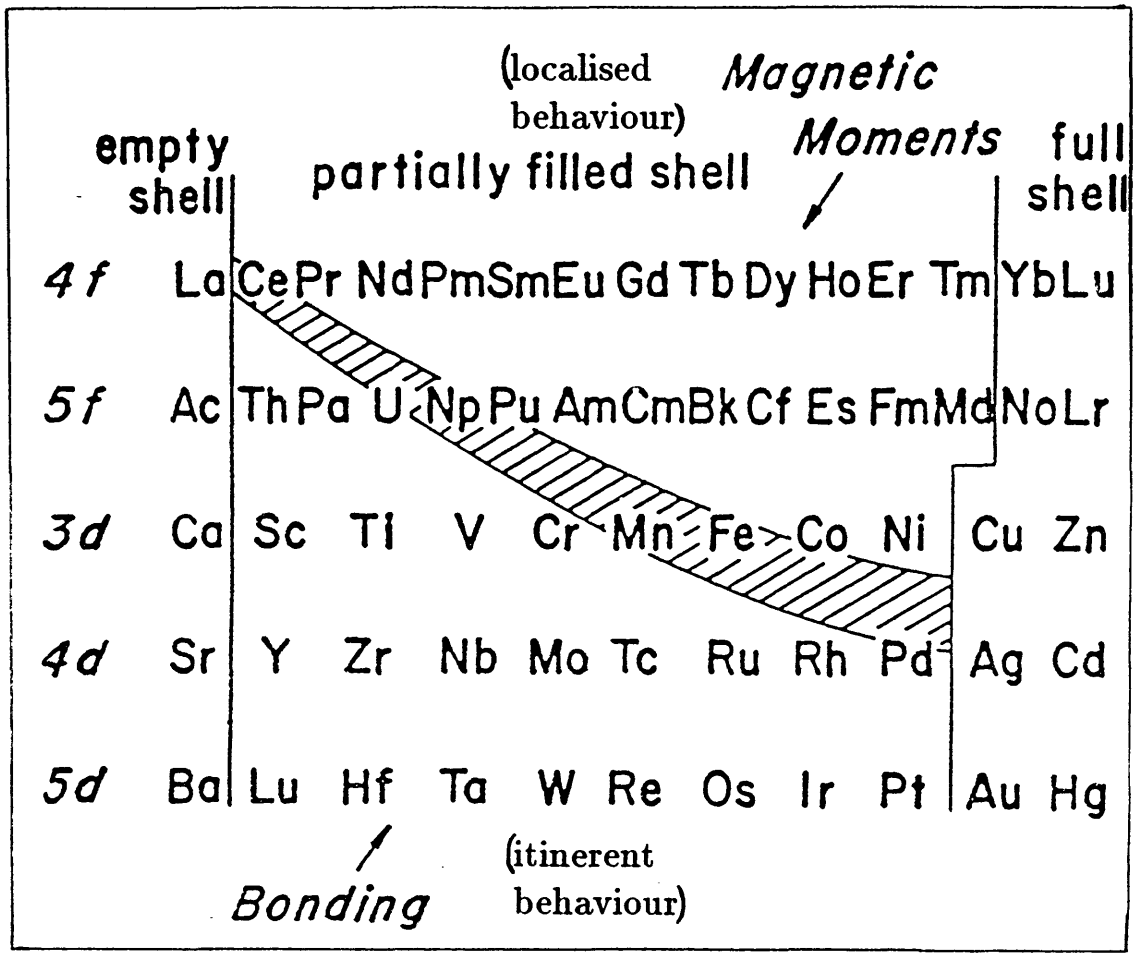


The five long periods arranged in order of increasing localisation. The boundary between conductivity and magnetism can be traced empirically down the diagonal of this table.

The Pseudo-periodic table
(after Smith and Kmetko 1983)

Figure 5.10

# Chapter VI

# Gadolinium and its fluoride $GdF_3$

## 6.1 Summary

In this chapter we present a case of a *pure* profile and we see how identical the *giant resonance* remains in going to the fluoride.

A simple theory with which the giant resonance profile can be reproduced is introduced based on the ideas of quantum scattering and effective range theory.

We present a universal curve for giant resonances and show the connection with giant resonances dropping below threshold, and the associated concept of controlled collapse.

## 6.2 Introduction

It is perhaps of interest to note that gadolinium is the only element other than the ferrous element to be ferromagnetic. Investigations of gadolinium metal and solid $GdF_3$ using a number of techniques have been reported. For example, Kowalczyk et al (1974) obtained 4d photoemission spectra of gadolinium. Similarly Gerken et al (1981) used the combined techniques of photoemission and electron excited Auger spectroscopy. Absorption spectra exist only from the pioneer work of Fomichev et al (1967) for metallic gadolinium, Olson and Lynch (1982) for $GdF_3$, and the work of Cukier et al (1980) for both.

However an absorption spectrum for gadolinium vapour was not available because of the extremely corrosive nature of the Gd liquid, and excluding promethium was the only atomic spectrum missing from the lanthanide series. We obtained the spectrum by containing the metal in a tungsten boat that was placed in a split tungten tube, the 1 mm gap being sealed with a strip of carbon foil. This assembly was placed inside our inductively heated furnace, as explained in chapter three (see figure 3.7).

## 6.3 Gadolinium and $GdF_3$

The absorption spectrum of gadolinium vapour in the wavelength region 50–120 Å is shown in figure 6.1 and that of $GdF_3$ in figure 6.2. It is immediately apparent that unlike the previous spectra of cerium and praseodymium, the giant resonance exhibits a *pure* profile. The multiplet structure present appears on the longer wavelength side of the resonance without distorting the giant resonance.

The close correspondence between the spectra of gadolinium vapour and the trifluoride vapour is demonstrated by direct superposition in figure 6.3. The reason for the almost identical spectra lies in the ground state configuration of neutral gadolinium, which is

$$4d^{10}\,4f^{7}\,5d6s^{2}\quad (^{9}\mathrm{D}_{2}^{0})$$

A $4d$ electron is being excited in this wavelength range and it interacts with the half-filled $4f$ shell and its associated continuum leading to the large absorption resonance, as already outlined in the previous chapters.

Non-relativistic Hartree–Fock analytical wavefunctions for $Gd^{+}$ have been calculated by Freeman and Watson (1962). Figure 6.4 plots the radial charge density as a function of $r$ for $4f$, $5s$, $5p$ and $6s$ electrons. This vividly illustrates that the $4f$ shell is indeed deeply imbedded inside the $5s$ and $5p$ shells, and are thus relatively unaffected by the valence $6s$ electrons.

Cukier et al (1980) have reported the spectrum of gadolinium metal and $GdF_3$ solid, and these too are almost identical to our spectra. The predominantly trivalent nature of gadolinium means that the $5d6s^2$ electrons are removed in the metal $Gd^{3+}$ ion, and are also the valence electrons involved in bonding in the trifluoride molecule. That our atomic spectra agree so well with the solid state data verifies our reasoning that the giant resonance is not unduly complicated by interactions with the valence electrons.

The wavelength values of the observed lines are included in the respective figure. We do not presume to identify the transitions involved in our spectra. As in the other lanthanide spectra we assume the giant resonance to arise from the localisation of a $\varepsilon f$ final state in the inner well region and this effect dominates the absorption to the extent that structure from other final states does not manifest itself.

The small energy shift between the atomic and $GdF_3$ spectrum is similar to that for the other lanthanide trifluorides, and could possibly be a purely chemical shift or result from the removal of the valence electrons, in particular of the $5d$ electron.

We however consider the essentially unperturbed cross-section of the giant resonance to be the feature of main interest.

## 6.4 The Giant Resonance Profile

Hitherto (Gerken et al 1982), the profile of the $4f$ partial photoionisation cross-sections (the main component of the giant resonance) for gadolinium has been fitted with a Beutler–Fano profile. Examination of the theoretical fit and the experimental curve reveals that agreement is not exceptional. The typical minimum of the Fano profile is not evident in the empirical data, and the agreement on the high energy side is poor.

This really highlights the intrinsic difference between an autoionising line profile and the giant resonance which leads to a quite different line profile. Let us first look at the reason why an autoionising state occurs.

### 6.4.1 Autoionisation

Discrete states above the photoionisation threshold are stationary states only within the independent particle model, where the interaction between the discrete level and the continuum is neglected. If this so-called configuration interaction is taken into account, then the discrete level will decay or autoionise. Thus the discrete state becomes broadened through configuration mixing effects and relies on two distinctly seperate channels. The breadth of the line depends on the strength of the interaction and in principle it could be turned down to zero, leaving a perfectly sharp structure. Fano (1961) analysed the lineshape and is hence known as the *Fano profile*

in the literature.

The configuration interaction $\mathcal{V}$ with the Hamiltonian $\mathcal{H}$, between the discrete level $\varphi$ and the continuum $\psi$, can be represented by the matrix element

$$\mathcal{V} = \langle \varphi \mid \mathcal{H} \mid \psi \rangle$$

Fano (1961) obtained for the cross-section $\sigma(\epsilon)$ the parametrisation

$$\sigma(\epsilon) = \sigma_b + \sigma_a \frac{(\epsilon + q)^2}{\epsilon^2 + 1}$$

where $q$, the line profile index, is a constant and $\sigma_b$ and $\sigma_a$ are slowly varying functions of energy $\epsilon$, with

$$\epsilon = \frac{E - E_o}{\Gamma}$$

$E_o$ being the resonance energy and $\Gamma$ is the half-width of the resonance which characterises the lifetime $\tau$ of the quasi-discrete state

$$\tau = \frac{\hbar}{2\Gamma}$$

Figure 6.5 shows the so-called Fano lineshape and how it changes for various values of the channel interaction parameter $q$, and one sees that the minimum in the cross-section occurs close to the resonance energy.

In contrast giant resonances encorporate a fundamental difference in that they arise from a single channel effect, due to the radial potential of the atom possessing a short-range inner well almost sufficiently binding to trap an eigenfunction of its own, which leads to a *semi*-virtual state. Thus we do not have a bound state and hence no way of decoupling it from the continuum, of which it is an integral part. This yields a profile of a profoundly different form to the Fano profile.

We now wish to introduce a general formula for the profile of a giant resonance. The simple theory is related to the concept of quantum scattering and effective range theory.

### 6.4.2 A General Formula for Giant Resonances

The term *giant resonance* originates from nuclear scattering to describe abnormally large cross-sections observed in certain scattering processes near threshold. It is therefore fruitful to look more closely at the analysis of such nuclear processes and to draw comparisons, and relate the physics involved, to the atomic processes we are interested in.

The scattering of non-relativistic particles by a spherically symmetric rectangular well was considered as far back as 1930 by Guido Beck (1930), in connection with the Ramsauer-Townsend effect. He observed that ... *when the well depth decreases, the bound levels are pushed into the continuous spectrum giving rise to broad virtual levels.*

Similarly the virtual level of the deuteron was suggested by Wigner and Eisenbud (1947) to account for the large cross-section in neutron–proton scattering.

Resonances are not uniquely defined in in the literature and there have been several such attempts to define a *virtual level* at small energy and the arguments are given in the context of effective range theory. The crucial ingredient in such a partial wave analysis is the assumption of spherical symmetry of the scatterer. In nuclear physics only partial waves of low angular momentum contribute to the scattering cross-section and phase-shift, and in fact at low energies the $\mathcal{S}$-wave scattering ( $\ell = 0$ ) dominates. The reason is that the larger the angular momentum, the more formidable is the potential barrier due to the centrifugal force, and the harder it is for the particles to penetrate to the central region where most of the potential energy is concentrated, and so participate in the scattering. In this case the cross-sectiom depends only on the range and depth of the potential and is hence known as the *shape independent* approximation. It is only at higher energies that the higher partial waves become important, but there the effective range theory begins to break down and is thus not applicable.

Also crucial for identifying an authentic resonance is that the phase shift should *increase* sharply through $\pi/2$ with increasing energy, with a *total* change in value of the phase shift of a little under $\pi$ (see figure 6.6).

Connerade (1984) has related the analogy between effective range theory and the atomic giant resonances as follows.

If we consider a square well

$$V(r) = \begin{cases} -D & \mathrm{r} < \mathrm{a} \\ 0 & \mathrm{r} > \mathrm{a} \end{cases}$$

then the dimensionless parameters

$$z' = \kappa' a = [\,2m(\,E + D\,)\,]^{\frac{1}{2}}\, a\hbar$$

and

$$z = \kappa a = (\,2mE\,)^{\frac{1}{2}}\, a\hbar$$

correspond to the wave number inside and outside the potential well.

A formula for the scattering phaseshift $\delta_\ell$ in the continuum of such a square well is given by Mott and Massey (1965, p.35 eqn. (37)) which when converted into spherical Bessel functions and for $\ell = 3$ becomes

$$tan\,\delta_3 = \frac{z j_3(z') j_2(z) - z' j_3(z) j_2(z')}{z j_3(z') j_{-3}(z) + z' j_{-4}(z) j_2(z')} \tag{6.1}$$

Explicit formulae for numerical evaluation in terms of elementary functions can be obtained by using standard formulae (Abramowitz and Stegun 1964)

$$j_n(z) = f_n(z)\sin(z) + (-1)^{n+1} f_{-n-1}(z)\cos(z)$$

where

$$f_2 = \left(\frac{3}{z^3} - \frac{1}{z}\right) \quad f_{-3} = \frac{3}{z^2}$$

$$f_3 = \left(\frac{15}{z^4} - \frac{6}{z^2}\right) \quad f_{-4} = -\left(\frac{15}{z^3} - \frac{1}{z}\right)$$

It is thus an easy matter to calculate the phaseshift $\delta_3$ and hence also the cross-section $\sigma(\kappa)$

$$\sigma(\kappa) = \frac{28\pi}{\kappa^2}\sin^2\delta_3$$

having used only two parameters, namely $D$ the well depth, and $a$ the radius.

We can further define a well range-depth parameter $A$

$$A^2 = \frac{2m}{\hbar^2} a^2 D$$

Figure 6.7 shows the fit obtained for gadolinium with $a = 1.89$, and $D = 3.40$ (in atomic units). Where the atomic unit of length is $a_0 = 0.53$ Å

(the Bohr radius) and the atomic unit of energy is $e^2/4\pi\epsilon_0 a_0 = 27.2\,\mathrm{eV}$ (a Hartree). A sloping background was necessary for the fit. This points to the fact that the calculated cross-section is only that for the $f$ partial-wave and that other partial-waves also contribute in the real spectrum, leading to the additional absorption. We conclude that the simple formula (6.1) that Connerade (1984) first applied to this area of physics gives a remarkably good representation of the giant resonance. In reality though the situation is probably more complex and involves a mixture of single and two-channel processes. The subject of scattering at low energies is also clearly presented by Gasiorowicz (1974, p.388*ff*).

A progression of such profiles as calculated by Connerade (1984) are shown in figure 6.8 together with the path of the unitary limit $\mathrm{E}^{-1}$. Connerade (1984) notes that as $\kappa \to 0$, $\sigma(\kappa) \to 0$, provided that $\ell \neq 0$ which means that a zero in the partial cross-section occurs at threshold, which is not necessarily close to the resonance energy. This is in marked contrast to a Fano profile where the minimum in cross-section is not tied to the threshold, and instead is linked to the resonance energy and the interaction strength, and occurs close to the autoionising line.

In figure 6.9 we show the calculated phaseshifts with the calculated fit for gadolinium vapour and we see that the change in value of the phase shift is large. So the peak does qualify as a resonance in the true sense of scattering theory. Thus with our data we show that a giant resonance occurs in the $d^{10} \longrightarrow d^9 f$ singlet channel above the associated $4d$ ionisation limit in both the atomic and the trifluoride vapour (Connerade and Pantelouris 1984).

## 6.5 A Universal Curve

Let us now pause to reflect on what a resonance implies in a scattering regime. It corresponds to the physical situation whereby the incident particle is captured by the target to form a long-lived compound state, before emerging again. Thus a resonance by its very nature will give rise to a time delay.

By appealing to the uncertainty principle an empirical universal curve has been obtained by Connerade (1984) which plots the resonance width at half maximum against the energy of the maximum referred to threshold

This is shown in figure 6.10. It is of use when the atomic threshold is not known, since we are able to work backwards from the experimental resonance width to obtain an indication of its magnitude.

This very simple model is remarkably successful in interpreting the available data. It applies however to virtual states in the continuum and hence above the potential barrier level. If the level drops below the top of the barrier it is no longer a true continuum state but can decay by tunneling through the barrier, and if it drops further it will eventually become bound. Connerade (1978a) has suggested an experiment on *controlled collapse*, which by exciting an outer electron to various states of a Rydberg series, the localisation of another electron can be influenced. This possibility has been predicted on the basis of Hartree–Fock calculations for the caesium $4f$ wavefunction, and the effect of progressively exciting an outer electron is to perturb the inner well.

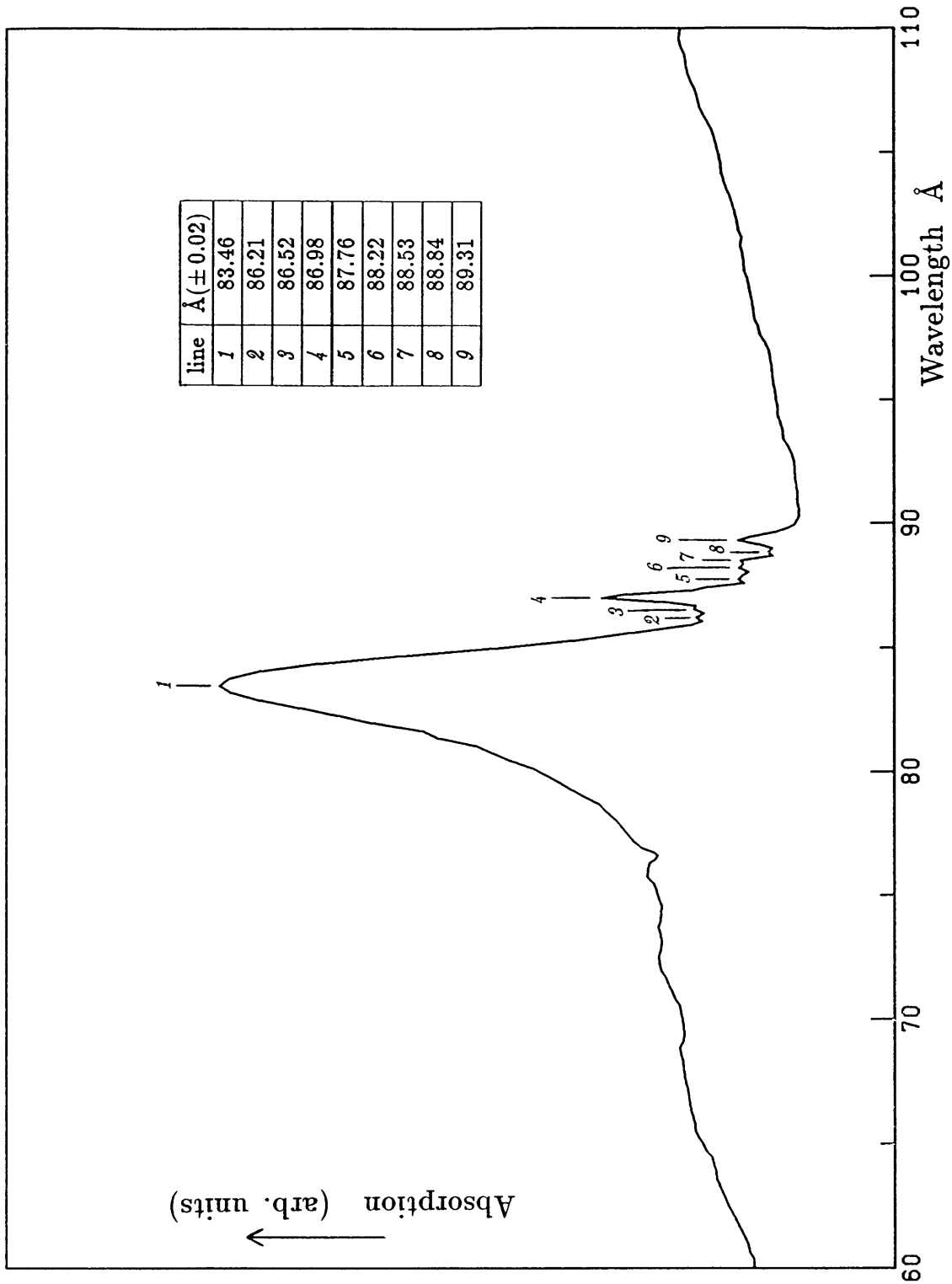


The $4d$ absorption spectrum of gadolinium vapour.

Figure 6.1

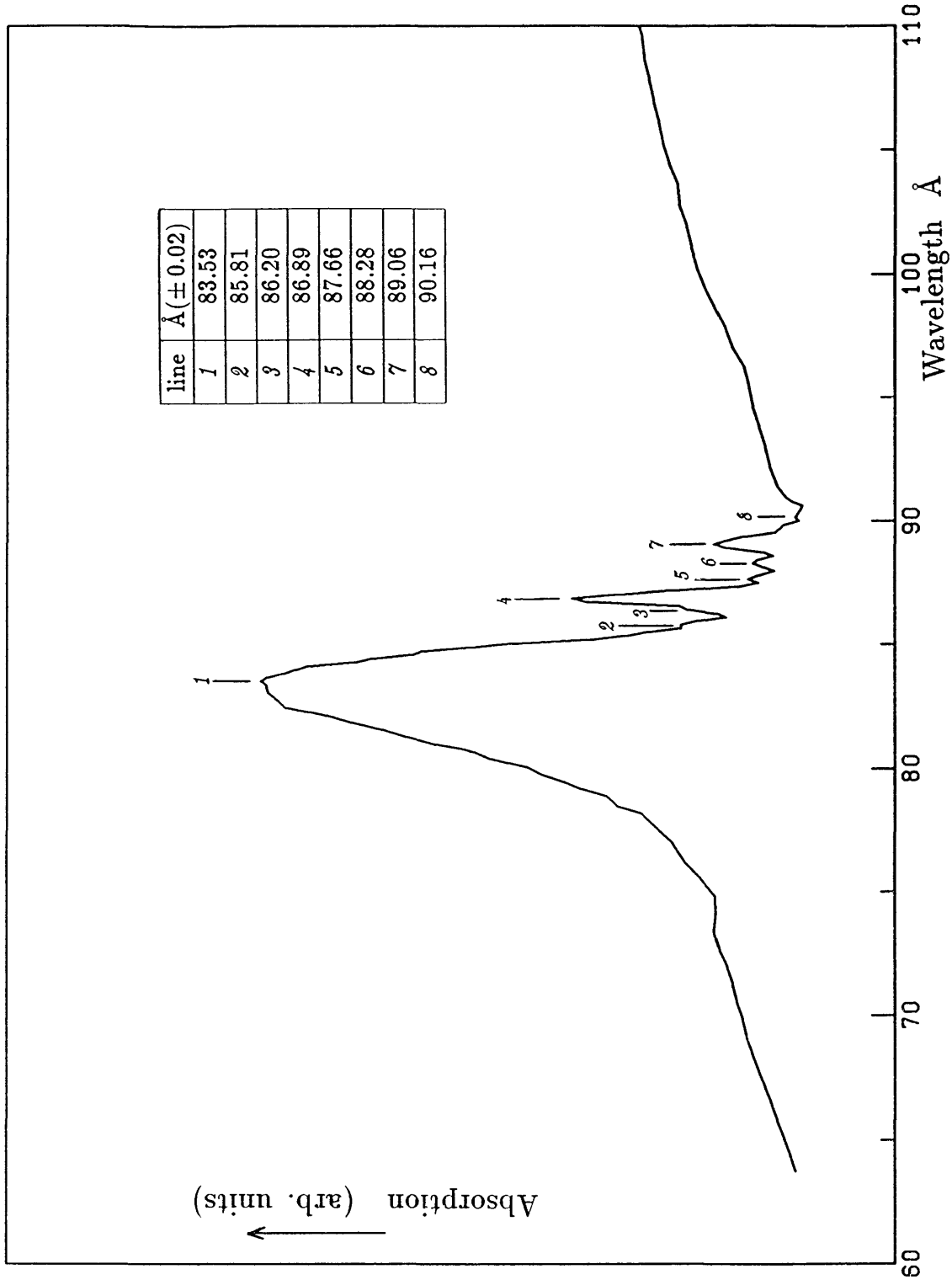


The $4d$ absorption spectrum of $GdF_3$ vapour.

Figure 6.2

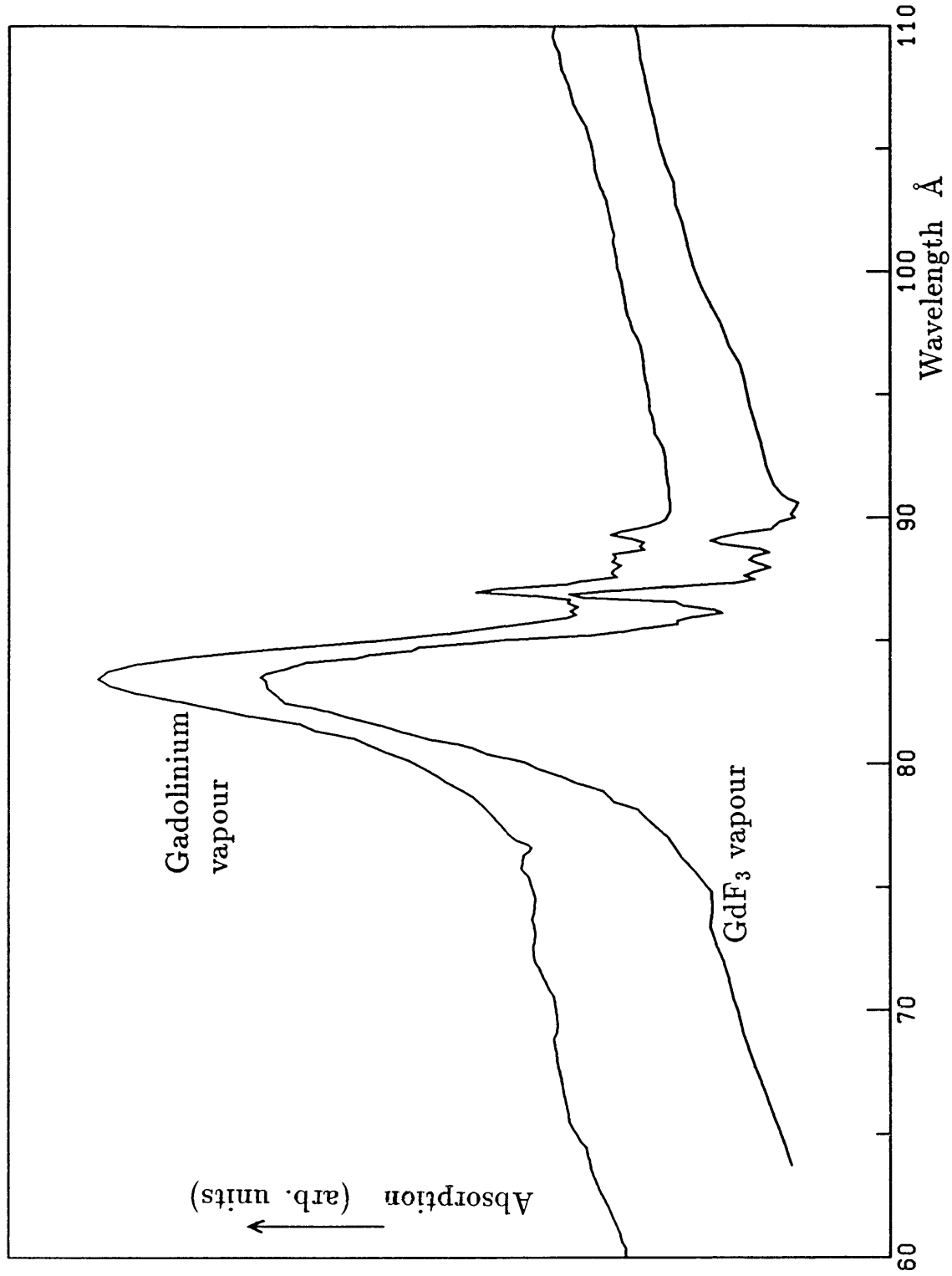


Comparison of the Gadolinium and $GdF_3$ spectra.

Figure 6.3

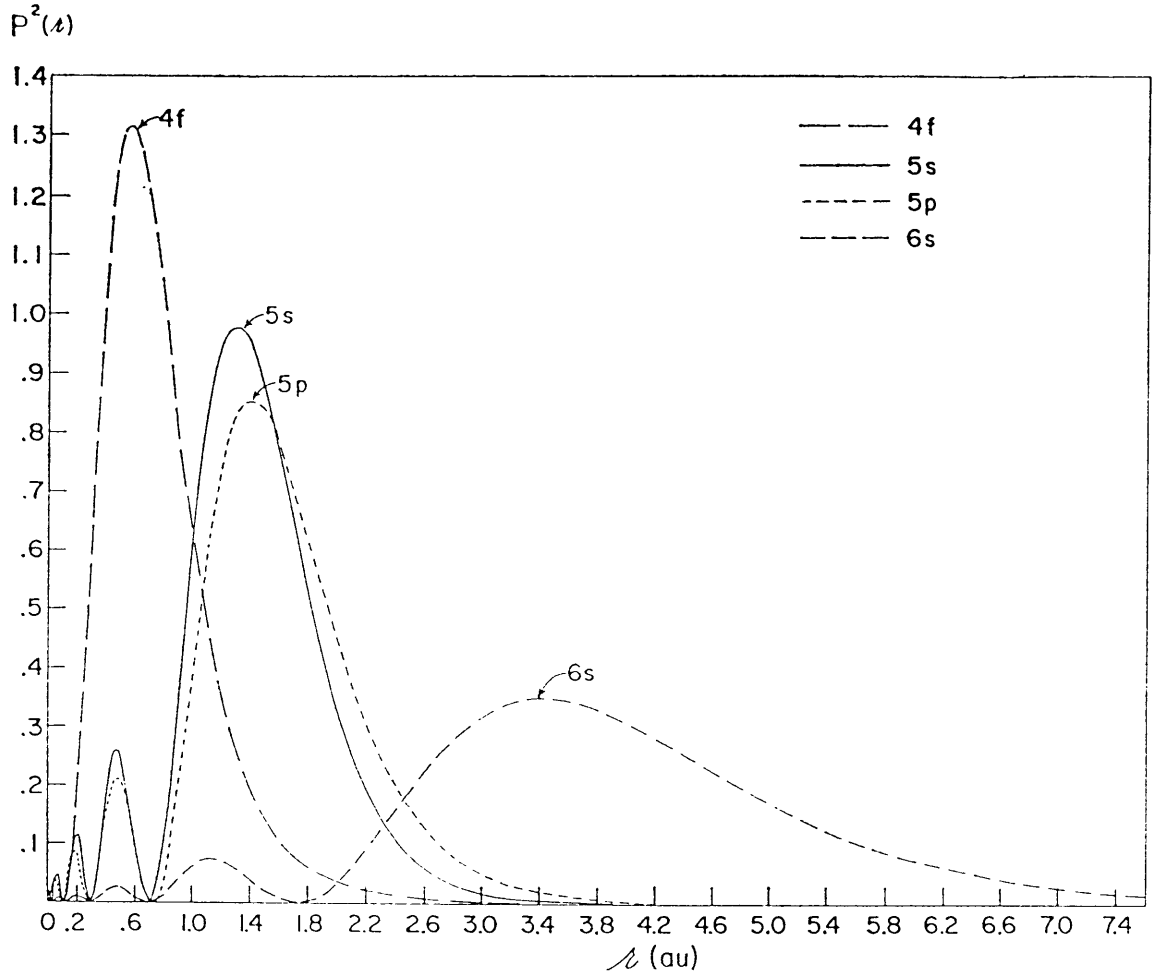


The radial charge distribution for the $4f$, $5s$, $5p$, and $6s$ electrons of $Gd^+$.

(from Freeman and Watson 1962)

Figure 6.4

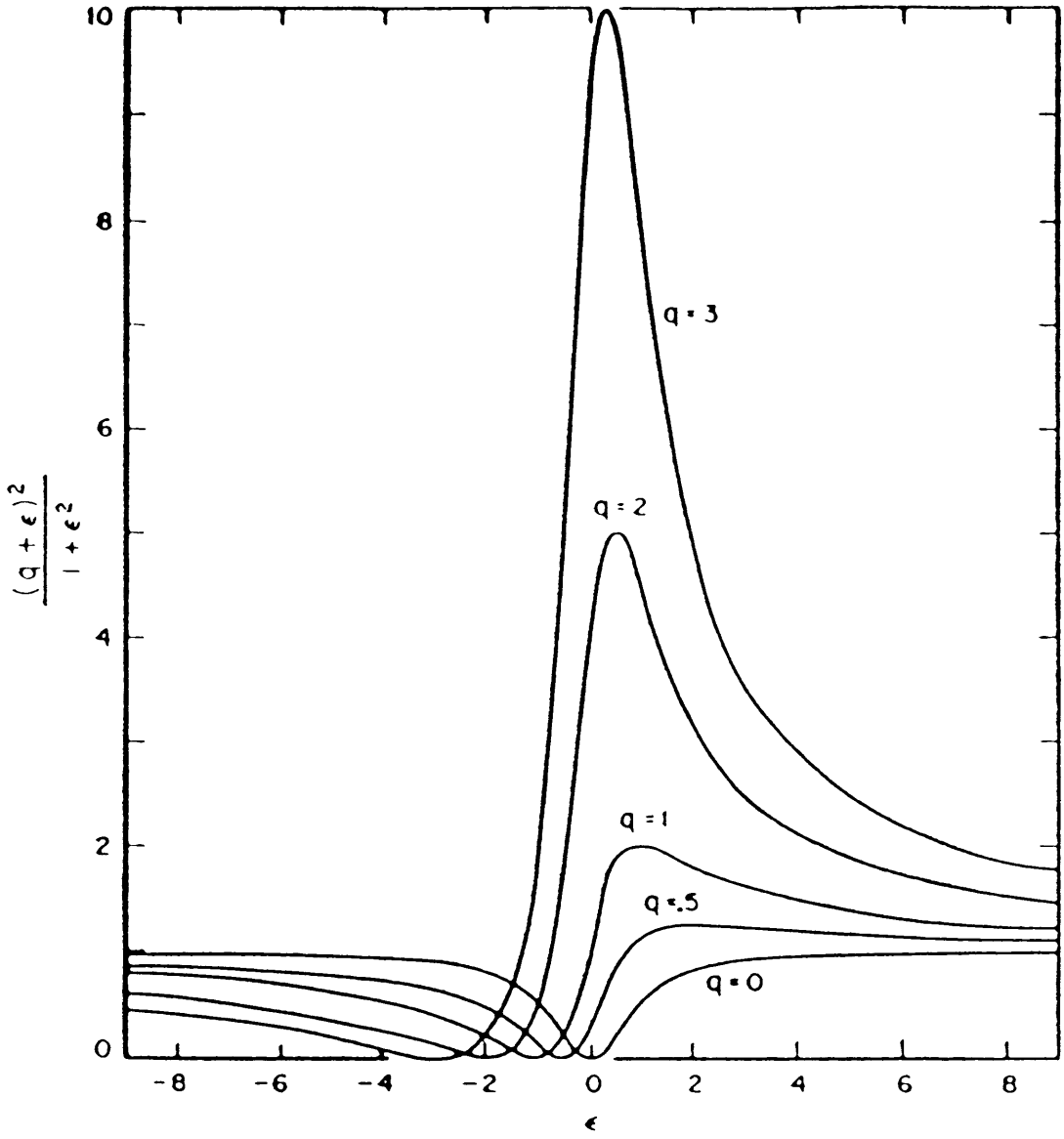


The zero in the cross-section is linked to both the resonance energy and the interaction strength and generally occurs near to the autoionising line.

Fano lineshapes for various values of the parameter $q$.

(from Fano 1961)

Figure 6.5

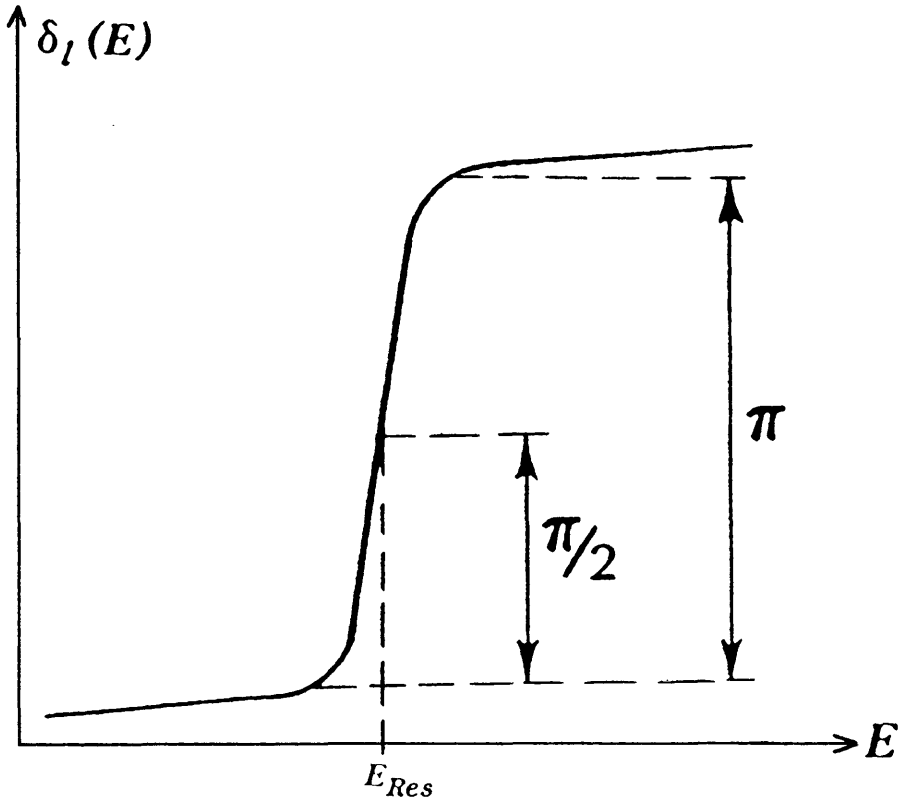


Schematic representation of the partial-wave phase shift of $\pi$ associated with a resonance.

Figure 6.6

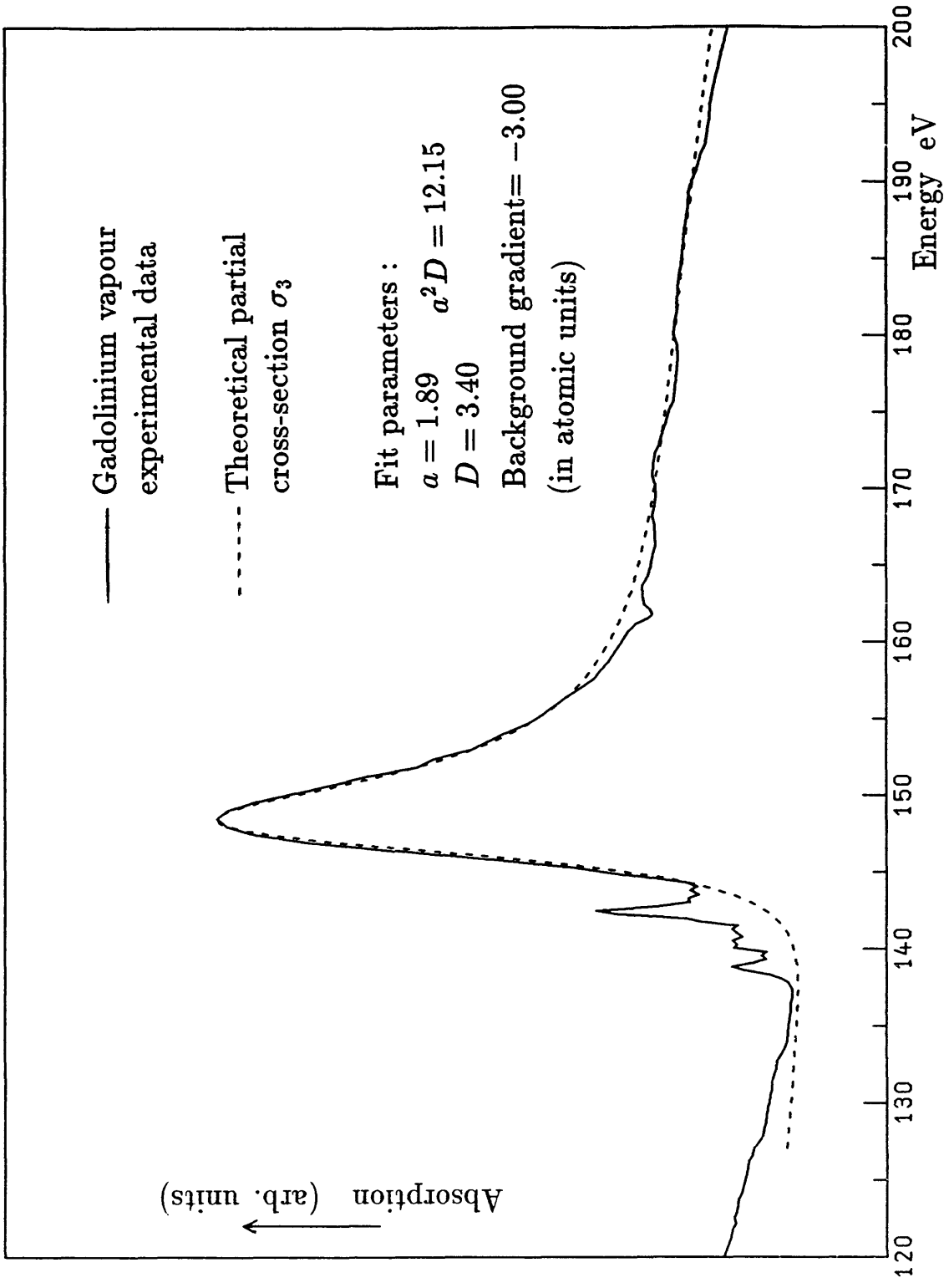


The fit to the experimental data for gadolinium vapour using formula (6.1) and the parameters $a = 1.89$, $D = 3.40$

Figure 6.7

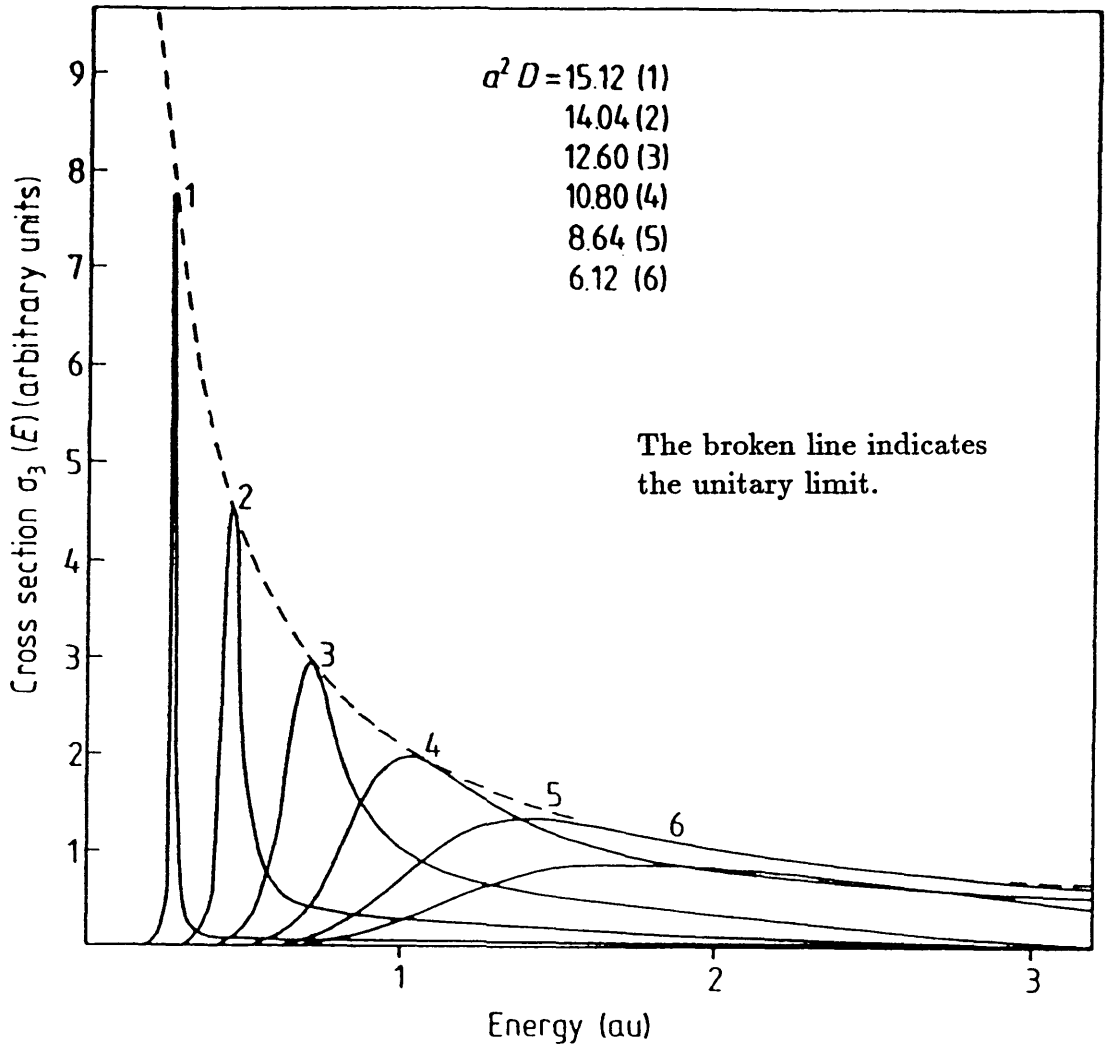


In contrast to the autoionisation profile, the zero in the cross-section occurs at threshold, which is not necessarily close to the resonance energy.

A plot of the evolution of the profiles as calculated from equation (6.1), for different strengths of the scattering potential.
(from Connerade 1984)

Figure 6.8

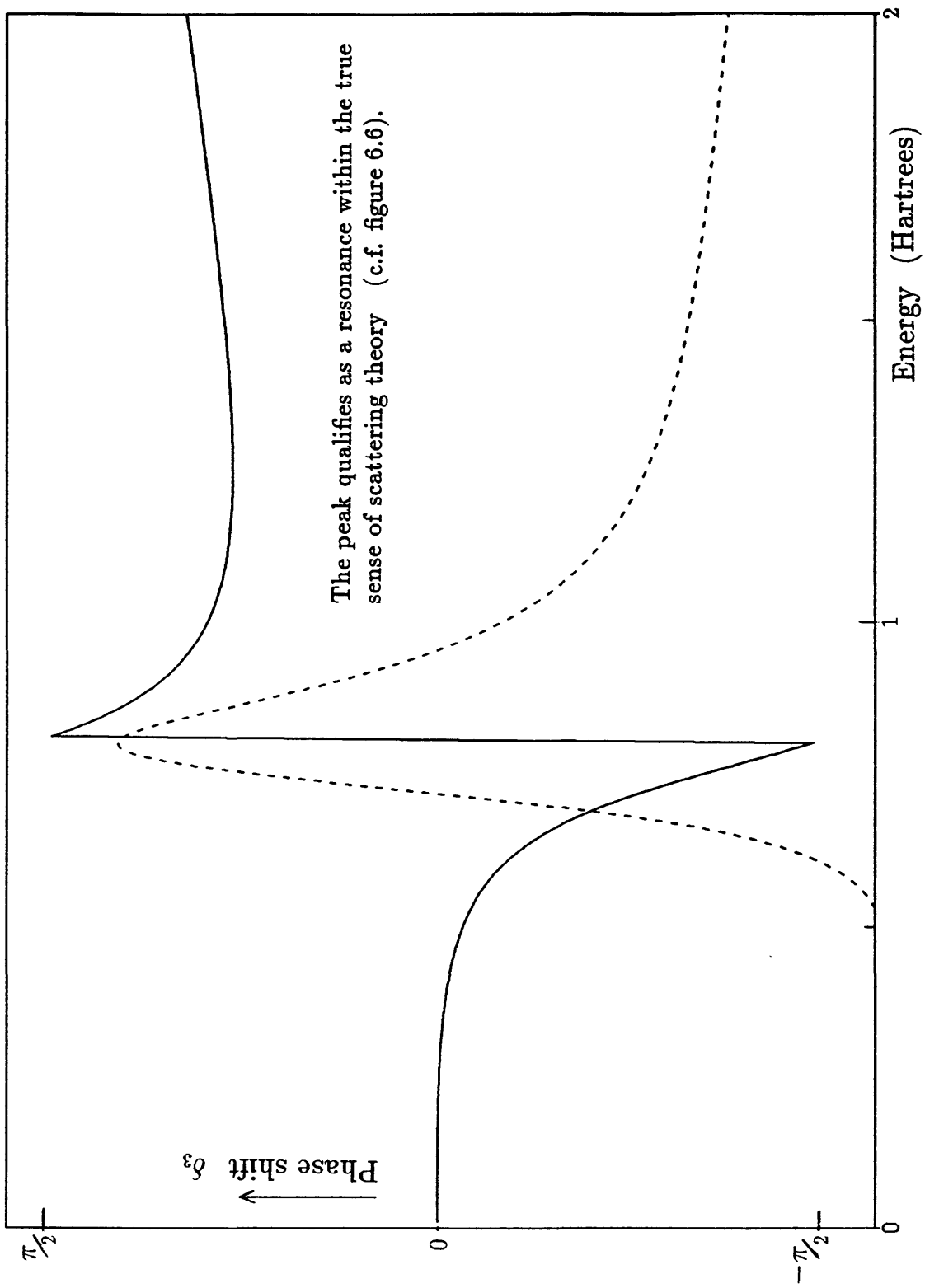


The calculated phase shift $\delta_3$ for gadolinium together with the calculated resonance profile.

Figure 6.9

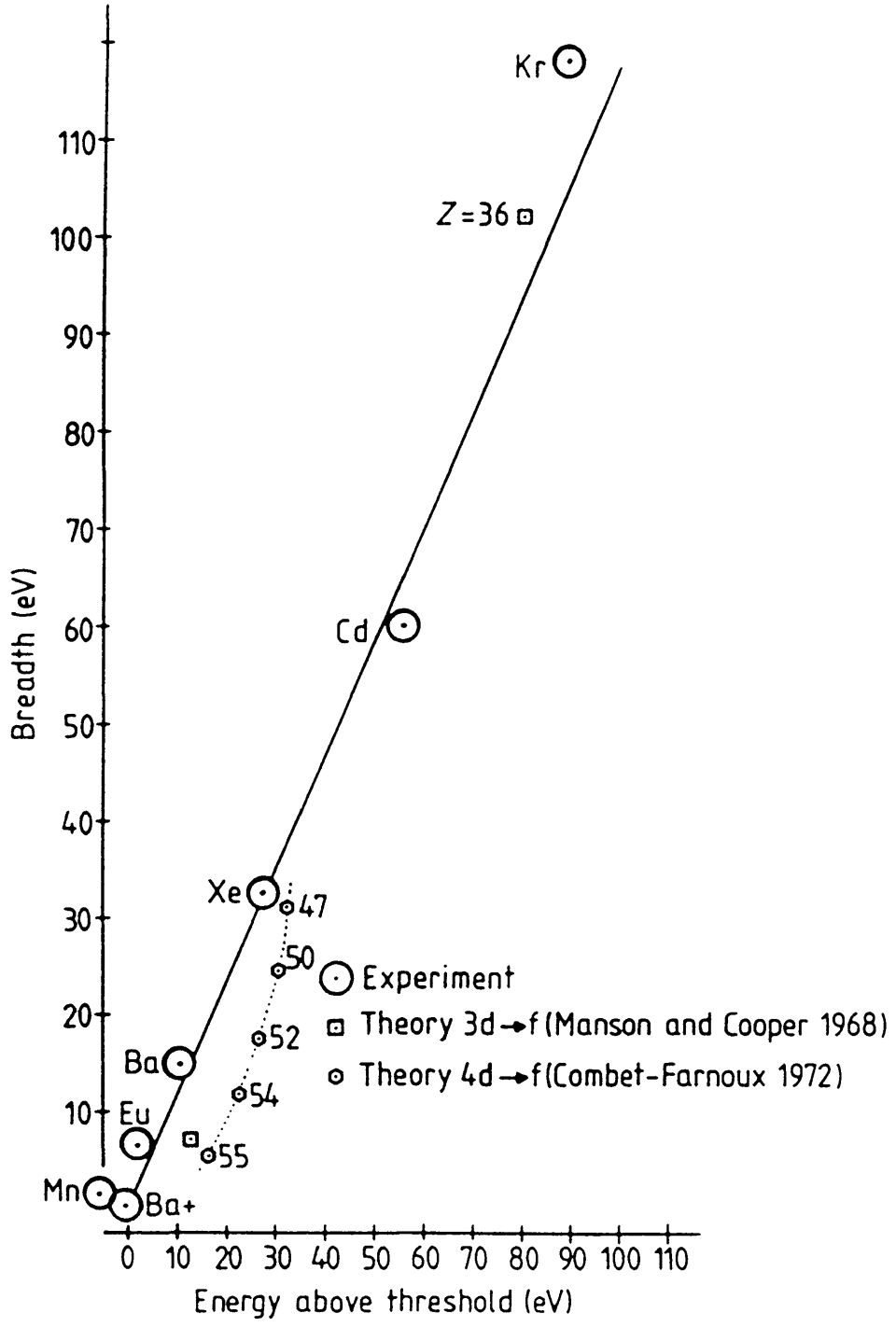


A universal curve for giant resonances showing the resonance width at half maximum against the energy of the maximum referred to threshold.
(from Connerade 1984)

Figure 6.10

# Chapter VII

# The Tetrafluorides of Thorium and Uranium

## 7.1 Summary

A *giant resonance* feature dominates the absorption spectra of $ThF_4$ and $UF_4$, due to excitation of a $5d$ electron to a resonantly localised $\overline{5,\varepsilon f}$ continuum state. The lack of experimentally determined binding energies for the actinides is discussed.

## 7.2 Introduction

Work in France had produced data on solid thorium and uranium (Cukier et al 1974), but it was debatable if the observed spectra were atomic in nature. The $5f$ situation was considered to be different ~~the~~ from $4f$'s before the present experiments. Solid state physicists were inclined to argue that the $5f$ wavefunction in solids is not quasi-atomic because it is less localised. Because the $5f$ wavefunctions have an extra node and extend into the outer well, they ought therefore be influenced much more by the external environment. So the original interpretation of the French data by some, was that it was due to solid state effects. Others who held for a quasi-atomic view were unsure as to the extent of the solid state influence.

The clinching experiment was to vapourise $ThF_4$ and $UF_4$. We present our data and qualitatively interpret them. Because the $ThF_4$ spectrum is also of *pure* profile, we give a fit using the effective range theory introduced

in the previous chapter.

## 7.3 The Actinides

A feature common of both the actinides and the lanthanide elements is the occurence of partially filled $f$ shells. This leads us to expect a certain similarity to manifest itself when we look at the transitions to the $5f$ shell in the actinides. However, unlike the $4f$ electrons in the lanthanides, the $5f$ orbitals of the actinides extend spatially into the outer valence regions of the atom. Hence because they are less localised and extend into the outer well of the effective radial potential, they are less effectively shielded by the outer electrons, and should have lower binding energies than is the case with the $4f$ electrons. Thus in marked contrast to the lanthanides, these factors enable the actinides to form a wider range of compounds, and although $f$ electrons are not as important as $d$ orbitals in bonding, the contribution of the former cannot be neglected (Brown 1968).

It is well known that the actinide elements exhibit a much greater tendency to exist in multiple oxidation states than do the lanthinides elements. Uranium ( $5f^36d7s^2$ ) forms for example the largest number of halides with a great multiplicity in oxidation state. It also forms compounds known as *intermediate fluorides* of fractional valence. Thorium ( $6d^27s^2$ ) on the other hand gives no indication of existing in any other than a tetravalent state (Katz and Sheft 1960).

This lends weight to the statement above, that the stability of these multiple valence states and ions is attributable to $f$ orbital participation. It must however be stressed that the electronic structure of uranium compounds is very complex and attempts to study it thoroughly are still rather limited. Indeed there is much discussion about the role and nature of the $5f$ electrons in the actinide series in general.

For example, uncertainties in the electronic configuration of the lighter actinides arise because the $6d$ and $5f$ binding energies are very similar even in uranium. It can be said that much of what is known of the electronic configuration of the actinides has been learned from experiments with their halides (Bagnall 1967). Uranium has the largest and perhaps the most studied array of halides of any of the actinide elements. Particularly the hexafluoride $UF_6$ is of considerable technological significance, primarily for

uranium isotope enrichment and hence unfortunately for its subsequent military applications.

## 7.4 Thorium and Uranium Tetrafluorides

Absorption spectra of $UF_4$ in the visible spectral range date back to 1954 (Gruen and Fred 1954), which reflects the ease with which this fluoride compound can be handled. The work on the actinide tetrafluorides presented in this chapter was originally the first to be undertaken in the course of this study. The success and experience so collected spurred us to follow this line of work and to investigate further the lanthanides as described in the previous chapters.

In figure 7.1 we present the absorption spectra we obtained for $ThF_4$ vapour, and figure 7.2 that of $UF_4$ vapour, both in the energy range 70–150 eV.

The spectra exhibit two large peaks in the range of $5d$ electron excitations, typical features which are very similar in the two actinide fluorides. However in $UF_4$ clear structure within the peaks is evident, and the shoulder at 97 eV in the $ThF_4$ spectrum is real, being present on all plates.

A rigorous interpretation for these absorption peaks is not really possible, other than attributing them to transitions from the $5d$ shell. However comparison with the lanthanides does make it possible to draw a similar qualitative picture.

But first let us compare the corresponding solid state photoabsorption spectra of the metal (Cukier et al 1978) with our fluoride vapour spectra (figures 7.3 and 7.4). It was held possible that the surroundings about the metal ions would influence the $5f$ states much more profoundly than in the rare earths, and that these solid state effects could broaden the $5d \longrightarrow 5f$ transitions. However the comparison with our fluoride vapour data invalidates this argument. Thus as in the case of the lanthinides, all the spectra have a common atomic origin, in this case transitions to $\overline{5, \varepsilon f}$ resonantly localised continuum states.

We see that the agreement between the metal and the fluoride vapour of thorium is almost perfect (figure 7.3). This is perhaps not so surprising since the situation for thorium is comparable to that of gadolinium in the rare earths. As thorium is tetravalent, the electronic configuration in the

metal ion and in the fluoride is the same, with the four ( $6d^2 7s^2$ ) valence electrons either in the conduction band or transferred to the halide ion. Thus the spectrum is not complicated by structures due to interactions with open valence shells. There is also no shift in energy between the two spectra indicating that the inner well where the $5f$ wavefunctions are localised is unaffected by the chemical environment. Although the geometry of the fluoride molecule in the gas phase has not as yet been conclusively determined, electron diffraction studies indicate that they have a distorted trapezoid structure (Dyke et al 1980) with all metal–halogen inter-nuclear distances equal (eg. U—F bond length is 1.994 Å ). We thus have a sort of fluorine *cage* surrounding the metal atom (Rosen 1979) which does not have a large effect.

On the other hand, the spectrum of $UF_4$ vapour displays much more structure within the peaks and there is a real shift of about 1 eV between the metal and the molecular spectrum (figure 7.4).

Thus thorium probably provides the purest $5d \longrightarrow \overline{5,\varepsilon f}$ giant resonance yet investigated (Connerade et al 1980). A fit of the profile, using the procedure outlined in the previous chapter is shown in figure 7.5, with $a = 1.84$ and $D = 3.60$ (atomic units). In comparison to gadolinium (figure 6.7) the well is somewhat narrower and deeper.

Along the lanthanide sequence we observed a gradual modification of the strong absorption maxima due to the excitation of the $4d$ electrons. With increasing atomic number, the maxima move to higher energies and the profiles become narrower. The latter is attributed to the increasing localisation of the $4f$ states as the $4f$ shell is filled. An actinide contraction entirely similar to this well-known lanthanide contraction is well established (Wybourne 1965).

It is therefore a surprising contadiction to observe that the thorium peaks are narrower than in uranium, indicating that $5f$ localisation is more pronounced in thorium. Although this broadening can partly arise from the interaction between unpaired valence electrons and the core hole, we cannot give a satisfactory explanation.

No relativistic multichannel *ab initio* calculations of the $5d$ cross-sections have been performed yet for elements as heavy as thorium and uranium. Calculations by Combet-Farnoux using average configuration Hartree–Fock wavefunctions have been quoted by Cukier et al (1978). The results suggest that for thorium the $5f$ states lie in the outer well (ie. not localised),

whereas only in uranium are they localised within the inner well. This does not correspond to our observed spectra. The inability of the independent particle model to make correct predictions shows how necessary it is to include many-body effects and, in heavy atoms such as the actinides, relativistic effects have a significant influence. The inclusion of many-electron correlations within a relativistic approach remains a challenge. We will touch on this point again in the next chapter.

## 7.5 The Question of Binding Energies

It is now important to turn our attention to the core level binding energies marked on our figures. They have been experimentaly determined by Fuggle et al (1974) and are the binding energies for the metal in the solid state:

| *Binding energies in eV* | | |
|---|---|---|
| | $5d_{3/2}$ ( $O_{IV}$ ) | $5d_{5/2}$ ( $O_V$ ) |
| Thorium | 92.5 | 85.4 |
| Thorium oxide | 94.0 | 87.0 |
| Uranium | 102.8 | 94.2 |
| Uranium oxide | 104.9 | 97.1 |

Table 7a: The $5d$ binding energies for solid thorium and uranium

Experimental work from other workers (Siegbahn et al 1967, Park and Houston 1973 and Bancroft et al 1977) also exist, but there are major discrepancies in their results. The probable reason for this lies in the uncertainty of chemical composition, particularly of surface layers (oxidisation), and also non-rigorous calibrations. Fuggle et al (1974) investigated the effect of oxidation as also shown in table 7a. Confirmation of the above data for thorium is given in the more recent work of Aono et al (1981). However, these binding energies cannot simply be transferred to our spectra of the vapour phase.

Rigorously speaking, binding energy should be defined as the energy required to remove a specific electron completely from an atom, without changes in the $n\ell$ values of any of the other electrons.

Binding energies for solids are however only the energy required to move an electron from its particular orbit to the Fermi level in the solid. This energy has to be augmented by the electronic work function of the material, to remove the electron completely. There then remains to be taken into account the energy of extracting the resulting inner vacancy ion from the solid. Although no accurate values for the actinides exist, the former is of the order of 3–5 eV, and the latter is extremely difficult to estimate let alone to measure. Thus these corrections may total an appreciable 5–10 electron-volts, but in principle this shift should be the same for all thresholds. It is therefore not really possible to comment on the relative positions of the observed maxima in the vapours with respect to the $5d_{3/2}$ and $5d_{5/2}$ thresholds. However it does appear that in the case of solid thorium and uranium the two main transitions both occur above their associated thresholds. This is in contrast with the lanthanides where in the solid at least we know that only one transition lies above threshold (see figure 4.8).

We have as yet not considered how the binding energies shift within a molecular environment and in order to emphasise this whole point of uncertainties in binding energies we finally draw attention to the recent work of Mårtensson et al (1984) on $UF_6$. Their photoelectron spectrum of $UF_6$ recorded in the vapour phase is shown in figure 7.6. We have also added to the figure their measured binding energies for uranium in $UF_6$ also in the gas phase. Comparison with the values in the solid phase shows a shift of $\sim 11\,eV$ between the binding eneries for uranium in the metal and in the hexafluoride. This is even after taking into account a work function energy of $\sim 3.5\,eV$. However the whole spectrum has also been shifted unlike the tetrafluoride spectrum. We can offer no explanation for this, and we will not consider $UF_6$ further, but it serves to emphasise our point. We will consider further the question of binding energies in the next chapter.

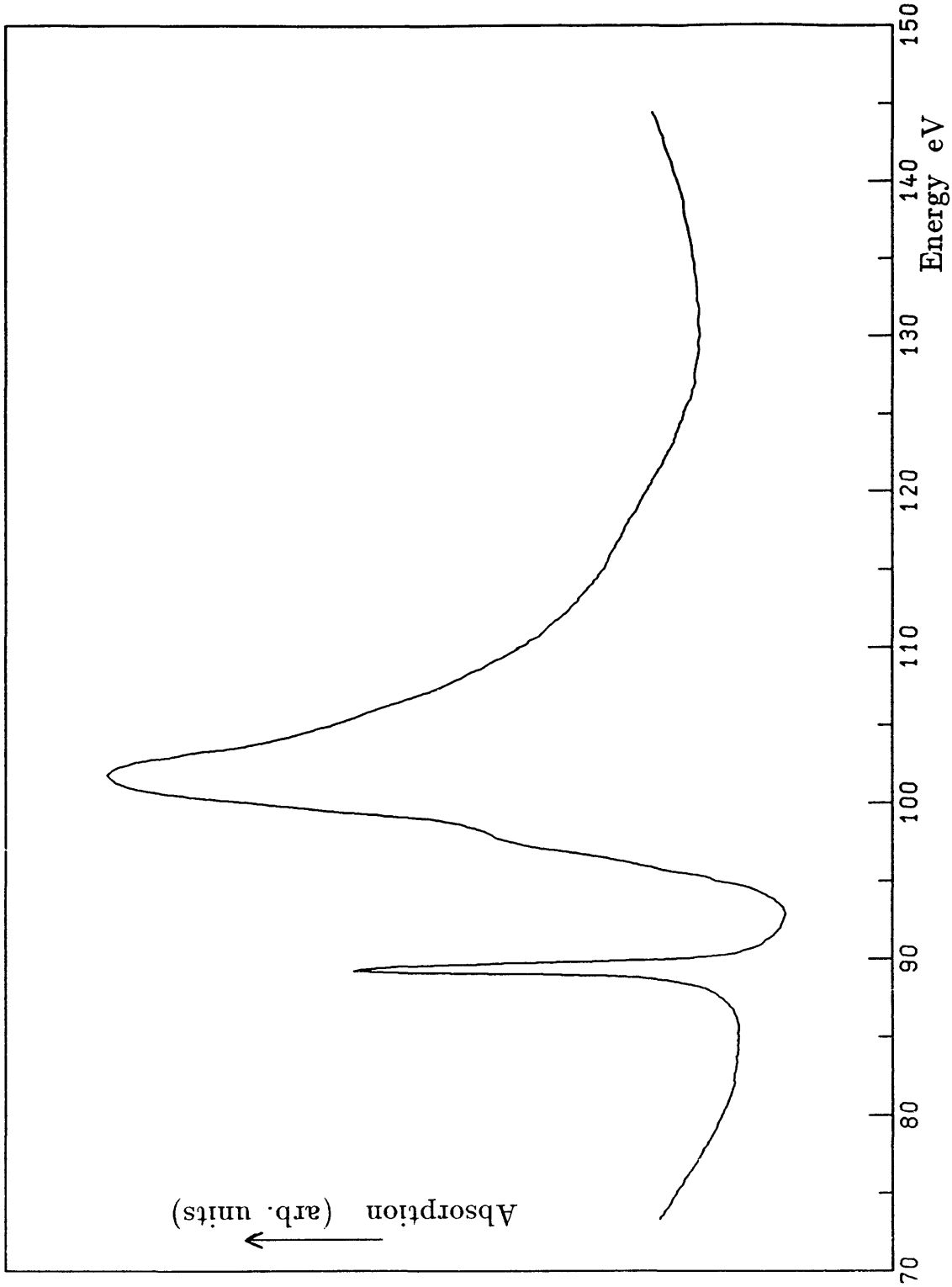


The $5d$ absorption spectrum of $ThF_4$ vapour.

Figure 7.1

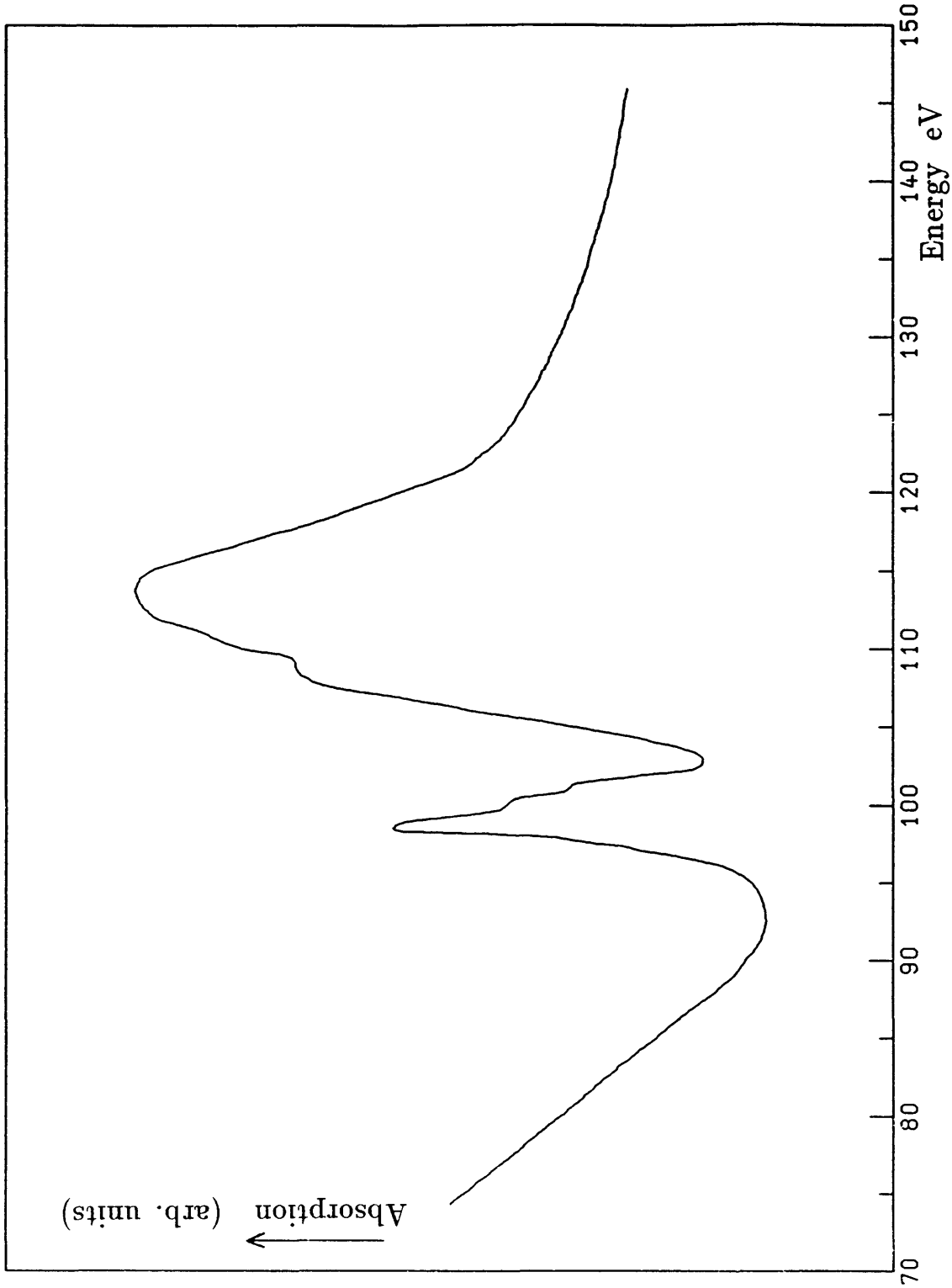


The $5d$ absorption spectrum of $UF_4$ vapour.

Figure 7.2

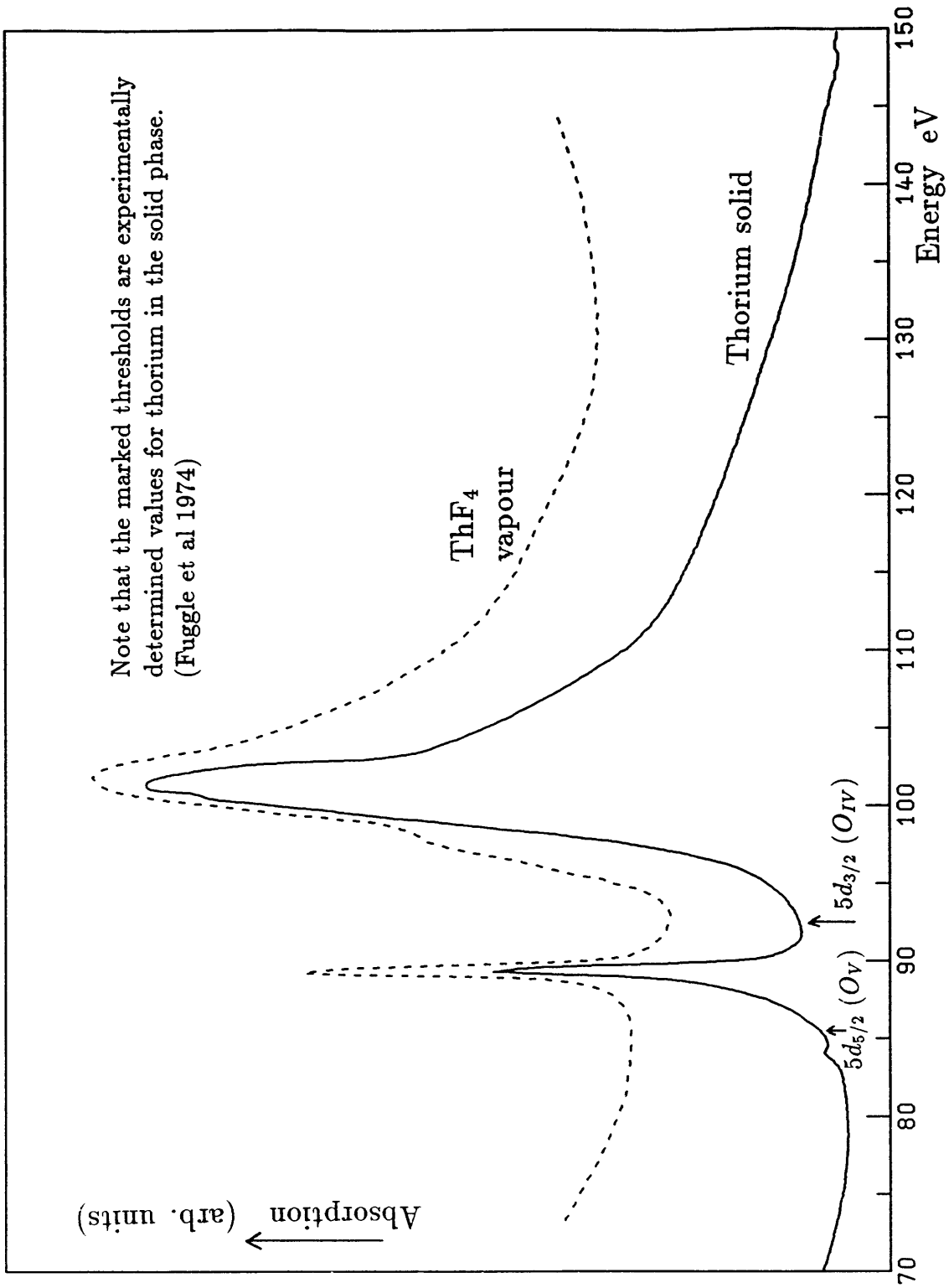


Comparison between the data of Thorium in the solid state and $ThF_4$ in the vapour phase.

Figure 7.3

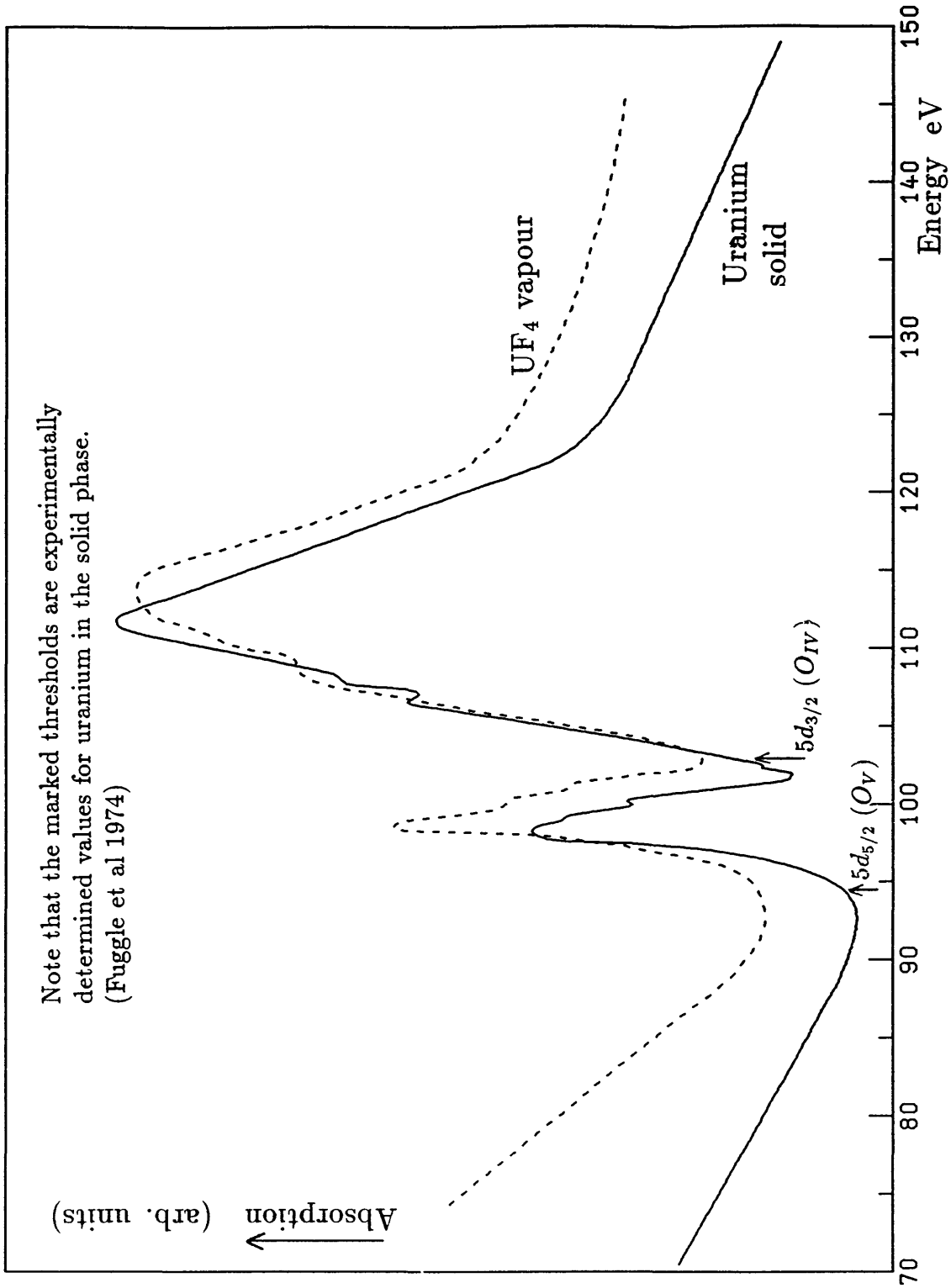


Comparison between the data of Uranium in the solid state and $UF_4$ in the vapour phase.

Figure 7.4

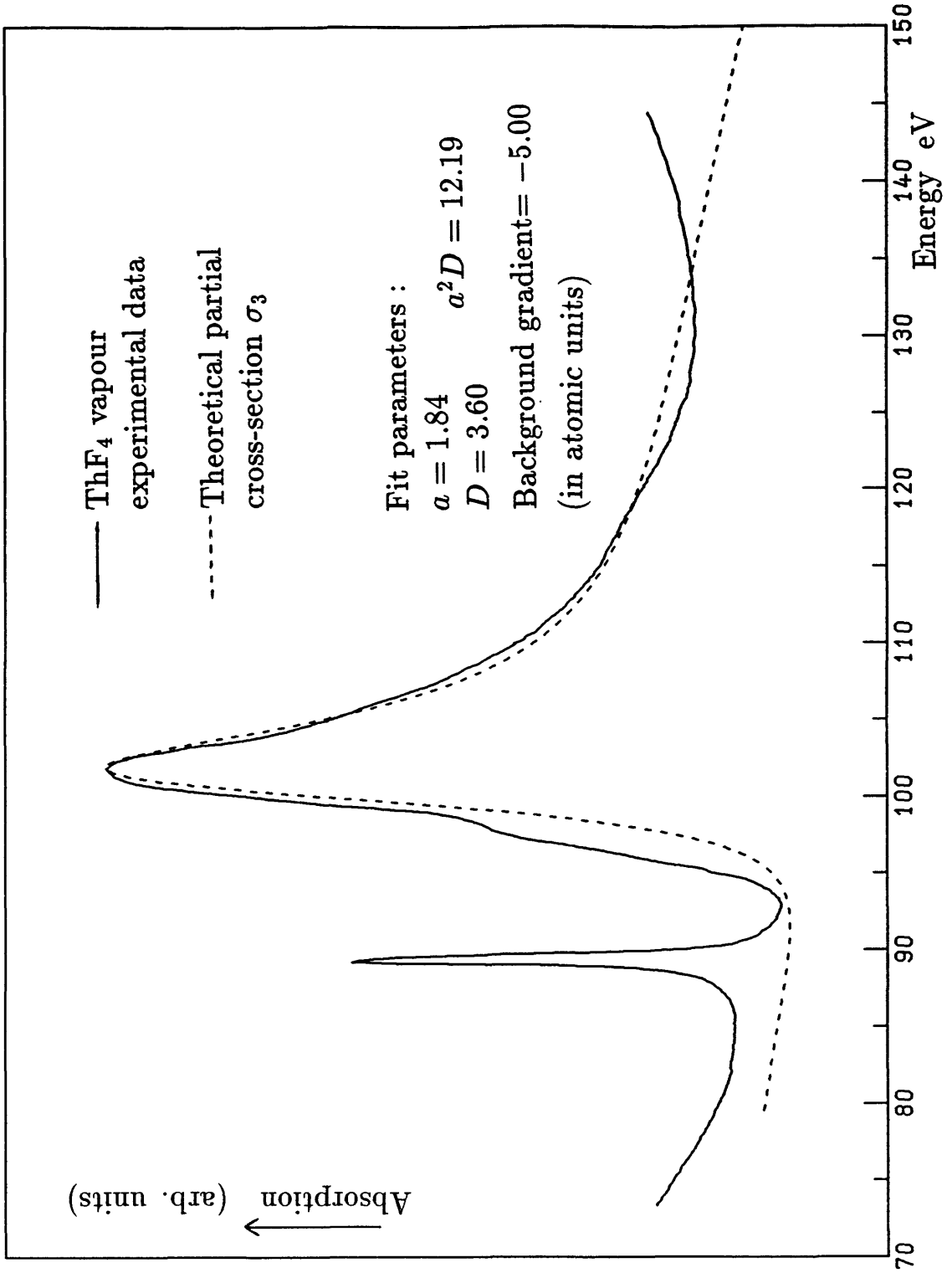


The fit to the experimental data for $ThF_4$ vapour using formula (6.1) and the parameters $a = 1.84$, $D = 3.60$

Figure 7.5

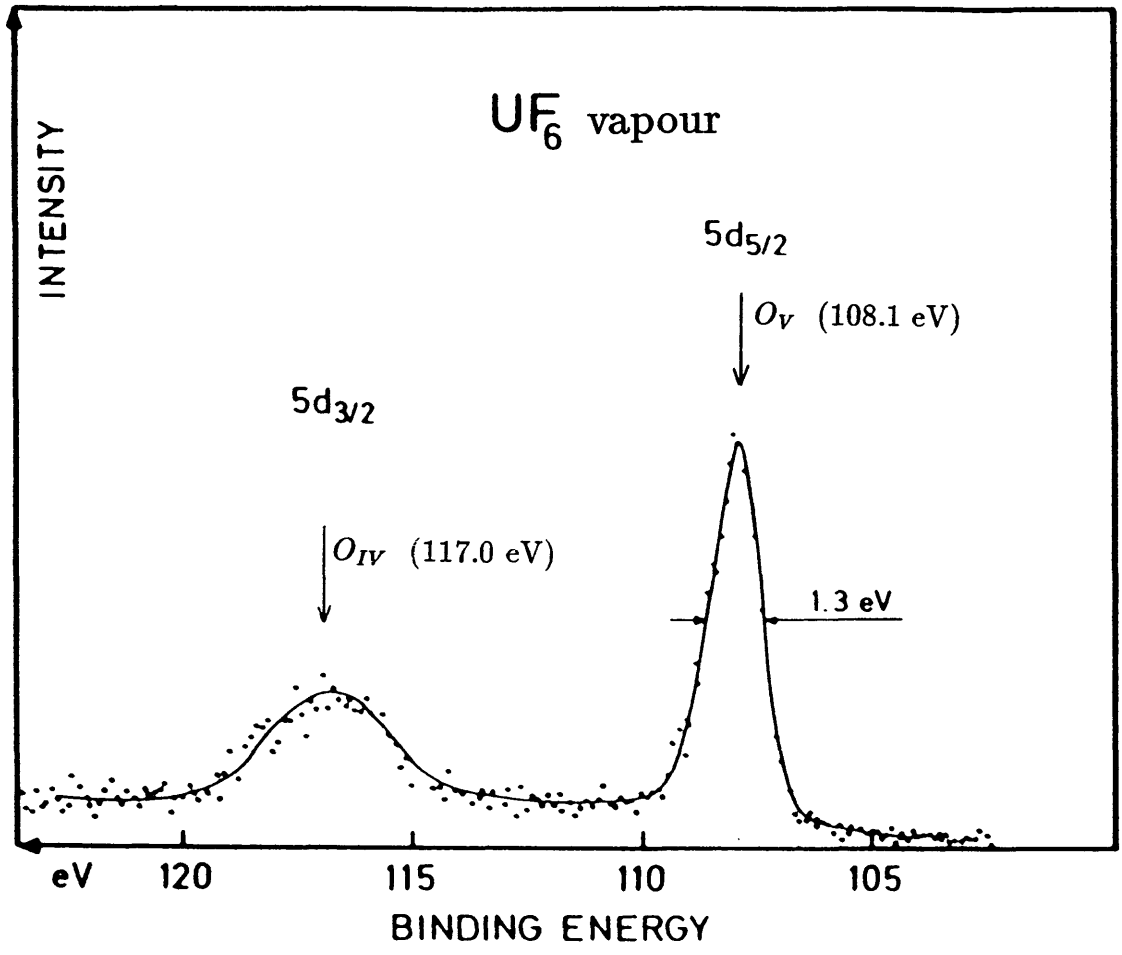


Note that the marked thresholds were experimentally determined for $UF_6$ in the vapour phase.

The $5d$ absorption spectrum of $UF_6$ vapour. (from Mårtensson et al 1984)

Figure 7.6

# Chapter VIII

# Uranium — the surprise experiment

## 8.1 Summary

The $5d$ absorption spectrum of uranium vapour yields the remarkable result of a single sharp line observed at the energy of the expected giant resonance. This unexpected behaviour is discussed in relation to the tetrafluoride and solid state uranium spectra.

## 8.2 Introduction

The distinguishing property of *giant resonances* from the experimenters point of view is their insensitivity to the environment. True, the theory indicates how critical the inner well can be, but in the periodic table only one example $Ba^+$ is actually on a knife edge.

The present work showed the first example of how a giant resonance can be induced to recur below threshold and in this example, the molecular field was the perturber. As discussed in chapter 4 similar effect has been achieved in the Ba, $Ba^+$, $Ba^{2+}$ sequence by Lucatorto et al (1981). These two experiments bring out a new feature of giant resonances, namely their sensitivity to the potential in the inner region, which is more difficult to disturb. We can regard the experiment by Lucatorto et al (1981) as a perturbation of the inner well by an increase in nuclear charge, which preserves atomicity, and the uranium case as a perturbation in which the effective

charge near the nucleus stays the same. It is perhaps not surprising that the $5f$ orbitals are more sensitive to this perturbation than the $4f$ orbitals because their localisation is less complete.

## 8.3 Uranium

We have now come to uranium the heaviest of the naturally occuring elements. As explained in the previous chapter, the measurements on metallic thorium and uranium show broad resonances lying above the $5d$ metallic thresholds. Our subsequent absorption experiments on the respective fluorides confirmed the atomic nature of these giant resonances and by analogy to the lanthanides we identified them as arising from transitions to $\overline{5,\varepsilon}\,f$ states. This was clear since as they are observed in both the solid actinide and the fluoride vapour, they cannot originate from lattice or molecular effects.

The strong parallels with the $4d$ excitation spectra in the lanthanide elements led us to expect that we would once again observe a $\overline{5,\varepsilon}\,f$ continuum resonance in atomic uranium. This was not to be the case.

Previous attempts to produce the spectrum had been unsuccessful due to the extremely corrosive nature of the liquid uranium, which on contact instantaneously destroyed our tantalum and tungsten furnace tubes. We eventually succeeded in containing the molten uranium in a tantalum carbide boat which remained unscathed. The uranium vapour itself caused no damage to our furnace tubes.

Our data for uranium vapour is shown in Figure 8.1. The startling result is that the $5f$ state does *not* give rise to a broad giant resonance but appears as a sharp transition, corresponding to a bound state. This means that the $5f$ state has dropped so deep in the inner well that it lies below the level of the outer well as depicted in Figure 8.2.

The transition appears as a sharp line peaking at $107.33 \pm 0.01$ Å at very nearly the same energy as the peak of the broad continuum resonances in $UF_4$ and metallic uranium as shown in Figure 8.3. We detected only one transition to what we assume to be a $5f$ state, but it is possible that we were unable to obtain a high enough vapour pressure to observe any other weaker transitions.

Clearly this is a bound state, but it exhibits the characteristic asym-

metric Beutler–Fano profile of an autoionising line. This is very similar to the observed discrete state in thulium (Radtke 1979a) lying near the end of the lanthanide sequence.

The most readable paper by Shore (1967) outlines a simple method of determining the profile parameters of an autoionising line from empirical data. This method yielded the profile parameters

$$q = 5.15 \pm 0.05$$
$$\lambda_o = 107.328 \pm 0.01 \text{ Å}$$
$$\Gamma/\hbar = (1.59 \pm 0.06) \times 10^{14}\ s^{-1}$$

and figure 8.4 shows the result. Thus the $5f$ state is interacting with continuum states and the interaction gives rise to the characteristic autoionisation profile as already discussed in chapter six. We will return to this shortly.

We also note that on close examination of the photographic plates evidence of two further lines can be seen at shorter and longer wavelength (at $\approx 105$ Å and 124 Å). These are so diffuse and weak that they do not show on the microphotometer traces although they appear consistently on all plates.

Since our experimental result is so surprising it is at this point necessary to expand a little on the experimental procedure, since it could be argued that the observed line originates from an impurity or from some component part of the furnace. Except for the tantalum carbide boat, exactly the same furnace setup as for gadolinium was used, and we observed no impurity during that experiment. The spectrum of gadolinium lies at higher energy and so if any impurity line had been present it would not have been obscured. However since a higher temperature was to be needed for uranium, an empty furnace was raised to the temperature that was needed for uranium. A plate was taken and no absorption whatsoever was detected, other than the usual carbon edge at $\sim 50$ Å. With uranium metal loaded, a total of four plates were taken, and a systematic evolution in absorption intensity was observed as the temperature (and hence the vapour pressure) was raised. That a uranium vapour was produced is evidenced by the fact that no uranium was left in the boat and that uranium metal was found condensed in the *Tracy liner* tube. These consistent facts lead us to support the view that the observed absorption spectrum is that of uranium metal vapour and not of some impurity. It is otherwise difficult to understand how an expected strong absorption resonance could be swamped by

a weaker impurity line.

It is now of paramount importance to stress that although the continuum resonances appear only within a molecular or solid state environment, they are nevertheless still of quasi-atomic nature. The external environment does not drastically influence the inner well potential of Figure 8.2 that is inherent to the uranium atom. Therefore the wavefunction of both the resonantly localised state and the bound state are very similar in the core region (see figure 8.2). This is what we understand by the *quasi-atomic* nature of the continuum resonance and the metallic or fluoride spectra are not a result of lattice or molecular effects.

However the critical factor is the depth of the inner well, and small changes to the inner potential valley can result from the different environment. This can trigger the radical change that we see in our observed spectra. The potential well which is initially deep enough to support a $5f$ state in $5d$ excited uranium becomes too shallow to support a fully bound state in the fluoride. The $5f$ state ceases to be bound and becomes a resonant state that lies above threshold, as occurs in the solid phase. This experimental result is hard to understand and we are unable to suggest even a qualitative mechanism.

In our experience with the lanthanide sequence of elements the opposite appeared to be true. For example in lanthanum and praseodymium the resonance became narrower in the fluoride. We interpreted this as being due to the fluorine atoms deepening the inner well by drawing away charge from the metal atom thus reducing shielding and hence tending to increase the localisation of the resonant state. This is not applicable to the situation in uranium. It is therefore obvious that the spectrum of thorium would be of immense interest as a comparison. This is particularly so since the resonance in $ThF_4$ is narrower than in $UF_4$ and so indicates an even more localised $\overline{5,\varepsilon f}$ state than in uranium.

## 8.4 Perturbation of the Inner Well

Lucatorto et al (1981) reported the photoabsorption spectra for the $4d$ subshell of Ba, $Ba^+$ and $Ba^{2+}$, and the differences in the spectra are quite striking. Of particular interest in the sequence is the $Ba^{2+}$ spectrum which in contrast to the uranium spectrum exhibits several discrete autoionis-

ing lines, and these can be ordered into a highly perturbed rydberg series (Connerade 1983). Calculations for the barium ionic series indicate that in conjunction to a deepening of the inner well a parallel removal of the potential barrier allows the higher $nf$ states to partially enter into the inner well region (Cheng and Froese–Fischer). In the case of uranium we see only one line which seems to indicate that the $5f$ is collapsed but that the higher $nf$ wavefunctions remain localised in the outer well, and hence the Rydberg series are suppressed. This potential barrier remains intact in the solid and fluoride.

Thus in the case of uranium the inner well potential which is being *tuned* by the molecular or solid state field, and these are providing a more *gentle* perturbation that primarily affect only depth of the inner well. We stress however that the mechanism for this perturbation is not understood and that the fluorine atoms lead to a delocalisation of the $5f$ state contrary to our results with the lanthanides. This crossing over from the continuum into the bound spectrum relates to our discussions of controlled collapse in chapter six.

## 8.5 Theoretical Calculations

This sensitive area of atomic physics where a small perturbation causes a magnified response is obviously an excellent testing ground for *ab initio* theory. However few of the current sophisticated methods have as yet been applied specifically to the actinides.

Kahn et al (1978) used an approximate method to include relativistic effects within a Hartree–Fock routine (Cowan and Griffin 1976) and calculated the $5f$ wavefunction (figure 8.5) and the effective radial potential (figure 8.6) for the uranium atom.

Another theoretical treatment is that of Band et al (1981) who use Dirac–Fock theory which implicitly includes exchange and relativistic effects. This has been applied to demonstrate wavefunction collapse in the lanthanides but as yet has to be used with the actinide elements. Relativistic effects are important, and $5f$ wavefunction collapse in neutral atoms is predicted to occur in non-relativistic calculations (Griffin et al 1969) at actinium, whereas relativistically it does not occur till thorium. This is a result of the relativistic spatial expansion of the outer $d$ and $f$ wavefunc-

tions as a result of the greater shielding from the nucleus by the relativistic $s$ and $p$ functions.

Recently Wendin (1985) has used a local density based random phase approximation to calculate the photoionisation cross-section for uranium. Although the calculation is atomic and not for the metal ion, the calculated spectrum agrees well with the fluoride and metal absorption cross-section. The fact that the atomic spectrum has been reported to be drastically different (Pantelouris and Connerade 1982) is evaded. This is not meant as a criticism of the theory which is playing a leading role in many-body theory, but only highlights how critical this area of the periodic table is to electron correlation effects. These have been considered in non-relativistic (Wendin and Ohno 1976) but not in relativistic calculations. We admit that our empirical result is hard to understand and further refinements to the theoretical treatments are necessary.

Theoretical calculations of binding energies also do not compare well with experimental results either. Calculations for uranium metal thresholds lie about 10 eV higher than measured values (Shchornak et al 1979).

## 8.6 Binding Energy Considerations

Let us now return to our spectrum of uranium vapour. It is once again important to note that the thresholds depicted in figure 8.3 are experimental values obtained for the solid (Fuggle et al 1974). Now the discrete state we observe in uranium lies at approximately the same energy as the maximum of the localised resonance in the metal. Since for the observed $5d \longrightarrow 5f$ transition, the discrete $5f$ state must lie at least below the $5d^9\ ^2D_{3/2}$ based threshold, the $5d$ threshold must in the free uranium atom lie at much higher energies than in the solid. Thus for consistency with our spectrum an energy shift of the thresholds of at least 1 Rydberg (13.6 eV) must be involved. Further the narrow autoionising profile we observe indicates that the interaction with the continuum is relatively weak. This suggests that the observed $5f$ state is not interacting with its associated $\varepsilon f$ continuum but is only weakly coupled with continua of other $\ell$. This requires that the observed state should lie below both the $^2D_{3/2}$ and the $^2D_{5/2}$ based thresholds, implying a shift of more than 25 eV. Such a level below threshold can only interact with its associated $\varepsilon f$ continuum through second and

higher order processes which do not cause autoionisation, and can only autoionise to other underlying continua.

The suggested shift of the ionisation limits may at first sight seem a very large value, but as mentioned in the previous chapter a difference of 14 eV has been observed between the uranium metal and $UF_6$ vapour (Mårtenson et al 1984), and so a difference of such magnitude to uranium vapour is feasible. It is also generally accepted that core electrons are more tightly bound in the gas phase than they are in the metallic phase. The reason given is the final state screening by the surrounding conduction electrons in the metal (Johansson and Mårtensson 1980). Obviously an independent empirical determination of the atomic threshold energies would therefore in itself yield an insight into our spectrum and provide a check of our interpretation. It appears however to be much easier to determine core-level binding energies for the metallic state than it is for the free atom. It is to be hoped that this will be rectified in the near future, and that atomic threshold data will become as freely available as they are for the metallic phase at present.

## 8.7 Conclusion

We have thus demonstrated that although the inner well that occurs in the effective radial potential for $f$ electrons is not greatly affected by the external environment, dramatic changes in the absorption cross-section can nevertheless be observed in certain elements. This occurs in those situations where the atomic wavefunctions are on a thread-like balance and where a small perturbation can *push out* or *suck in* the wavefunction and thus greatly influence the spectra observed.

It is therefore not surprising that uranium exhibits such a multitude of valence states and that external pressure can so easily change its crystal structure. It is also no coincidence that we obtained such unexpected results from an element that lies on the diagonal of critical behaviour in the pseudo-periodic table that we introduced in chapter five.

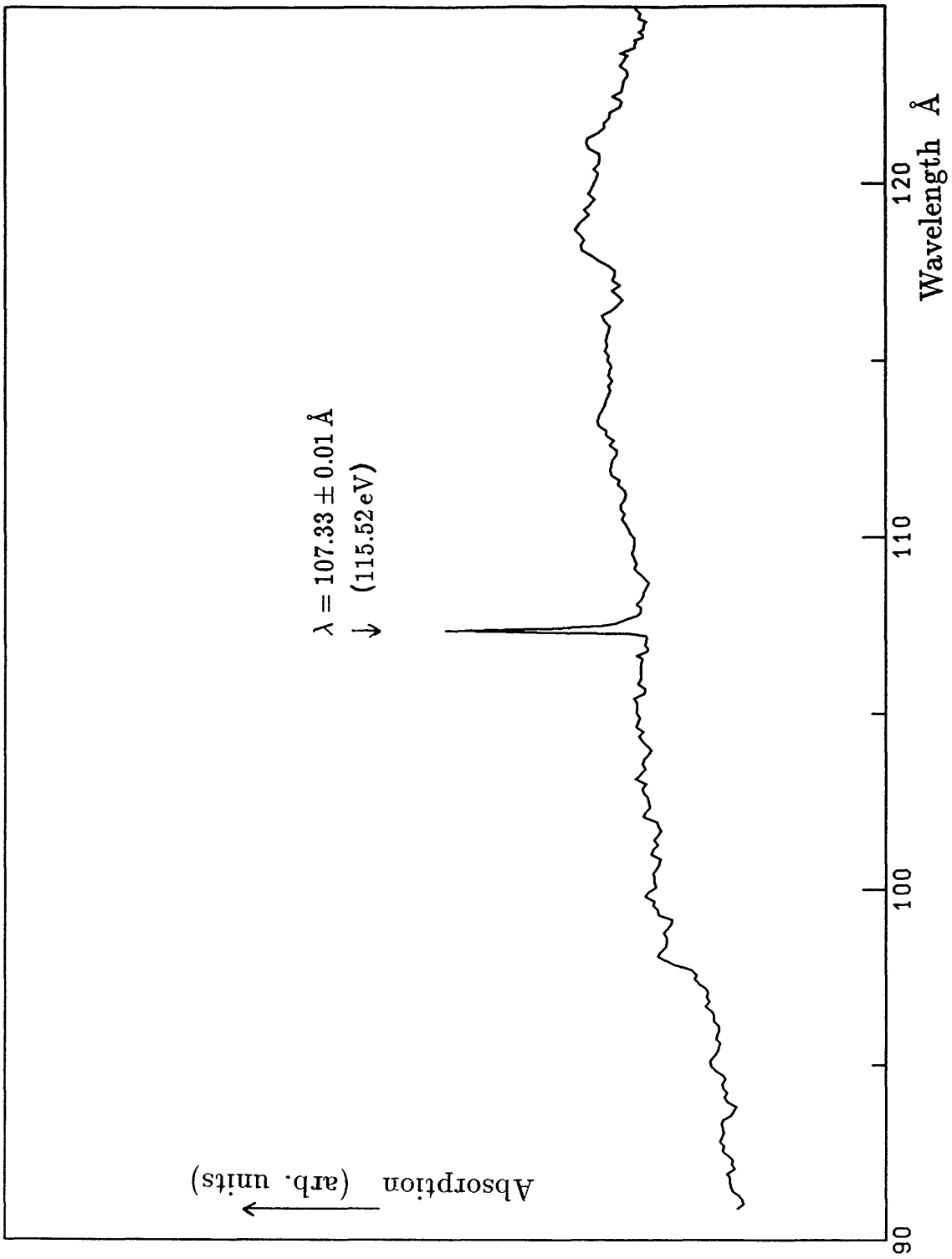


The $5d$ absorption spectrum of uranium vapour.

Figure 8.1

Depending on the energy of the excited $5f$ state the following solutions are possible. (i) $E > E_B$: the solution is a continuum state which can become resonantly localised. (ii) $E_B > E > 0$: the solution is a quasi-bound state that can tunnel through the barrier into the $f$ continuum. (iii) $0 > E > E_V$: the solution is a bound state which can be a hybrid of inner- and outer-well eigenfunctions. (iv) $E_V > E > E_W$: the solution is a bound state of the inner well that can only be broadened by autoionisation into continua of other channels.

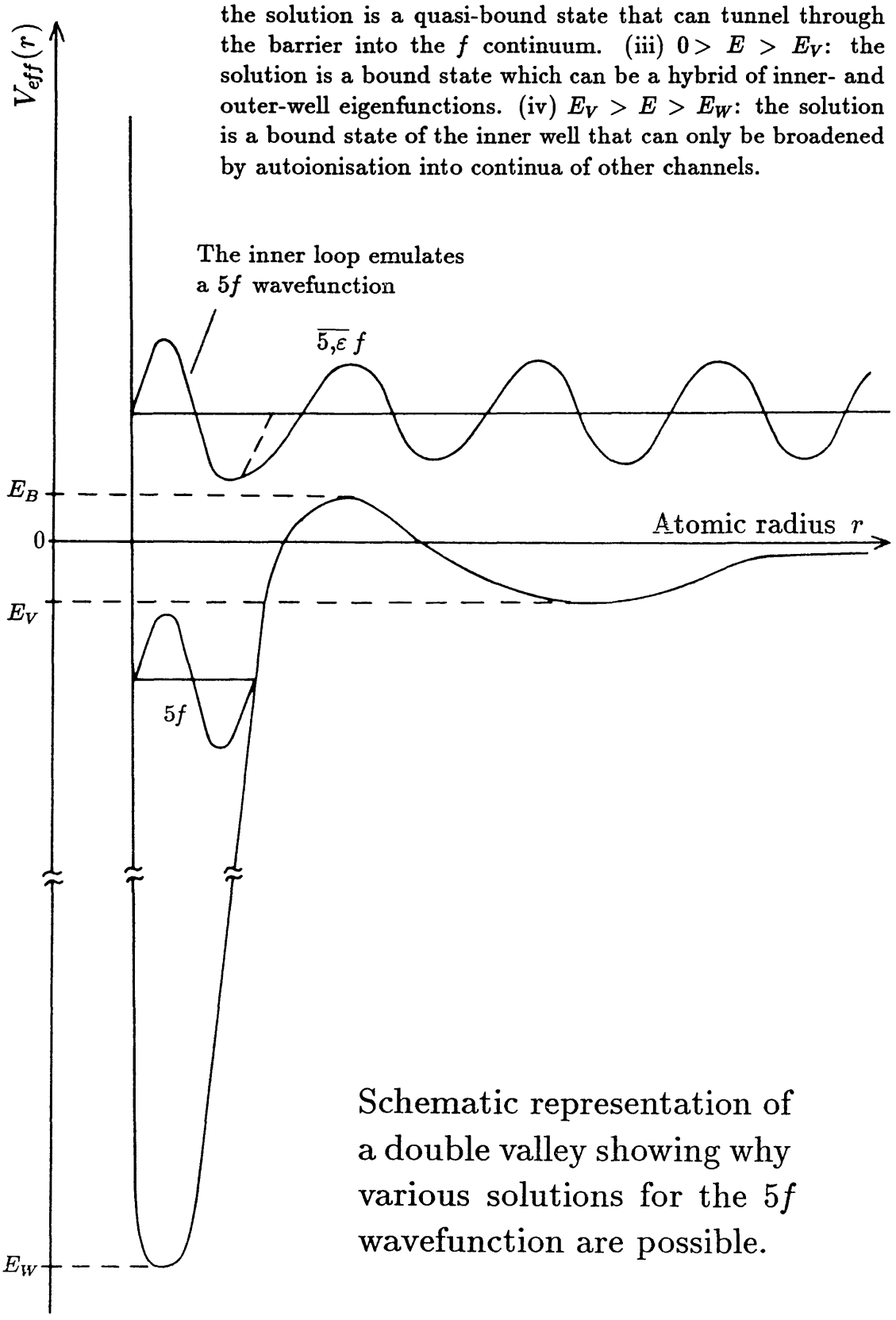


Schematic representation of a double valley showing why various solutions for the $5f$ wavefunction are possible.

Figure 8.2

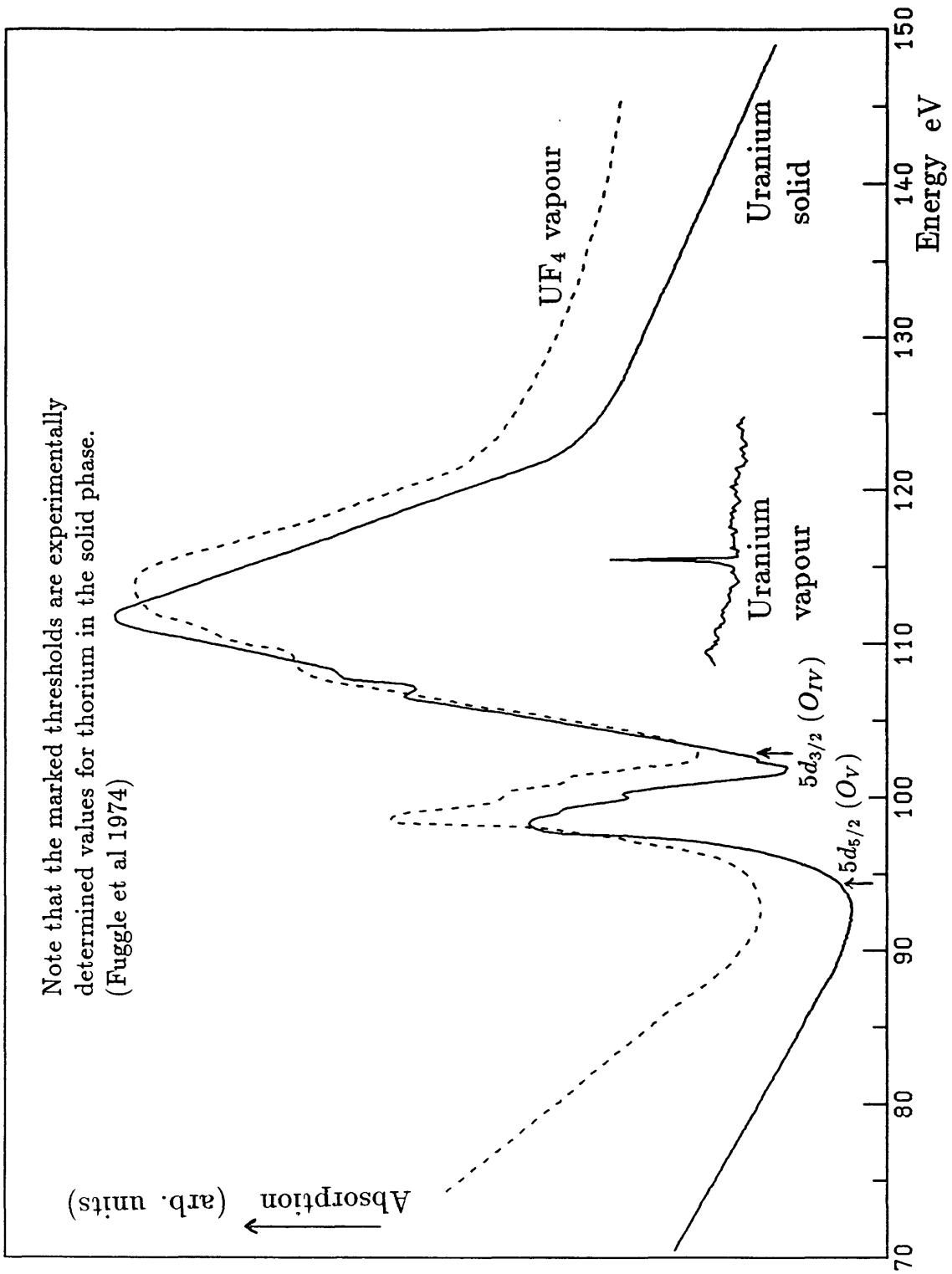


Comparison of the uranium vapour data with that of metallic uranium and $UF_4$ vapour.

Figure 8.3

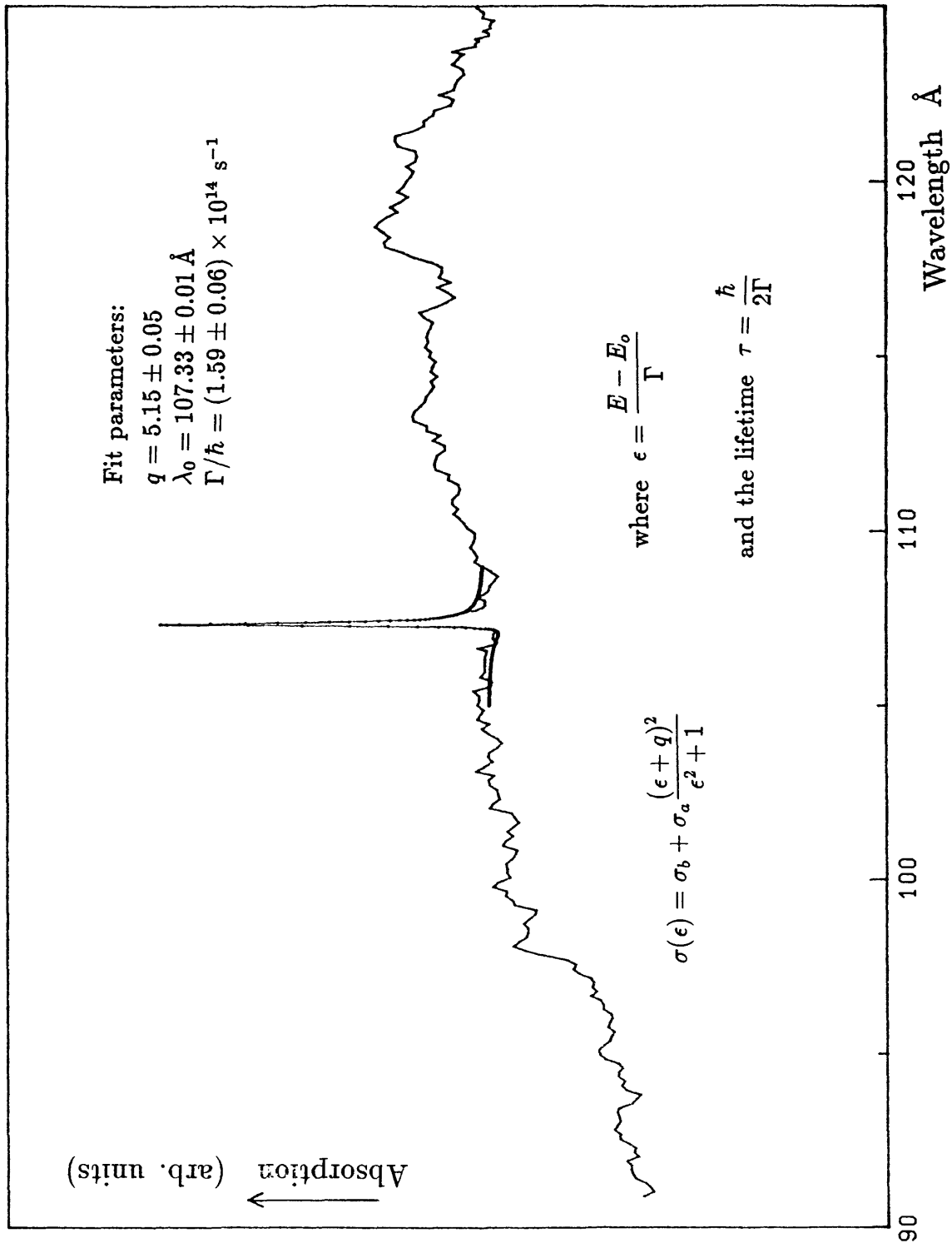


The Fano profile fitted to the uranium vapour data.

Figure 8.4

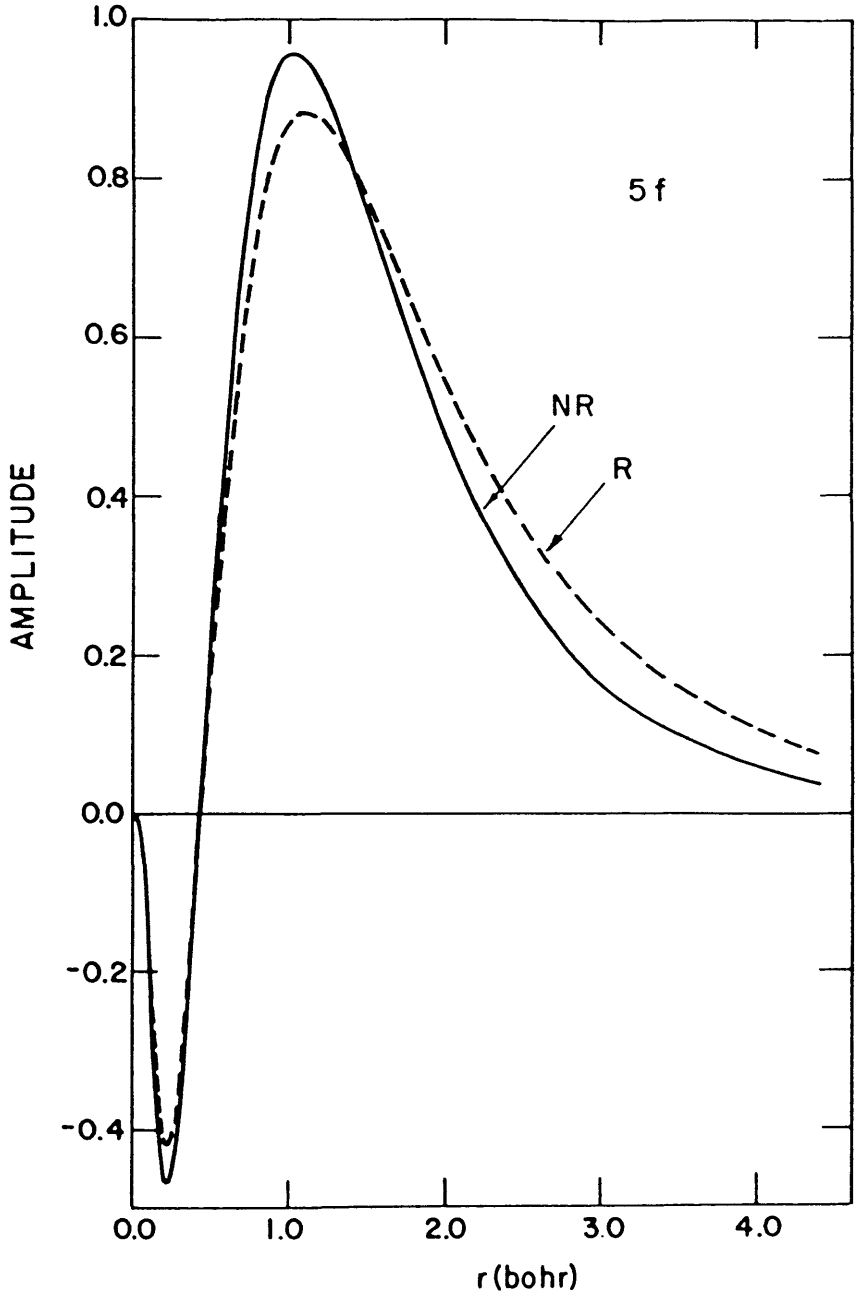


Nonrelativistic (NR) and relativistic (R) $5f$ orbitals in the uranium atom. (from Kahn et al 1978)

Figure 8.5

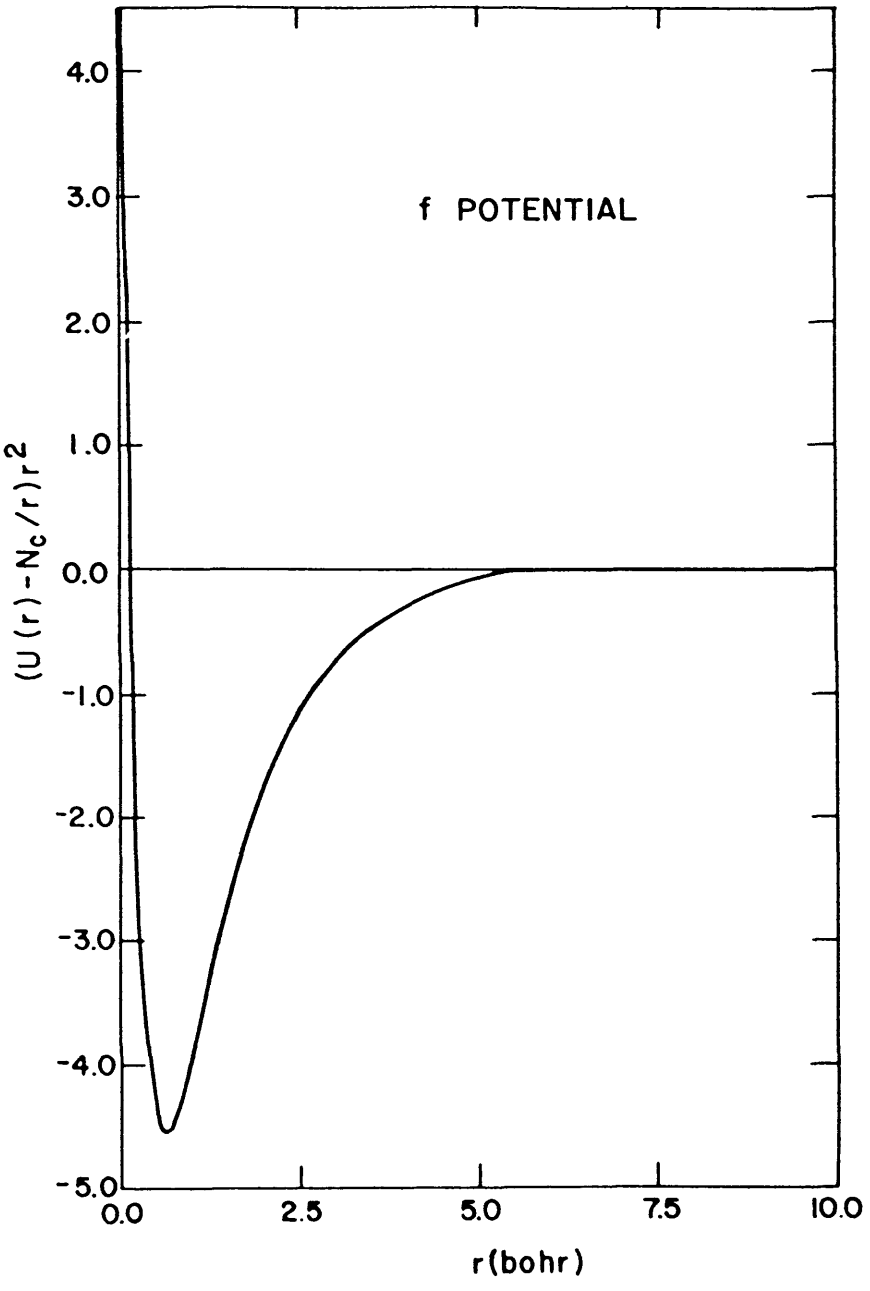


The relativistic $f$ effective radial potential for the uranium atom. (from Kahn et al 1978)

Figure 8.6

# References


Abramowitz, M. and Stegun, I.A. (Eds.) 1964 *Handbook of Mathematical Functions*, National Bureau of Standards, Washington D.C.

Althoff, K.H., Bätzner, K., Drees, J., Febel, A., Gildemeister, O., von Holtey, G., Knop, G., Lütter, P., Netter, H., Paul, W., Schittko, F.J., Schultz von Dratzig, A., Stier, H.E. and Weisse, E. 1968 *Nucl. Instr. Meth.* **61**, 1

Aono, M., Chiang, T.-C., Knapp, J.A., Tanaka, T. and Eastman, D.E. 1980 *Phys. Rev.* **B21**, 2661

Amusia, M. Ya, Cherpkov, N.A. and Chernyshevaa, L.V. 1971 *Sov. Phys. JETP* **33**, 458

Amusia, M. Ya and Sheftel, S.I. 1976a *Phys. Letts.* **55A**, 469

Amusia, M. Ya, Ivanov, V.K. and Chernysheva, L.V. 1976b *Phys. Letts.* **59A**, 191

Amusia, M. Ya, Ivanov, V.K., Sheĭnerman, S.A. and Sheftel, S.I. 1980 *Sov. Phys. JETP* **51**, 458

Aono, M., Chiang, T.C., Weaver, J.H and Eastman, D.E. 1981 *Sol. State Commun.* **39**, 1057

Bagnall, K.W. 1967 *Coordin. Chem. Rev.* **2**, 145

Ballafet, G., Romand, J. and Vodar,B. 1961 *C. R. Acad. Sci. Paris* **252**, 4139

Bancroft, G.M., Sham, T.K. and Larsson, S. 1977 *Chem. Phys. Lett.* **46**, 511

Band, I.M. and Fomichev, V.I. 1980 *Phys. Lett.* **75A**, 178

Band, I.M., Fomichev, V.I. and Trzhaskovskaya, M.B. 1981 *J. Phys. B: Atom. Molec. Phys.* **14**, 1103

Beck, G. 1930 *Z. Physik* **62**, 331

Bohm, D. and Pines, D. 1953 *Phys. Rev.* **92**, 609

Bohr, N. 1913 *Phil. Mag.* **26**, 1

Brown, D. 1968 *Halides of Lanthanides and Actinides*, Wiley, London

Brueckner, K.A. 1955 *Phys. Rev.* **97**, 1353

Cheng, K.T. and Froese–Fischer, C. 1983 *Phys. Rev.* **A28**, 2811

Cheng, K.T. and Johnson, W.R. 1983 *Phys. Rev.* **A28**, 2820

Chiang, T.C., Eastman, D.E., Himpsel, F.J., Kaindl, G. and Aono, M. 1980 *Phys. Rev. Letts.* **45**, 1846

Codling, K. 1973 *Rep. Prog. Phys.* **36**, 541

Collins, G. and Price, W.C. 1934 *Rev. Sci. Instr.* **5**, 523

Combet–Farnoux, F. 1969 *J. de Physique* **30**, 521

Connerade, J.P. 1978a *J. Phys. B: Atom. Molec. Phys.* **11**, L381

Connerade, J.P. 1978b *Contemp. Phys.* **19**, 415

Connerade, J.P. 1982 *Les Houches Summer School: New Trends in Physics, Vol. 2*, p643 (Eds. G.Grynberg and R.Stora, North–Holland, Amsterdam)

Connerade, J.P. 1983 *J. Phys. B: Atom. Molec. Phys.* **16**, L257

Connerade, J.P. 1984 *J. Phys. B: Atom. Molec. Phys.* **17**, L165

Connerade, J.P. and Mansfield, M.W.D. 1973 *Proc. R. Soc. Lond.* **A335**, 87

Connerade, J.P. and Mansfield, M.W.D. 1974 *Proc. R. Soc. Lond.* **A341**, 267

Connerade, J.P. and Mansfield, M.W.D. 1976 *Proc. R. Soc. Lond.* **A348**, 239

Connerade, J.P. and Mansfield, M.W.D. 1982 *Phys. Rev. Lett.* **48**, 131

Connerade J.P. and Pantelouris, M. 1984 *J. Phys. B: Atom. Molec. Phys.* **17**, L173

Connerade, J.P., Tracy, D.H., Mansfield, M.W.D. and Thimm, K. 1974 *Proc.* IV *Int. Conf. VUV Rad. Phys.*, p99 (Ed. E.E. Koch, R. Haensel and C. Kunz), Pergamon-Vieweg, Braunschweig

Connerade, J.P., Pantelouris, M., Baig, M.A., Martin, M.A.P. and Cukier, M. 1980 *J. Phys. B: Atom. Molec. Phys.* **13**, L357

Connerade, J.P, Dietz, K., Mansfield, M.W.D. and Weymans, G. 1984 *J. Phys. B: Atom. Molec. Phys.* **17**, 1211

Coqblin, B. 1977 *The Electronic Structure of the Rare-Earth Metals and Alloys: the Magnetic Heavy Rare-Earths*, (Academic Press, London)

Cowan,R.D. 1967 *Phys. Rev.* **163**, 54

Cowan, R.D. and Griffin, D.C. 1976 *J. Opt. Soc. Am.* **66**, 1010

Cukier, M., Dhez, P., Wuilleumier, F. and Jaegle,P. 1974 *Phys. Lett.* **48A**, 307

Cukier, M., Dhez, P., Gauthe, B., Jaegle, P., Wehenkel, C. and Combet–Farnoux, F. 1978 *J. Physique Lett.* **39**, L-315

Cukier, M., Gauthe, B. and Wehenkel, C. 1980 *J. Physique* **41**, 603

Darnell, A.J. and Keneshea, F.J. 1958 *J. Phys. Chem.* **62**, 1143

Dehmer, J.L. 1974 *Phys. Fennica* **9**, Supplement S1, 60

Dehmer, J.L. and Starace, A.P. 1972 *Phys. Rev.* **B5**, 1792

Dehmer, J.L., Starace, A.F., Fano, U., Sugar, J. and Cooper, J.W. 1971 *Phys. Rev. Lett.* **26**, 1521

Desclaux, J.P. 1975 *Comp. Phys. Commun.* **9**, 31

Dietz, K., Lechtenfeld, O. and Weymans, g. 1982 *J. Phys. B: Atom. Molec. Phys.* **15**, 4315

Dietz, K. and Weymans, G.. 1984 *J. Phys. B: Atom. Molec. Phys.* **17**, 2987

Dirac, P.A.M. 1928 *Proc. Roy. Soc.* **117**, 610; **118**, 351

Dworkins, A.s. and Bredig, M.A. 1971 *J. Phys. Chem.* **75**, 2340

Dyke, J.M., Fayad, N.K., Morris, A. and Trickle, I.R. 1980 *J. Chem. Phys.* **72**,3822

Ederer, D.L. 1964 *Phys. Rev. Lett.* **13**, 760

Ederer, D.L. and Tomboulian, D.H. 1964 *Phys. Rev.* **A133**, 1525

Ederer, D.L., Lucatorto, T.B., Salomen, E.B., Madden, R.P. and Sugar, J. 1975 *J. Phys. B: Atom. Molec. Phys.* **8**, L21

Edlén, B. 1975 *Phys. Scr.* **11**, 366

Fano, U. 1961 *Phys. Rev.* **124**, 1866

Fano, U. and Cooper, J.W. 1968 *Rev. Mod. Phys.* **40**, 441

Fermi, E. 1928 in *Quantentheorie und Chemie, Leipziger Vorträge*, (Ed. H. Falkenhagen, S. Hirzel Verlag, Leipzig)

Feynman, R.P. 1949 *Phys. Rev.* **76**, 749,769

Fliflet, A.W., Chase, R.L. and Kelly, H.P. 1975 *J. Phys. B: Atom. Molec. Phys.* **7**, L443

Fock, V. 1930 *Z. Physik* **61**, 126

Fomichev, V.A., Zimkina, T.M., Gribovskiĭ, S.A. and Zhukova, I.I. 1967 *Sov. Phys. Solid State* **9**, 1163

Freeman, A.J. and Watson, R.E. 1962 *Phys. Rev.* **127**, 2058

Froese–Fischer, C. 1972 *Comp. Phys. Commun.* **4**, 107

Froese–Fischer, C. 1977 *The Hartree–Fock method for atoms*, Wiley, New York

Fuggle, J.C., Burr, A.F., Watson, L.M., Fabian, D.J. and Lang, W. 1974 *J. Phys. F: Metal Phys.* **4**, 335

Gabriel, A.H., Swain, J.R. and Waller, W.. 1965 *J. Sci. Instrum.* **42**, 94

Garton, W.R.S. 1959 *J. Sci. Instr.* **36**, 11

Garton, W.R.S. 1966 *Adv. Atom. Molec. Phys.* **2**, 93

Garton, W.R.S., Connerade, J.P., Mansfield, M.W.D. and Wheaton, J.E.G. 1969 *Appl. Opt.* **8**, 919

Gasiorowicz, S. 1974 *Quantum Physics*, p.388 *ff*, Wiley, New York

Gerken, F., Barth, J. and Kunz, C. 1981 *Phys. Rev. Lett.* **47**, 993

Gerken, F., Barth, J. and Kunz, C. 1982 . *Am. Inst. of Phys. Conf. Proc.* **94**, 602

Godwin, R.P. 1969 *Springer Tracts in Modern Physics* **51**, Springer Verlag, Berlin

Goeppert–Mayer, M. 1941 *Phys. Rev.* **60**, 184

Goldstone, J. 1957 *Proc. Roy. Soc* **A239**, 267

Griffin, D.C. , Andrew, K.L. and Cowan, R.D. 1969 *Phys. Rev.* **177**, 62

Gruen, D.M. and Fred, M. 1954 *J. Am. Chem. Soc.* **76**, 3850

Gudat, W. and Kunz, C. 1972 *Phys. Rev. Lett.* **29**, 169

Haensel, R., Rabe, P. and Sonntag, B. 1970 *Sol. State Commun.* **8**, 1845

Hansen, J.E., Fliflet, A.W. and Kelly, H.P. 1975 *J. Phys. B: Atom. Molec. Phys.* **8**, L127

Hartree, D.R. 1928 *Proc. Camb. Phil. Soc.* **24**, 89

Hartree, R.D. 1957 *The calculation of atomic structures*, Wiley, New York

Hegerty, J. and Yen, W.M. 1980 *J. Appl. Phys.* **51**, 3545

Herman, F. and Skillman, S. 1963 *Atomic Structure Calculations*, (Prentice–Hall, Inc., Englewood Cliffs, New Jersey)

Hopfield, J.J. 1930 *Astrophys. Jour.* **72**, 133

Husmann, D. 1983 *IEEE Trans. Nucl. Sci.* **30**, 3252

Herzberg, G. 1944 *Atomic Spectra and atomic structure* (Dover Publications, New York)

Johanson, W.R., Crabtree, G.W., Edelstein, A.S. and McMasters, O.D. 1981 *Phys. Rev. Lett.* **46**, 504

Johansson, B. and Mårtenson, N. 1980 *Phys. Rev.* **B21**, 4427

Johnson, W.R. and Lin, C.D. 1979 *Phys. Rev.* **A20**, 964

Kahn, L.R., Hay, P.J. and Cowan, R.D. 1978 *J. Chem. Phys.* **68**, 2386

Karaziya, R.I. 1982 *Sov. Phys. Usp.* **24**, 775

Katz, J.J. and Sheft,I. 1960 *Advances in Inorganic Chemistry and Radiochemistry*, Vol. 2, p.195 (eds. H.J. Emuléus and A.G. Sharpe, Academic Press Inc., New York)

Kelly, H.P. 1964 *Phys. Rev.* **136 B**, 896

Kelly, H.P. 1969 *Adv. Chem. Phys.* **14**, 129

Kelly, H.P. 1976 *Photo-ionisation and other Probes of Many-electron Interactions,* p.83, (Ed. F.J. Wuilleumier, Plenum Publ. Corp., New York)

Kelly, R.L. and Palumbo, L.J. 1973 *Atomic and Ionic Emission Lines below 2000 Å*, Naval Research Lab. Report NRL 7599 (Washington D.C)

Koel, B.E., Loubriel, G.H., Stulen, R.H., Rosenberg, R.A. and Parks, C.C. 1982 *Phys. Rev.* **B25**, 5551

Koskenmake, D. and Gschneider, K.S. 1979 *Hand-book on the Physics and Chemistry of Rare Earths*, Chapter 4 (Ed. K.S. Gschneider and L. Eyring), North-Holland, Amsterdam

Kowalczyk, S.P., Edelstein, N., McFeely, F.R., Ley, L. and Shirley, D.A. 1974 *Chem. Phys. Lett.* **29**, 491

Kubaschewski, O., Evans, E.L. and Alcock, C.B. 1967 *Metallurgical Thermochemistry*, Pergamon Press, London

Kunz, C. 1979 *Topics in Current Physics* **10**, 1 (ed. C. Kunz, Springer Verlag, Heidelberg)

Ley, L. and Cardona, M. 1979 *Photoemission in Solids 2*, Topics in Applied Physics **27** (Springer Verlag, Berlin)

Lim, M. and Searcy, A.W. 1966 *J. Phys. Chem.* **70**, 1762

Lin, C.D. 1974 *Phys. Rev.* **A9**, 181

Lindgren, I. and Morrison, J. 1982 *Atomic Many-body Theory*, Springer Series in Chemical Physics **13**, (Springer Verlag, Heidelberg)

Lotz, W. 1970 *J. Opt. Soc. Am.* **60**, 206

Lu, K.T. and Fano, U. 1970 *Phys. Rev.* **A2**, 81

Lucatorto, T.B., McIlrath, T.J. Sugar, J. and Younger, S.M. 1981 *Phys. Rev. Lett.* **47**, 1124

Lukirskiĭ, A.P. and Zimkina, T.M. 1963 *Bull. Acad. Sci. USSR Phys. Ser* **27**, 808

Lukirskiĭ, A.P., Brytov, I.A. and Zimkina, T.M. 1967 *Sov. Phys. Sol. State* **9**, 1128

Lyman, T. 1924 *Astrophys. Jour.* **60**, 1

Maĭste, A.A., Ruus, R.E., Kuchas, S.A., Karaziya, R.I. and Élango, M.A. 1980 *Sov. Phys. JETP* **51**, 474

Mansfield, M.W.D. and Connerade, J.P. 1976 *Proc. Roy. Soc.* **A352**, 125

Manson, S.T. and Cooper, J.W. 1968 *Phys. Rev.* **165**, 126

Mar, R.W. and Searcy, A.W. 1967 *J. Phys. Chem.* **71**, 888

Mårtensson, N., Malmquist, P.-Å. and Svensson, S. 1984 *J. Chem. Phys.* **80**, 5458

McCreary, J.R. and Thorn, R.J. 1973 *High Temp. Sci.* **5**, 97

Morse, P.M. 1929 *Phys. Rev.* **34**, 57

Mott, N.F. and Massey, H.S.W. 1965 *The Theory of Atomic Collisions (third ed.)*, p.35 *ff* Clarendon Press, Oxford

Nuroh, K., Stott, M.J. and Zaremba, E. 1982 *Phys. Rev. Lett.* **49**, 862

Olson, C.G. and Lynch, D.W. 1982 *J. Opt. Soc. Am.* **72**, 88

Pantelouris, M. and Connerade, J.P. 1982 *J. Phys. B: Atom. Molec. Phys.* **16**, L23

Park, R.L. and Houston, J.E. 1973 *Phys. Rev.* **A7**, 1447

Pauli, W. 1925 *Z. Phys.* **31**, 745

Petersen, H., Radler, K, Sonntag, B. and Haensel, R. 1975 *J. Phys. B: Atom. Molec. Phys.* **8**,31

Platau, A. and Karlsson, S.E. 1978 *Phys. Rev.* **B18**, 3820

Pratt, R.H., Ron, A. and Tseng,H.K. 1973 *Rev. Mod. Phys.* **45**, 273

Rabe, P. 1974 *Doktorarbeit DESY Internal Report F41-74/2*, Fachbereich Physik der Universität Hamburg

Rabe, P., Radler, K. and Wolff, H.W. 1974 *Proc.* IV *Int. Conf. VUV Rad. Phys.*, 247 (Ed. E.E. Koch, R. Haensel and C. Kunz), Pergamon-Vieweg, Braunschweig

Radler, K. and Sonntag, B. 1976 *Chem. Phys. Lett.* **39**, 371

Radtke, E-R. 1975 *Diplomarbeit BN-IR-75-13*, Physikalisches Institut, Universität Bonn

Radtke, E.-R. 1979a *J. Phys. B: Atom. Molec. Phys.* **12**, L71

Radtke, E.-R. 1979b *J. Phys. B: Atom. Molec. Phys.* **12**, L77

Radtke, E-R. 1980 *Doktorarbeit BN-IR-80-34*, Physikalisches Institut, Universität Bonn

Rathenau, G. 1934 *Z. Physik* **87**, 32

Rau, A.R.P. and Fano, U. 1968 *Phys. Rev.* **167**, 7

Rosen, A. 1979 *Chem. Phys. Lett.* **61**, 75

Samson, J.A.R. 1966 *Adv. Atom. Molec. Phys.* **2**, 2602

Samson, J.A.R. 1967 *Techniques in vacuum ultra-violet spectroscopy*, Wiley, New York

Schiff, L.I. 1949 *Quantum Mechanics (third edition)*, McGraw–Hill Book Co., New York

Seaton, M.J. 1966 *Proc. Phys. Soc.* **88**, 815

Seaton, M.J. 1978 *J. Phys. B: Atom. Molec. Phys.* **11**, 4067

Shchornak, G., Lemann, D., Muziol, G. and Myuller, G. 1979 *Opt. Spectrosc. (USSR)* **47**, 240

Schrödinger, E. 1926 *Ann. Phys.* **79**, 734

Schwinger, J. 1949 *Phys. Rev.* **75**, 1912

Shore, B.W. 1967 *J. Opt. Soc. Am.* **57**, 881

Siegbahn, K., Nordling, C., Fahlman, A., Nordberg, R., Hamrin, K., Hedman, J., Johansson, G., Bergmark, T., Karlsson, S.-E., Lindgren, I. and Lindberg, B. 1967 *Nova Acta Regiae Soc. Sci. Ups. (Ser.* IV*)* **20**, 1

Skinner, H.B. and Searcy, A.W. 1968 *J. Phys. Chem.* **72**, 3375

Slater, J.C. 1930 *Phys. Rev.* **81**, 385

Smith, J.L. and Kmetko, E.A. 1983 *J. Less Common Metals* **90**, 83

Spedding, F.H. and Henderson, D.C. 1971 *J. Chem. Phys.* **54**, 2476

Spedding, F.H., Beaudry, B.J., Henderson, D.C. and Moorman, J.C. 1974 *J. Chem. Phys.* **60**, 1578

Sugar, J. 1972 *Phys. Rev.* **B5**, 1785

Suzuki, S., Ishii, T. and Sagawa, T. 1975 *J. Phys. Soc. Japan* **38**, 156

Taylor, J.R. 1972 *The quantum theory of nonrelativistic collisions* (Wiley: New York)

Thimm, K. 1965 *Diplomarbeit*, Physikalisches Institut, Universität Bonn

Tomboulian, D.H. and Hartman, P.L. 1956 *Phys. Rev.* **102**, 1423

Tomkins, F.S. and Ercoli, B. 1967 *Appl. Opt.* **6**, 1299

Tracy, D.H. 1975 *Proc. Roy. Soc. Lond.* **344**, 563

Uhlenbeck, G.E. and Goudsmit, S.E. 1925 *Naturwiss.* **13**, 593

Wendin, G. 1972 *J. Phys. B: Atom. Molec. Phys.* **5**, 110

Wendin, G. 1973a *Phys. Lett.* **46A**, 101

Wendin, G. 1973b *Phys. Lett.* **46A**, 119

Wendin, G. 1976 *J. Phys. B: Atom. Molec. Phys.* **9**, L297

Wendin, G. 1985 *Phys. Scr.* **32**, 286

Wendin,G. 1976 *Photo-ionisation and other Probes of Many-electron Interactions,* p.61, (Ed. F.J. Wuilleumier, Plenum Publ. Corp., New York)

Wendin, G. and Ohno, M. 1976 *Phys. Scr.* **14**, 148

Wendin,G. and Starace, A.F. 1978 *J. Phys. B: Atom. Molec. Phys.* **11**, 4119

Wheaton, J. 1964 *Appl. Opt.* **3**, 1247

Wigner, E.P. and Eisenbud, L. 1947 *Phys. Rev.* **72**, 29

Winick, H. and Doniach,S. 1980 *Synchrotron Radiation Research*, Plenum Press, New York

Wolff, H.W., Bruhn, R., Radler, K. and Sonntag, b. 1976 *Phys. Letts.* **59A**, 67

Wybourne, B.G. 1965 *Spectroscopic Properties of Rare Earths* (Wiley: New York)

Zangwill, A. and Soven, P. 1980 *Phys. Rev. Lett.* **45**, 204

Zimkina, T.M. and Gribovskiĭ, S.A. 1971 *J. de Physique*, Colloque **C4**, 282